AN INVESTIGATION OF THE MOMENTUM DISTRIBUTIONS OF POSITRON - ELECTRON PAIRS ANNIHILATING IN CONDENSED MEDIA

A Thesis

Submitted to the

Faculty of Graduate Studies

University of Manitoba

in partial fulfillment of the

requirements of the degree of

Doctor of Philosophy

by

Donald P. Kerr

Winnipeg, Canada

September, 1964

TABLE OF CONTENTS

LIST OF FIGURES

LIST OF PLATES

ACKNOWLEDGEMENTS

The author would like to express his sincere thanks to Dr. B. G. Hogg for his valuable advice and constant encouragement throughout this research.

Acknowledgement is due to Dr. K. I. Roulston for designing some of the electronics, and to Dr. E. Bock and Dr. E. Schaeffer for their participation in discussions on some aspects of this work.

Thanks are due also to Mr. R. S. Foulds for his assistance in building and maintaining the electronic instruments, and to Mr. R. H. Batten for his assistance in the construction of the apparatus.

The financial assistance of the National Research Council of Canada, the American Chemical Society and the Research Corporation of America is gratefully acknowledged.

ABSTRACT

The time spectra and the angular correlation of the annihilation photons for positrons annihilating in a number of organic liquids have been measured. In the present work, the angular correlation data are converted to momentum distributions of the annihilating positron-electron pairs in contrast to previous experiments in liquids where the experimental accuracy has not been sufficient to allow such a conversion. It is found that whenever positronium is formed, two momentum components appear in the momentum distributions. Measurements are made of the intensities of the low momentum components which are then seen to be equal to one third the intensities of the long lived components in the corresponding time spectra. This confirms the view that the low momentum component is due to the self annihilation of singlet positronium.

The variation in width of the low momentum component among different compounds is then examined and discussed in terms of the Ore model of positronium formation. These results imply that, although a lower bound exists for the Ore gap, a precise upper bound does not exist.

Finally, evidence is presented indicating that the high momentum component is a direct measure of the momentum distribution of the electrons involved in the annihilation process.

Chapter 1.

INTRODUCTION

1.1 General.

The positron has become a significant research tool in the study of atomic and molecular systems. The positron is able to penetrate a sample, become a member of its electronic system before annihilation, and then send back to the observer information pertinent to the structure of the sample by means of its positron - electron annihilation gamma rays.

The use of the positron as a probe is limited however, since the free positron, because of its charge, perturbs the electronic configuration within the sample. If a positron can form a bound system with an electron, that system being electrically neutral, its interaction with the electronic configuration will not be as great. Then, however, direct information about the medium can be obtained only to the extent that the positron-electron pair depends upon its environment and not upon its internal properties.

Information relative to the positron, prior to and during annihilation, is necessary for the effective use of the positron as a research probe. The annihilation process itself is well understood on the basis of quantum electrodynamics. The experiment of Weinstein, Deutsch and Brown[1] in which the fine stucture splitting of the ground state of positronium

was measured, very decisively confirmed the predictions of quantum electrodynamics in this matter. The problem of determining the behaviour of the positron prior to its annihilation has not been as clearly resolved. However, many important advances have been made in recent years in both the theoretical and experimental aspects of this problem. Several comprehensive reviews[2-5] have been written on the subject and certain pertinent facts are reviewed in the next few sections.

1.2 The Annihilation of Free Positrons.

It has been shown[6] that approximately 98% of all positrons injected into a sample reach the end of their path of ionization without annihilating. In this discussion we shall therefore consider only positrons that have reached thermal energy or have at most an energy of a few electron volts.

An S state positron-electron pair can exist in one of two forms, namely, the ^1S state with spin zero, or the ^3S state with spin one. The states of higher angular momentum are not of interest since in these states the positron and electron wave functions do not overlap sufficiently for a significant number of annihilations to occur.

From conservation arguments[3] it can be shown that, to first order, the spin zero or singlet state annihilates with the emission of an even number of quanta, the probability of annihilation decreasing rapidly with an increase in the order of the process. Thus, the singlet state normally undergoes

two quantum annihilation. Similarly, to first order, the triplet state can only annihilate with the emission of an odd number of quanta. Annihilation with the emission of a single quantum requires the presence of an external field and therefore the triplet state normally undergoes three quantum annihilation. Ore and Powell[7] have calculated the ratio of the two gamma to three gamma annihilation cross sections to be 372:1 for randomly oriented spins.

1.3 The Formation and Annihilation of Positronium.

Prior to the discovery of a bound system consisting of an electron and a positron, its existence had been postulated and its properties had been discussed by several authors.[7-11] Ruark gave this bound system the name positronium. To a first approximation, the equations describing positronium are the same as those for the hydrogen atom except that the reduced mass is one-half the electron mass. The Bohr radius is therefore 1.06 Angstroms and the ground state energy is 6.8 electron volts.

The ground state can exist in either a singlet (spins antiparallel) or triplet (spins parallel) configuration. As in the case of the unbound positron-electron pair, annihilation proceeds via two quantum emission from the singlet state and three quantum emission from the triplet state. The lifetimes of the singlet and triplet states have been calculated to be 1.25×10^{-10} seconds and 1.39×10^{-7} seconds respectively.[7]

Since the triplet configuration has three substates ($m=0,\pm1$) one expects three times as many positronium atoms to be formed in the triplet state as are formed in the singlet state.

If positrons decay from an unbound state in a rarefied medium such as a gas, then according to the theory of Dirac,[12] the annihilation rate should be proportional to the gas pressure. Also, the ratio of the number of two gamma annihilations to the number of three gamma annihilations should be 372:1 as mentioned above. However, if positronium is formed, its lifetime should be pressure independent since the positron annihilates its own electron. A ratio of somewhat less than 372:1 would be expected for the number of two gamma to the number of three gamma annihilations. If all positrons formed positronium the ratio would be 1:3.

In 1949 Shearer and Deutsch[13] investigated the annihilation of positrons in gases and found that the decay rate was not proportional to the pressure indicating that positronium was being formed. In a later experiment Deutsch[14] found the mean life of triplet positronium to be 1.5×10^{-7} seconds in excellent agreement with the value calculated by Ore and Powell. Further support was given the results of Shearer and Deutsch by other experiments[15] showing that the ratio of the number of two gamma to the number of three gamma annihilations differed appreciably from 372:1. Thus, the fact that positronium was being formed in gases was well established.

Ore[10] postulated the following model to describe the energetics of positronium formation. Consider a high energy positron entering some condensed medium. (In most experiments the positron has a maximum energy of about 0.5 Mev.) The positron is slowed down initially by a series of inelastic collisions in which atomic electrons are excited. When the positron has reached an energy V (see Figure 1.1) just above the first excitation level V_1 of the surrounding molecules, one more inelastic collision results in an energy loss of V_1 for the positron leaving it with an energy $V' = V-V_1$. Now the free space binding energy, V_p, of positronium is approximately 6.8 ev and it is probably slightly less in a condensed medium. Therefore, in order that positronium formation be possible, we must have $V'+6.8>V_i$ where V_i is the ionization potential of the molecule i.e. there must be sufficient residual energy for the positron to capture the atomic electron. To meet this requirement V' must be in the energy range between V_1 and $V_i-6.8$. The difference $V_1-(V_i-6.8)$ has been termed the Ore gap. The capture of an electron by a positron at energies greater than V_1 is possible but the cross section is small compared to that for inelastic scattering.

Support has been given to the Ore model of positronium formation by the results of experiments[16] where static or high frequency electric fields have been applied to samples in which positronium is formed. These fields increase the yield

FIGURE 1.1

THE ORE MODEL OF POSITRONIUM FORMATION

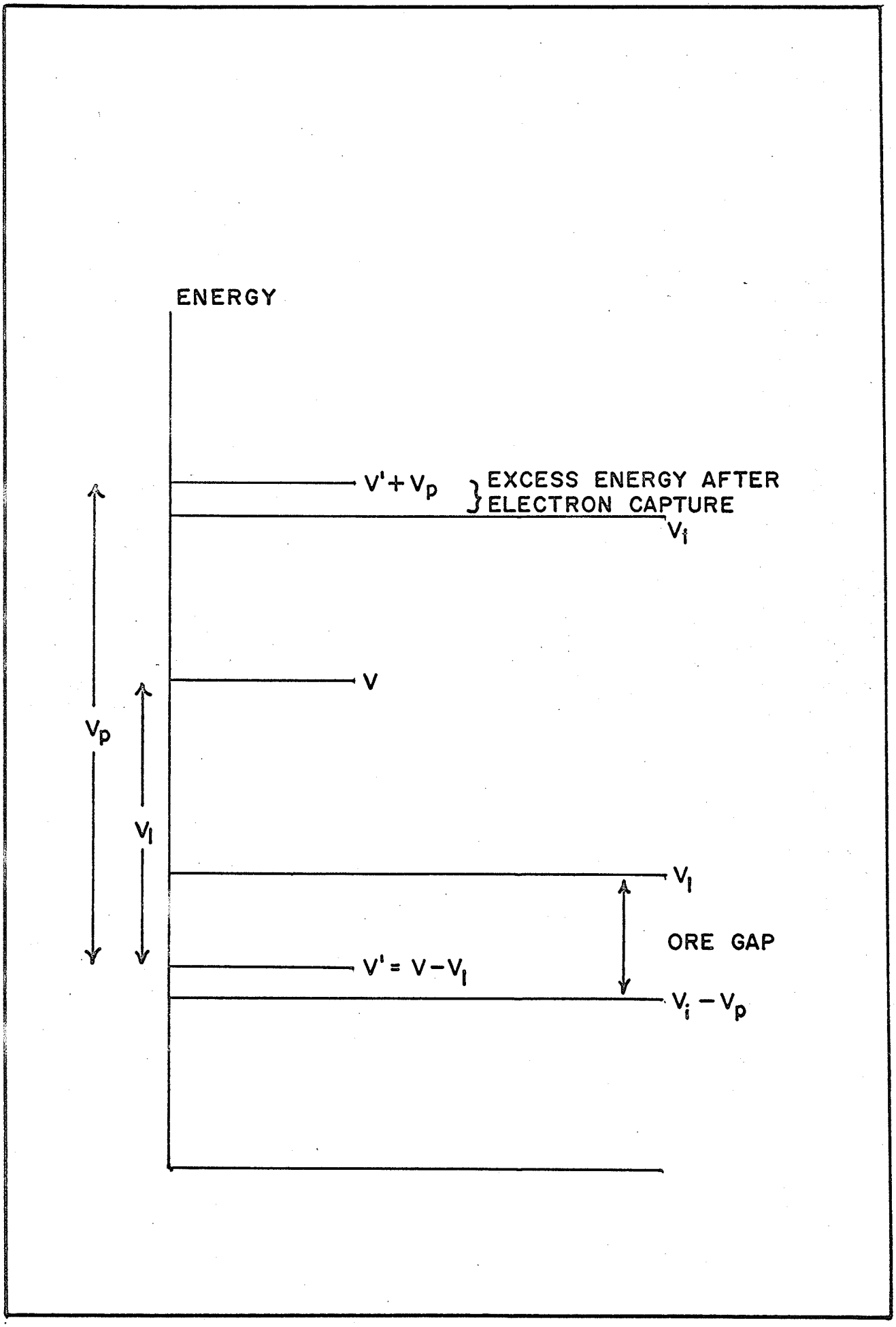
ENERGY
V' + Vp
EXCESS ENERGY AFTER ELECTRON CAPTURE
Vi
V
Vp
Vl
Vl
ORE GAP
V' = V − Vl
Vi − Vp

of positronium since, according to the Ore model, positrons which have passed through the Ore gap without forming positronium are recycled through it and given another opportunity to capture an electron.

1.4 Methods of Investigation of Positrons and Positronium.

There are a number of methods for detecting and investigating positronium. The most direct method is the detection of three gamma coincidences which indicate the presence of triplet positronium. One can examine the gamma ray energy spectrum of the .511 Mev annihilation radiation where, as usual, a photopeak and a Compton distribution appear separated by a well defined valley. If positronium is being formed, then the gamma rays resulting from three quantum annihilations have energies which are distributed continuously from 0 to .511 Mev. This results in a smaller peak to valley ratio than for pure two gamma annihilations thus indicating the formation of positronium. Positronium formation is also implied by a decrease in the number of two gamma coincidences in counters correlated at 180 degrees.

Two methods most widely used in recent and current experiments are the measurement of the time spectra of positron annihilations and the measurement of the angular correlation of the annihilation quanta.

1.5 The Time Spectra of Positron Annihilations.

To obtain the time spectra of positron annihilations a Na^{22} source which emits a positron and a 1.28 Mev nuclear gamma ray simultaneously is commonly used. The time difference between the detection of the nuclear gamma ray and the annihilation radiation is measured giving the lifetime of the positron. This was done originally by employing the method of delayed coincidences. With the advent of multichannel analysers, fast time to amplitude converters were developed which greatly facilitated time measurements.

Following the investigations of positron annihilations in gases, de Benedetti and Richings[17] and Bell and Graham[18] turned to an investigation of annihilations in condensed media. It became immediately apparent that there were two broad classifications for the materials studied. In one group, consisting of metals and ionic and valence crystals, a single and almost constant lifetime of the order of 10^{-10} seconds was found. The other group, consisting generally of organic and amorphous materials, exhibited a complex decay scheme. As in metals, a short lifetime of about 10^{-10} seconds was present, and in addition the time spectra had a separate, well defined exponential tail corresponding to a second, longer lifetime of approximately 10^{-9} seconds. In other words, at least two different modes of decay were clearly indicated. The percentage of positrons decaying with the longer lifetime appeared at

first to be about 30% in all the materials studied, but improved apparatus and techniques showed that this value could vary from a few percent to about 50% depending on the compound in which annihilation occurred.

The materials showing only the short lifetime have a variety of electron densities. If the Coulomb attraction between the positron and the electron is ignored, then the positron should have a mean life which is inversely proportional to the density of electrons with which the positron can annihilate. Since the positron lifetime remains fairly constant in spite of large variations in electron density, it is necessary to conclude that the Coulomb attraction of the positron to electrons is the governing factor. It appears that as the positron approaches thermal energy electrons cluster about it and annihilation occurs.

More recently Bell and Jørgensen[19] have remeasured the lifetime of positrons in aluminum and the alkali metals. They used an improved apparatus which allowed the lifetimes to be read directly from the logarithmic slopes of the time spectra rather than having to employ the relatively unreliable method of measuring centroid shifts. They found larger variations in the short lifetimes than had been previously reported but it was still apparent that the Coulomb attraction plays an important role. Their decay curves appeared to be complex indicating a second, longer lifetime of approximately 5×10^{-10} seconds

which has remained unexplained. This is the lifetime one would expect if positronium were being formed and a rapid triplet - singlet conversion were occurring. However, angular correlation studies have indicated that no positronium is being formed in these cases.[20]

The materials having a complex decay scheme with the longer lifetime of the order of 10^{-9} seconds can be classified generally as molecular materials. In contrast to the metals and crystals which have free electrons, these materials allow for electron exchange only within the individual molecules. The 10^{-9} second lifetime is too short to be attributed to annihilations directly from the triplet state of positronium. Furthermore, the annihilations connected with this lifetime have been shown to result in the emission of only two quanta and therefore it has been interpreted as arising from the process of "pickoff" annihilations. This process is described as follows. If positronium is being formed in these materials, one quarter will be formed as singlet positronium and will decay by self annihilation with a mean life of approximately 10^{-10} seconds. Three quarters will be formed as triplet positronium which will undergo scattering by the molecules of the material. In such scattering the positronium atom may collide with an electron whose spin state relative to it is singlet and therefore annihilate. Thus, the 10^{-9} second lifetime is the lifetime of the triplet state against pickoff. Of course pickoff could also occur from the singlet state but due to the very short singlet state lifetime, the probability of

such an occurrence is small.

The only alternative explanation of the long lifetime would be a triplet to singlet conversion due to collisions. However, Ore[21] has calculated that spin flip through magnetic interaction would require about 10^{-5} seconds. An exchange collision at the energies involved is possible only if the molecule has an unpaired electron but the long lifetime appears when no unpaired electrons are present. Hence, the pickoff process appears to be the only allowable explanation.

This explanation implies that the short lifetime in the complex decay scheme is itself complex. It should arise from the annihilation of singlet state positronium and from the annihilation of free positrons. Investigations of annihilations in liquid helium[22,23] have given support to this interpretation. In these experiments three components were discovered in the decay scheme, the short lifetime arising from singlet positronium annihilations, the intermediate one arising from free positron annihilations and the long lifetime arising from the decay of triplet positronium. More recently, the time spectra of positrons annihilating in various amorphous solids and plastics such as polyethylene have been shown to consist also of three distinct components.[24,25] There is some doubt however, as to the origin of the intermediate component in these experiments. Some comments will be made with regard to this in Chapter 5.

1.6 The Angular Correlation of the Annihilation Quanta.

When a positron and an electron annihilate one another, an energy of very nearly $2mc^2$ is released, where m is the mass of the electron. If annihilation occurs with the emission of two photons, each will have a momentum mc and in the centre of mass system the photon pair must be correlated at 180 degrees to conserve momentum. If the positron-electron pair has some momentum p, then in the laboratory system the deviation from 180 degrees will be θ, where $\theta \doteqdot p/mc$ radians.

It will be useful to digress here and consider the history of a positron from the time it enters a sample until its annihilation. Initially the positron may have an energy of several kilovolts. It loses energy very rapidly at first due to collisions with electrons. Lee-Whiting[26] has calculated the slowing down time of a positron in a metal and obtained the following results. To decrease the positron's energy to a few electron volts requires $10^{-16}/E^{\frac{1}{2}}$ seconds, where E is the final energy in electron volts. In this stage the collisions result in the excitation of electrons to excited bands. Further energy loss from 4 ev to 1 ev, 1 ev to 0.1 ev and 0.1 ev to 0.025 ev require 3×10^{-15} seconds, 2×10^{-13} seconds and 3×10^{-12} seconds respectively. The last stages of the slowing down process are relatively time consuming but, in metals, thermalization should be complete before annihilation occurs.

In insulators the positron is again attenuated quite

rapidly at first by inelastic collisions resulting in ionization or electronic excitation of the molecules. As noted above, at least 98% of the positrons should survive this stage of the slowing down process which takes approximately 10^{-12} seconds. When the positron velocity becomes comparable with the velocity of the outer shell electrons of the molecule, the cross section for positronium formation becomes appreciable. In a particular energy range therefore, the positron can capture and lose electrons continually until either process is no longer energetically possible. If positronium is formed, it will lose energy more slowly than will a free positron because of its electric neutrality. Therefore, it would be expected that thermalization of positronium may not be complete before annihilation. This is substantiated by the work of Page et al[27] and by the present work.

Positrons which pass through the energy range favourable to positronium formation without capturing an electron also moderate quite slowly since they are not energetic enough to cause electronic excitation. They may then lose energy through inelastic scattering resulting in vibrational excitation of the molecules[28] or they may suffer elastic scattering. Both of these processes reduce the energy of the positron rather slowly.

De Benedetti et al[29] have calculated that thermalization of positrons by the mechanism of the excitation of lattice vibrations in gold requires 3×10^{-10} seconds. It has been pointed out[5] that these calculations more properly give the

thermalization time in insulators and hence, in insulators, free positrons may not be thermalized before annihilation.

If the positrons are thermalized prior to annihilation as appears to be so at least in the case of metals, then the main contribution to the centre of mass motion will come from the electron motion. Therefore, in performing this type of experiment one hopes to obtain some knowledge of the electron momentum distribution in a substance.

There are two experimental arrangements which can be used to investigate the angular correlation of the annihilation quanta. The one most commonly employed has parallel slits in front of the gamma ray detectors. This arrangement, which measures only one component of the momentum of the positron - electron pair, will be described in detail in Chapter 3.

An experimental arrangement having a cylindrical geometry has been used by some investigators.[30,31] In this apparatus one counter accepts a narrow cone of radiation while the other accepts a conical shell of radiation defined by an annular aperture. When the momentum distribution is isotropic it can be obtained by an inversion of the data yielded by either type of apparatus. However, the cylindrical geometry type has several inherent experimental disadvantages which discourage its use.

The first detailed theoretical and experimental investigation of the angular correlation of the annihilation

photons was done by de Benedetti et al[29] in 1950 followed by the work of Warren and Griffiths[32] in 1951. Since then many investigators have made contributions to this field.[30,31,33-44]

As in the case of time spectra, two broad classifications for the materials studied were apparent. Again, one group consisted of metals and ionic and valence crystals and the other of organic and amorphous materials. The angular distributions for the first group are generally wider than those for the second group.

In a series of experiments, Stewart[33-37] has investigated positron annihilations in metals and alkali halides obtaining the momentum distributions of the positron-electron pairs. It was found that metals further divided naturally into two groups, those for which the momentum distribution or the density in momentum space dropped sharply to zero at a certain momentum, and those for which no sharp drop took place. For the first group, consisting in part of the alkali metals, the sharp drop-off occurred at very nearly the Fermi energy (calculated from the free electron theory) in each case. This verified the belief that positrons were thermalized before annihilation i.e. the momentum distribution obtained was that of the outer shell electrons assuming that the annihilation probability is the same for electrons of all momenta.

A small tail was present on the momentum distributions beyond the Fermi energy which was attributed to annihilations

with inner shell electrons. Berko and Plaskett[20] performed precision measurements on the angular correlation of the photons from positrons annihilating in aluminum which belongs to the first group of metals. They obtained good agreement with a theoretical angular distribution which they calculated allowing for core annihilations.

In the second group of metals, the distributions extend well beyond the Fermi energy. This could be caused by core annihilations or an interaction with the lattice. Berko and Plaskett[20] also investigated annihilations in copper which falls into the second group of metals. Their calculations were in qualitative agreement with their experimental results indicating again that core annihilations were influencing the the angular distribution to some extent.

In 1955 Page et al[27] investigated positron annihilations in organic and amorphous substances. Some of the angular distributions appeared to consist of a rather narrow distribution superimposed on a broader distribution. A direct connection between the narrow component and the formation of positronium was indicated in these experiments when it was found that the distribution from crystalline quartz, which shows no long lived component, had no narrow component, while the distribution from fused quartz, which has a strong long lived component, was quite peaked.

In a condensed material a positron normally decays

by one of three modes. It can decay as a free positron, it can form triplet positronium and annihilate by the pickoff process, or it can form singlet positronium which subsequently undergoes self annihilation. Ferrell[38] pointed out that the narrow component could only arise from the decay of a bound positron with its own electron i.e. from the self annihilation of the singlet state. The other two modes of decay involve electrons with relatively high momenta which should therefore contribute to the broad distribution. Support was given this view by the results of magnetic enhancement experiments[39,40] in which a magnetic field was used to convert triplet to singlet positronium before destruction by pickoff. In these experiments an increase in the intensity of the narrow component was observed as expected.

Since three quarters of the total amount of positronium is formed in the triplet state and one quarter is formed in the singlet state, the narrow component should have an intensity equal to $I_2/3$, where I_2 is the intensity of the long lived component arising from the decay of the triplet state by pickoff. In their original experiment, Page et al[27] estimated the intensity of the narrow component to be almost double the value indicated by lifetime measurements. Their estimate was based on the difference between the purely broad distribution for crystalline quartz and the complex distribution for fused quartz. This method relied on the questionable

assumption of similar broad distributions for both samples. Ferrell[39] suggested the possibility of a triplet to singlet conversion due to spin flip by magnetic fields but he states that the process would probably be far too ineffective.

De Zafra[41] has compared the change in $I_2/3$ with the change in intensity of the narrow component for some materials under varying conditions and has found the difference to be zero within his experimental error. Although the errors are rather large, his results support the view that the narrow component is due to the self annihilation of singlet positronium.

In this work it will be shown that good agreement exists between the value $I_2/3$ determined from time measurements and the absolute intensity of the low momentum or narrow component estimated from the momentum distributions rather than from the angular correlation data.

1.7 Factors Influencing the Annihilation of Positronium.

A temperature dependence of the lifetime of the long lived component was first observed by Bell and Graham.[18] It was found that, for teflon, the lifetime decreased with decreasing temperature. Similar results for lucite, nylon, polyethylene and polystyrene were reported by Lundholm et al.[42] Stump[43] found that when some of these substances were subjected to pressure, the long lifetime decreased indicating that both the temperature and pressure effects were simply the result of

density variations. With increasing density one would expect the lifetime against pickoff annihilations to be reduced. A very marked change in the long lifetime of positrons in napthalene was observed by Landes et al[44] as the napthalene was taken through a change of phase. However, the change was so large that it suggested more than only density changes were involved in this case.

In the same experiment the intensity of the long lived component was found to increase sharply as the napthalene went from the solid to the liquid state. Stewart[34] investigated the angular distribution of the annihilation radiation from teflon and found that the distribution narrowed as the temperature increased indicating that more positronium was being formed. De Zafra[41] investigated annihilations in teflon and water measuring the "peak rate" (counting rate at 180 degrees) as a function of temperature. His results strongly indicated that the temperature effect on the amount of positronium formed was actually a density effect. The peak rate in teflon increased steadily with temperature and then dropped sharply when the sample was subjected to a high pressure. In water the peak rate increased or decreased as the density changed in the opposite direction even in the region of the anomolous density variation. Wallace[5] suggested that the decrease in positronium formation at lower temperatures or higher densities is due to a decrease in the size of the Ore gap as a result of

the positronium binding energy becoming weaker as the space available to the positronium atom becomes smaller.

There are various other factors affecting the annihilation of positronium. The quenching of the triplet state by the application of a magnetic field has already been referred to. This results from a mixing of the singlet state and the m=0 triplet state so that conversion between the states can occur.

Ferrell[45] suggested that triplet to singlet conversion should be possible through electron exchange collisions with paramagnetic ions or any molecule with at least one unpaired electron. The first evidence for such a process was found by Deutsch[1]. More recent work of this nature was done by de Zafra[41] in which he introduced paramagnetic ions in varying concentrations into water and noted that the narrow component in the angular distribution was enhanced. This result indicated that a conversion process was operating.

Finally, there is some evidence that positron or positronium compounds may be formed. Green and Bell[46] observed that the addition of $NaNO_2$ or $NaNO_3$ to water decreased the intensity of the long lived component while the lifetime remained constant. They suggested that positron compounds were being formed thus reducing the number of positrons available for positronium formation. De Zafra's angular correlation work was in agreement with this view and indicated other cases in which positron compounds were possibly being formed.

Chapter 2.

THE TIME MEASURING APPARATUS

2.1 Electronics.

This apparatus has been described in detail previously[47] and therefore only the general principle of operation of the circuits and any modifications made to them will be described here.

The function of the apparatus is to measure the time delay between the emission of a 1.28 Mev nuclear gamma ray from the positron source, and a .511 Mev annihilation gamma ray from a sample into which positrons have been injected. This is a measure of the lifetime of the positron in the sample since the positron is emitted essentially in coincidence with the 1.28 Mev gamma ray, and the appearance of a pair of .511 Mev gamma rays signifies the annihilation of the positron with an electron.

Figure 2.1 shows a block diagram of the apparatus. Pulses from the 1P21 photomultipliers are sent to their respective limiters where they are changed to pulses of constant height and length. These shaped pulses go to the time to pulse height converter where the amount of overlap between them is converted into a pulse height. This voltage pulse is then amplified and sent to the multichannel analyzer where it is recorded if there has also been a slow coincidence.

PLATE 1

THE TIME MEASURING APPARATUS

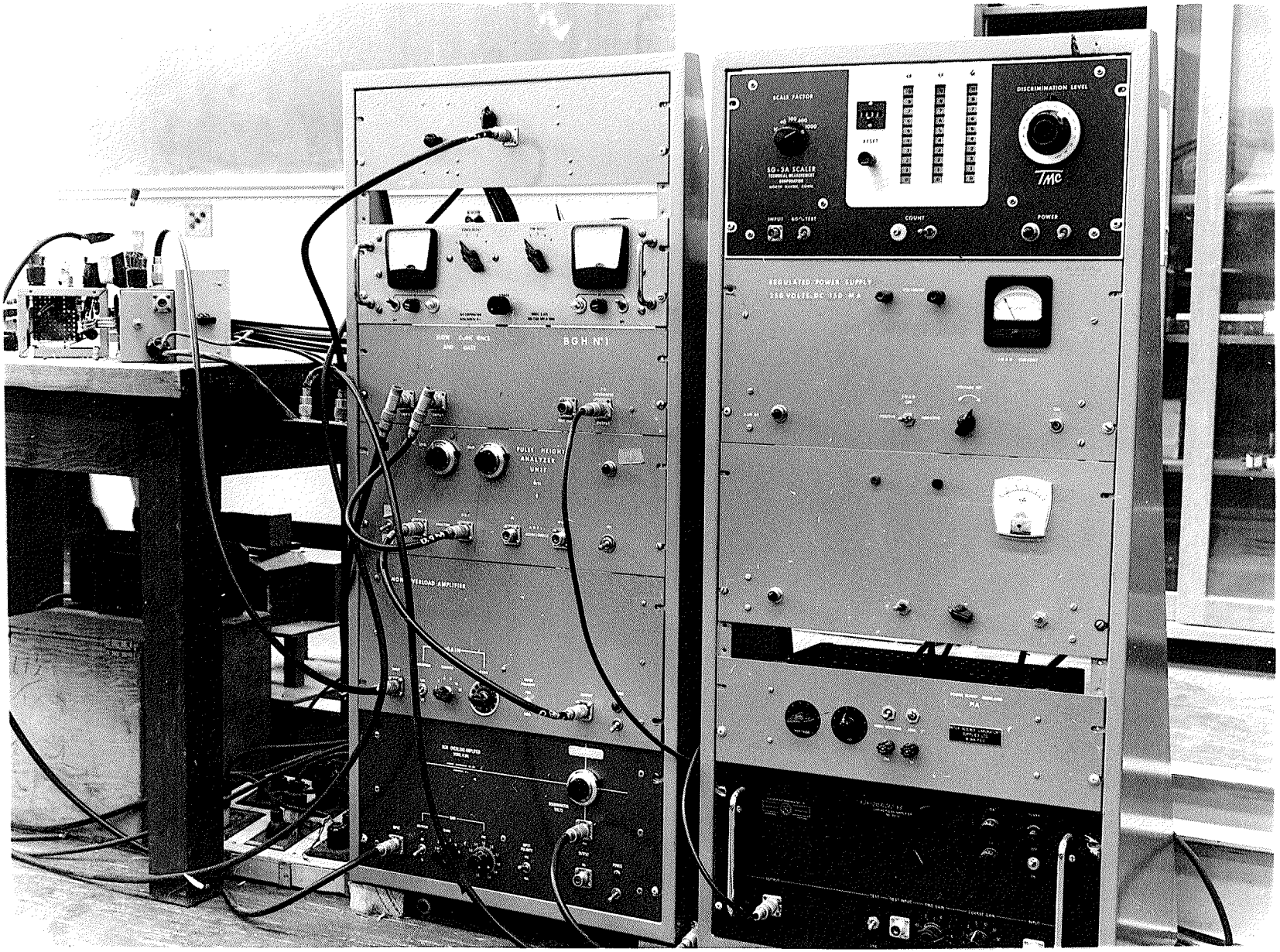
SCALE FACTOR
SQ-3A SCALER
DISCRIMINATION LEVEL
TMC
INPUT
COUNT
POWER
REGULATED POWER SUPPLY
BGH N°1
PULSE HEIGHT ANALYZER UNIT

FIGURE 2.1

BLOCK DIAGRAM OF THE TIME APPARATUS

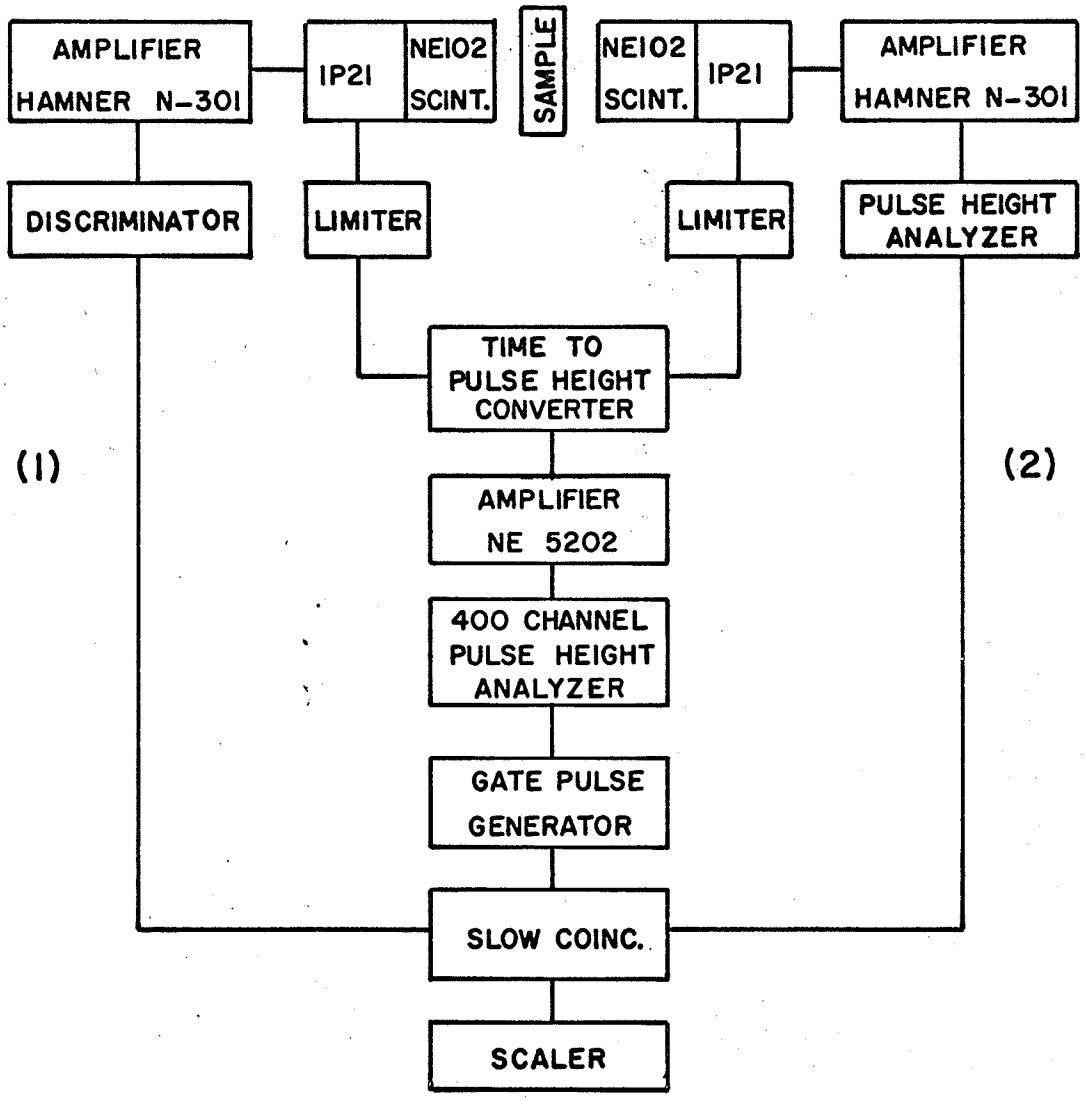
AMPLIFIER
HAMNER N-301
IP21
NE102
SCINT.
SAMPLE
NE102
SCINT.
IP21
AMPLIFIER
HAMNER N-301
DISCRIMINATOR
LIMITER
LIMITER
PULSE HEIGHT
ANALYZER
TIME TO
PULSE HEIGHT
CONVERTER
(1)
(2)
AMPLIFIER
NE 5202
400 CHANNEL
PULSE HEIGHT
ANALYZER
GATE PULSE
GENERATOR
SLOW COINC.
SCALER

The slow coincidence system operates as follows. The discriminator in side channel 1 is set to pass pulses to the slow coincidence unit corresponding to energies greater than .52 Mev. The pulse height analyzer in side channel 2 is set to pass pulses corresponding to energies between .2 and .5 Mev. Thus, side channels 1 and 2 accept the Compton distributions of the 1.28 Mev and .511 Mev gamma spectra respectively. If the two events occur within .5 microseconds of one another a gating pulse is sent to the multichannel analyzer from the gate pulse generator. All the slow coincidence circuitry is of standard design.

Detectors.

The detectors consist of NE102 plastic scintillators cemented to selected R.C.A. 1P21 photomultipliers. The plastic phosphors are cylindrical in shape, 2 cm. high and 2 cm. in diameter with a portion of the round surface ground to fit the face of the photomultiplier. These were wrapped with rough aluminum foil to provide diffuse reflection and then the assembly was wrapped in black electical tape for light tightness.

The counting efficiency and energy resolution is very poor for these plastic scintillators but they produce light pulses of very short mean time duration (approximately 2×10^{-9} seconds) which are required for fast coincidence work.

1P21 photomultipliers are normally operated at a maximum of 900 volts, but to ensure small electron transit time variations they were operated at 2300 volts. This was the

maximum permissible voltage; continuous discharge occurred if a higher voltage was applied.

Limiters.

The performance of the limiters is very critical in this type of fast coincidence circuit since the time to amplitude converter to be described is quite sensitive to pulse shape and size. The limiter tube must be a sharp cut-off tube capable of producing a flat topped pulse with a rise time of about one nanosecond. It must also be able to conduct a large plate current (15 - 20 milliamps) so that the pulse will have an amplitude of at least one volt. The E180F, a high gain, high current capacity, sharp cut-off pentode is used for this purpose. The limiter circuit as a whole must be such that the pulses produced are of constant amplitude and independent of the counting rate.

Figure 2.2 shows the limiter circuit diagram. Negative pulses about 10 volts in amplitude from the photomultiplier are applied to the grid of the E180F. The tube ceases to conduct and at the anode a fast rising flat topped 2 microsecond pulse is produced which travels to the junction of the shorting stub and the cable leading to the time to pulse height converter. In the present experiment the shorting stub was increased in length from 400 cm. to 500 cm. in an attempt to increase the linear range of time to pulse height conversion.

FIGURE 2.2

DETECTOR AND LIMITER

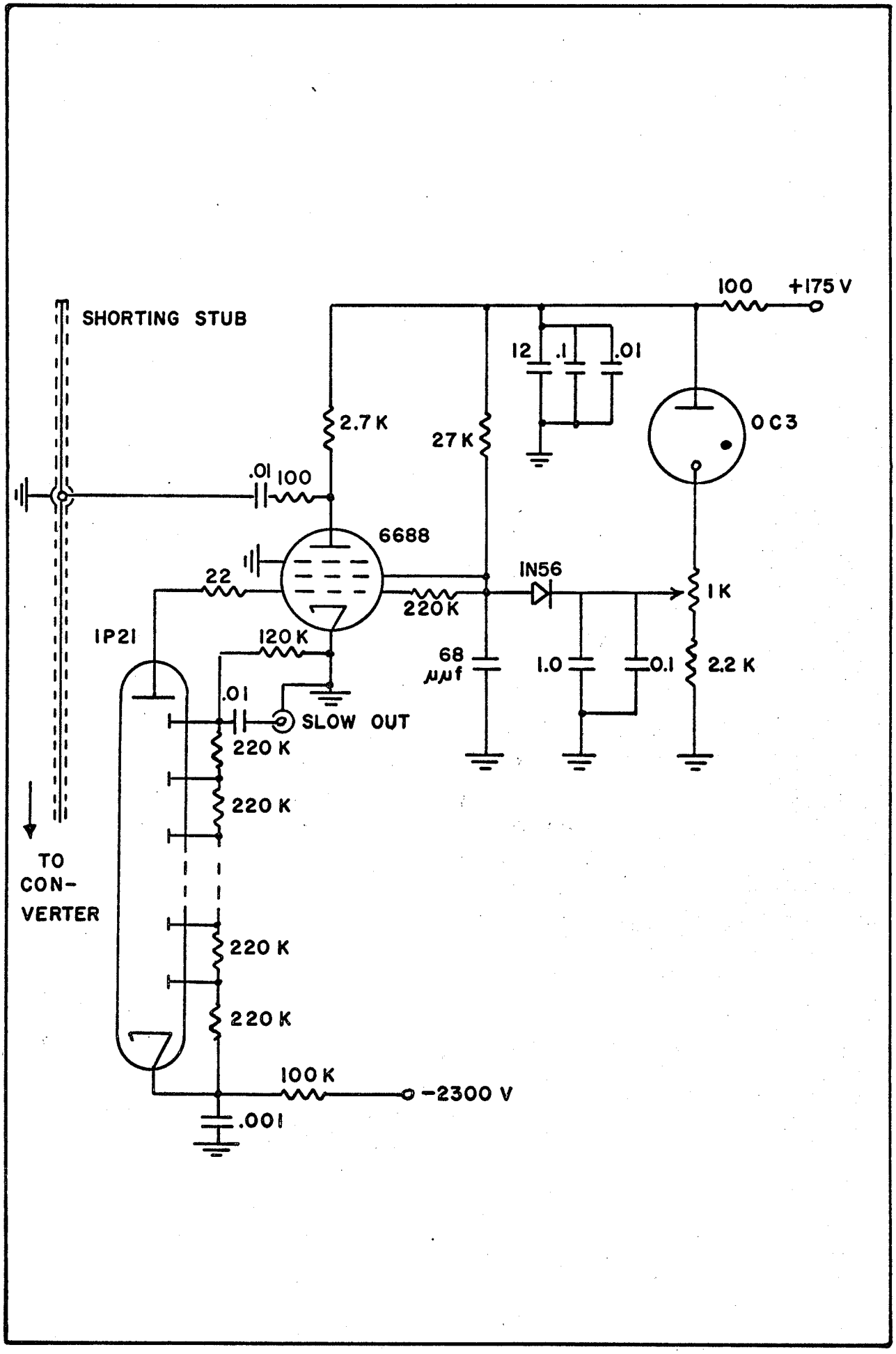
SHORTING STUB
100
+175 V
12
.1
.01
2.7 K
27 K
0C3
.01
100
6688
22
IN56
1 K
220 K
1P21
120 K
68
μμf
1.0
0.1
2.2 K
.01
SLOW OUT
220 K
220 K
TO
CON-
VERTER
220 K
220 K
100 K
-2300 V
.001

The two microsecond pulse travels down the shorting stub, is reflected negatively, and returns to the junction so that the resulting pulse arriving at the time to pulse height converter is 40 nanoseconds long. Thus, 40 nanoseconds is the maximum linear range of time to pulse height conversion. The effect of high counting rates is minimized by clamping the screen of the limiter tube with the 1N56 diode to limit its positive excursion. Short time constants in the associated circuitry allow fast recovery of the tube.

The only modification made to the limiter circuit itself was the insertion of a 100 ohm damping resistor between the plate of the E180F and the cable junction. The purpose of this resistor is to minimize the ringing of the limiter pulses.[48] Its value was chosen by the method of trial and error. With the damping resistor in place, a considerably more linear time to amplitude conversion resulted.

Time to Pulse Height Converter.

The time to pulse height converter is a unit which converts the degree of overlap of two pulses (i.e. the time difference between the pulses) into a voltage pulse suitable for analysis in a multichannel analyser.

The circuit employed here (Figure 2.3) is based on one described by Bell and Green[49] but it has several modifications. It employs a 6BN6 gated beam tube with two control

FIGURE 2.3

TIME TO PULSE HEIGHT CONVERTER

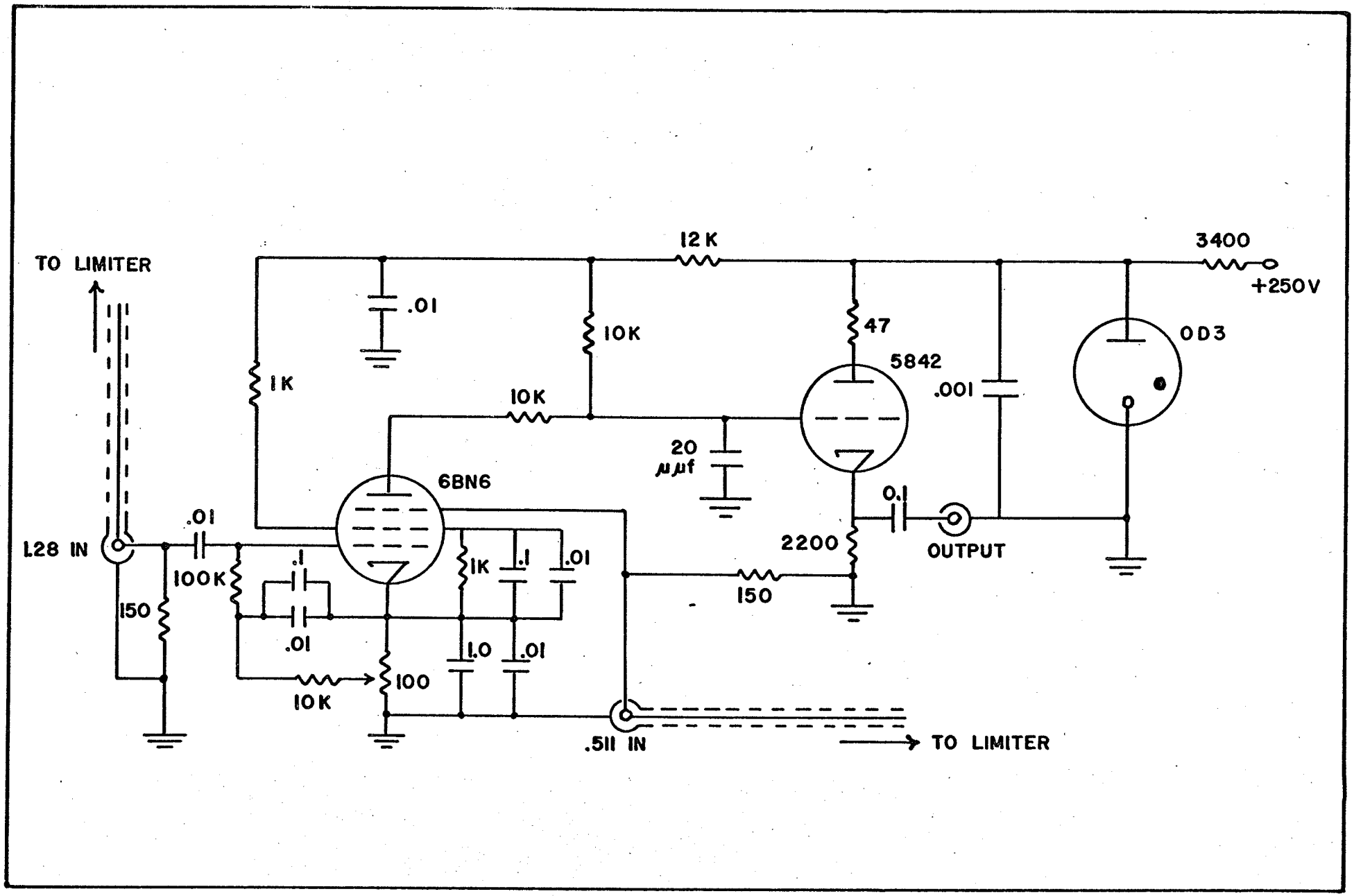
TO LIMITER
12 K
3400
+250V
.01
10K
47
5842
OD3
1K
10K
.001
20
μμf
6BN6
.01
0.1
1.28 IN
100K
2200
OUTPUT
.1
1K
.1
.01
150
150
.01
1.0
.01
100
10K
.511 IN
TO LIMITER

grids to which the limited pulses are applied. A significant plate current will flow only if both grids are driven positive simultaneously. Therefore, the tube conducts only when the limited pulses to the control grids overlap. The time during which conduction occurs (the length of the anode pulse) is determined by the amount of overlap. The length of the anode pulse is then converted to a pulse height by a standard integrating circuit employing a 5842 triode.

In actual operation the 1.28 Mev pulse is artificially delayed by approximately 30 nanoseconds so that the later the .511 Mev pulse originates, the larger the output from the converter. This results in the significant details of the time spectrum appearing on its high voltage side rather than on the low voltage side where a high non uniform background exists due to improperly limited pulses.

2.2 Calibration and Circuit Performance.

Calibrations were done previously using Co^{60} as a source of prompt coincidences and measuring the position of the centroid of the resulting time spectrum as a function of the delay inserted between the .511 Mev limiter and the converter. This procedure involved relatively long counting times during which electronic shifts sometimes occurred giving rise to questionable calibration curves. A calibration was attempted by pulsing the grids of the limiter tubes simultaneously with

a 60 cycle pulse generator. The calibration curves so obtained were more linear and they agreed with the Co^{60} calibrations within experimental error and therefore this method was adopted.

Also, in previous calibrations, the individual delay cables were inserted with Amphenol connectors. Slight electronic shifts would sometimes occur as a result of jarring the apparatus. The time to amplitude converter seemed particularly susceptible to this fault. To overcome this, the converter was rebuilt and rigidly rack mounted. Six position rotary switches were mounted on the .511 Mev limiter and on the corresponding input to the converter and six cables ranging in length from 100 cm. to 500 cm. (4 to 20 nanoseconds) were soldered to the switches. The delay could then be changed simply by switching from one cable length to another. All cable connections to the converter were soldered. With this system a six point calibration curve over a 16 nanosecond range could be obtained in less than a minute. Calibration over a larger range could be accomplished by varying the cable length between the 1.28 Mev limiter and the converter.

A typical calibration curve is shown in Figure 2.4. It is linear over a range of about 22 nanoseconds. As stated above, the maximum possible linear range for this apparatus is 40 nanoseconds. The departure from linearity at the upper end of the curve probably occurs because the integrator is no

FIGURE 2.4

TIME TO PULSE HEIGHT CALIBRATION CURVE

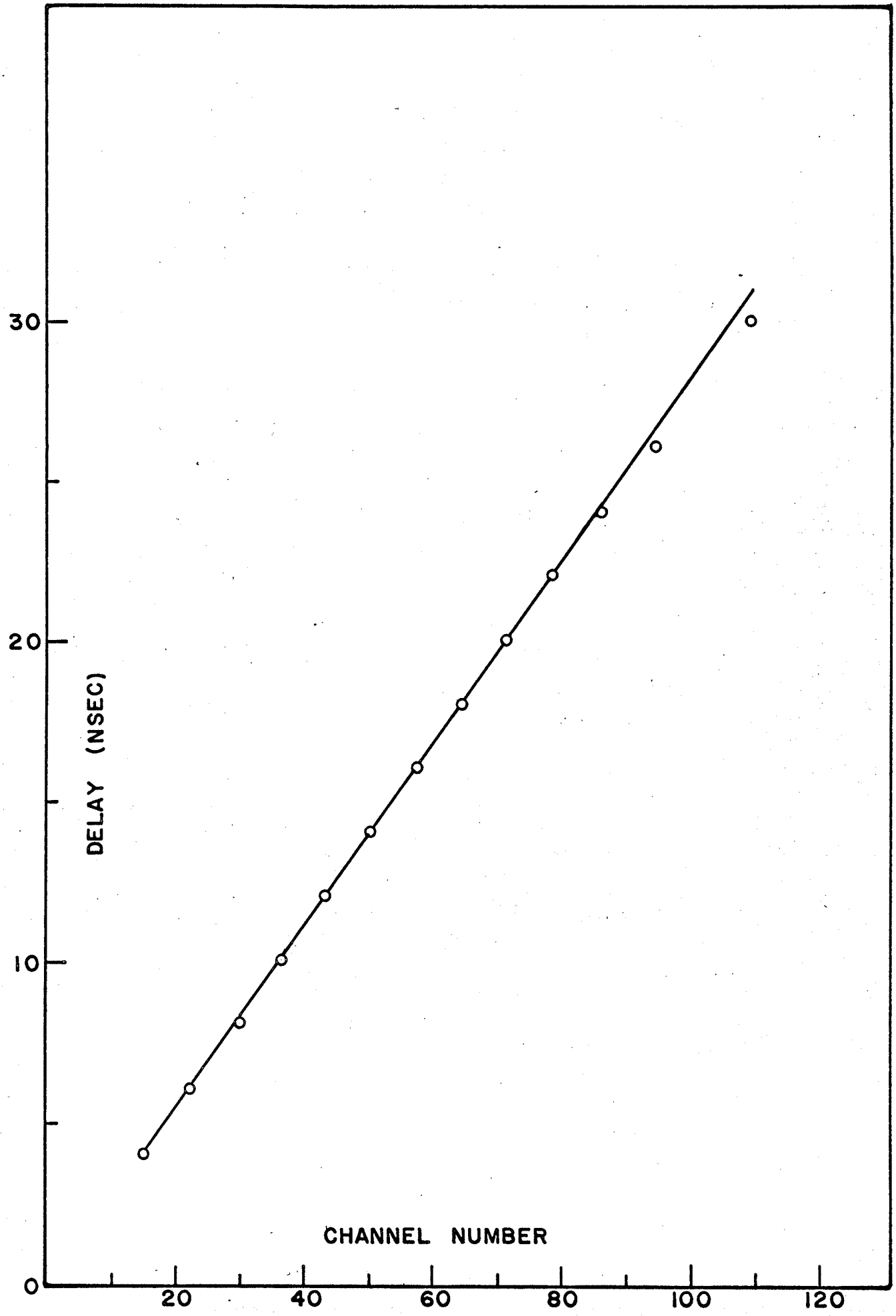
30
20
10
0
DELAY (NSEC)
20
40
60
80
100
120
CHANNEL NUMBER

longer operating in its linear region. This could be improved by adjusting the circuit parameters but only a 20 nanosecond range is required in actual operation. This calibration curve does not exhibit the slightly sinusoidal shape caused by the ringing of the limiter pulses indicating that the damping resistor reduced or eliminated this fault.

The time resolution of the apparatus (the full width at half maximum of a prompt coincidence spectrum) determined using a Co^{60} source was 1.3 nanoseconds. The long term stability of the apparatus was very good. Its sensitivity (in nanoseconds per channel) was constant to within 2% over an indefinite period.

2.3 Sources and Samples.

The source of positrons employed was Na^{22} in the form of NaCl which is insoluble in all the liquids studied. Therefore, an open source could be used in all cases. This consisted of a thin (2 mg/cm^2) roughened sheet of mica onto which about 40 microcuries of Na^{22} had been evaporated. The source was placed in a test tube containing the liquid to be investigated which was then mounted on the side of the two detectors. The high specific activity (1.97 mc/mg) permitted the use of a relatively strong source without encountering the problem of self absorption in the source material.

Only one source was used throughout the experiment

for all the different samples. A very small amount of contamination by a liquid exhibiting no long lived component has considerable effect on the time spectrum for a compound which does show the long lifetime. Therefore, when the investigation of one sample had been completed, the source was thoroughly rinsed in the liquid to be studied next and then allowed to stand for an hour in the same liquid. This was then discarded and replaced with a fresh sample.

2.4 Data Accumulation and Analysis.

Due to the much higher source strength used here than in previous experiments with the same apparatus, counting time was reduced by a factor of ten. For each result, at least five time spectra were obtained each with 10^5 to 10^6 counts at the peak.

The advantage of shorter counting times was somewhat offset by the more complicated background subtraction which was necessary resulting from the higher chance coincidence counting rate. (If the true coincidence counting rate increases by a factor of ten, the chance coincidence rate increases by a factor of one hundred.) The method of background subtraction used with smaller sources was to measure the counting rate in the region of the spectrum well beyond the exponential tail and to assume this to be a constant background over the whole range. With the higher counting rate it became apparent that

the background was not uniform. This fact was determined by examining the time spectrum of positrons annihilating in CCl_4 which does not exhibit a long lived component. The background was flat in a range well beyond the main peak in the spectrum but it then increased rather sharply 20 nanoseconds from the peak and continued to rise slightly in the range from 20 nanoseconds to 6 nanoseconds to the right of the peak where it then became impossible to distinguish the background from the true coincidence counts. This background was subtracted from all the time spectra after they had been normalized to the peak counting rate of the CCl_4 spectrum.

The slight change in the time to pulse height conversion factor as indicated by the departure from linearity in the calibration curve in Figure 4.4 would contribute to the sharp increase in the background mentioned above, but it is doubtful that it would completely account for it. Optical coupling[50] or pile up effects[49] also contribute to the nonuniformity. Results obtained earlier with smaller sources would not have been appreciably affected by this nonuniformity since the background was then a much smaller percentage of the true coincidence counting rate.

The method of data analysis followed that of Green and Bell.[46] After the background was subtracted, the logarithm of the coincidence counting rate was plotted vs time delay. A straight line was then drawn through the points on the

exponential tail and projected back to the position of zero time delay. The ratio of the area under the tail to the total area was obtained by numerical integration yielding I_2, the intensity of the long lived component. The lifetime of the long lived component is given by $\tau_2 = .434/m$ where m is the slope of the straight line portion of the spectrum.

Chapter 3.

THE ANGULAR CORRELATION APPARATUS

3.1 Mechanical Construction Details.

A diagram of the mechanical parts of the angular correlation apparatus is shown in Figure 3.1. To ensure rigidity, platforms for each of the two detectors, the source and sample housing and the associated collimating slits were mounted on two 3" by 6" aluminum I beams approximately 20 feet long. The I beams were placed 14" apart and bolted with cross bars at 5 foot intervals.

The movable gamma ray detector, detector A, and its collimating slits were mounted at one end of the I beam base on a steel plate which was free to rotate on top of a similar steel plate. The weight of the top assembly was about 20 pounds and therefore to allow for easy rotation, four ball races were set in wells in the corners of the bottom plate. A central shaft about which rotation occurred kept the two plates aligned. The lower plate was moved between a set of linear rails by a worm screw driven by a "Slo-Syn" 600 ounce - inch reversible motor.

The fixed gamma ray detector and its collimating slits were mounted at the other end of the I beam base. This detector was almost completely shielded with 3" thick lead blocks to reduce the background from scattered gamma rays and from other sources in the laboratory.

PLATE 2

THE ANGULAR CORRELATION APPARATUS

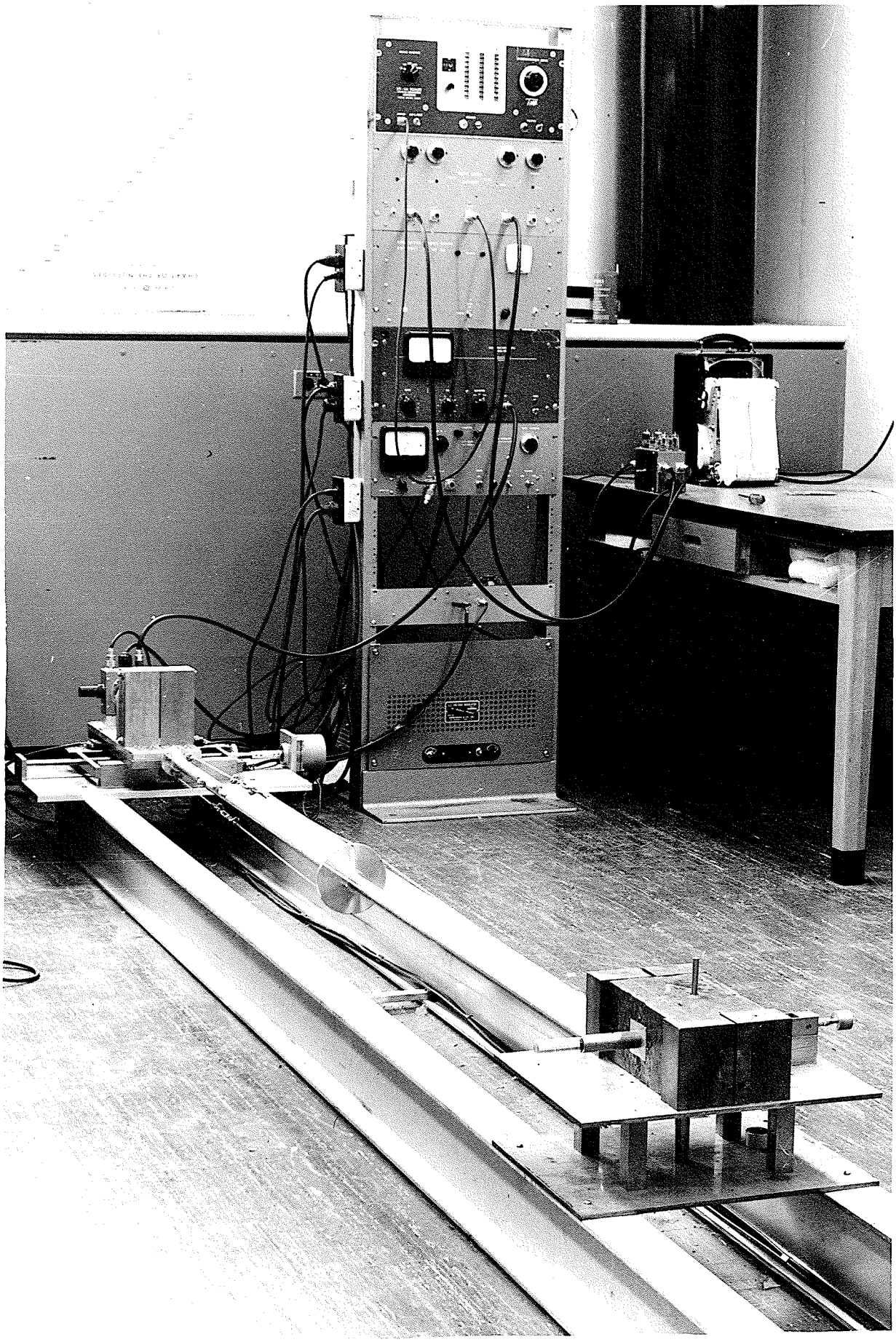

PLATE 3

THE MOVABLE DETECTOR

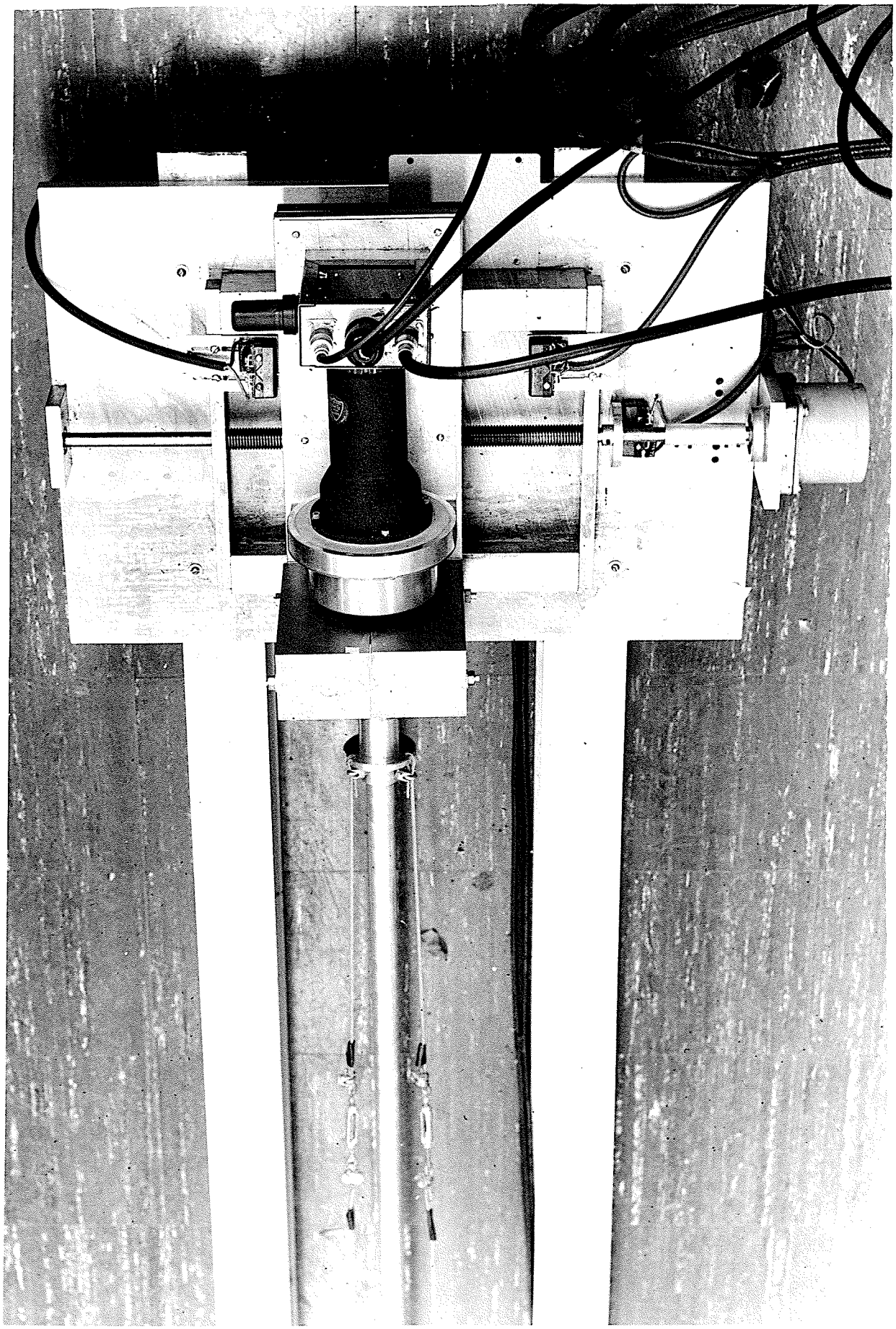

FIGURE 3.1

CONSRUCTION DETAILS OF THE

ANGULAR CORRELATION APPARATUS

A. Movable detector
B. Fixed detector
C. Positron source
D. Sample tank
E. Reversing switches
F. Cam operated switch
G. Motor

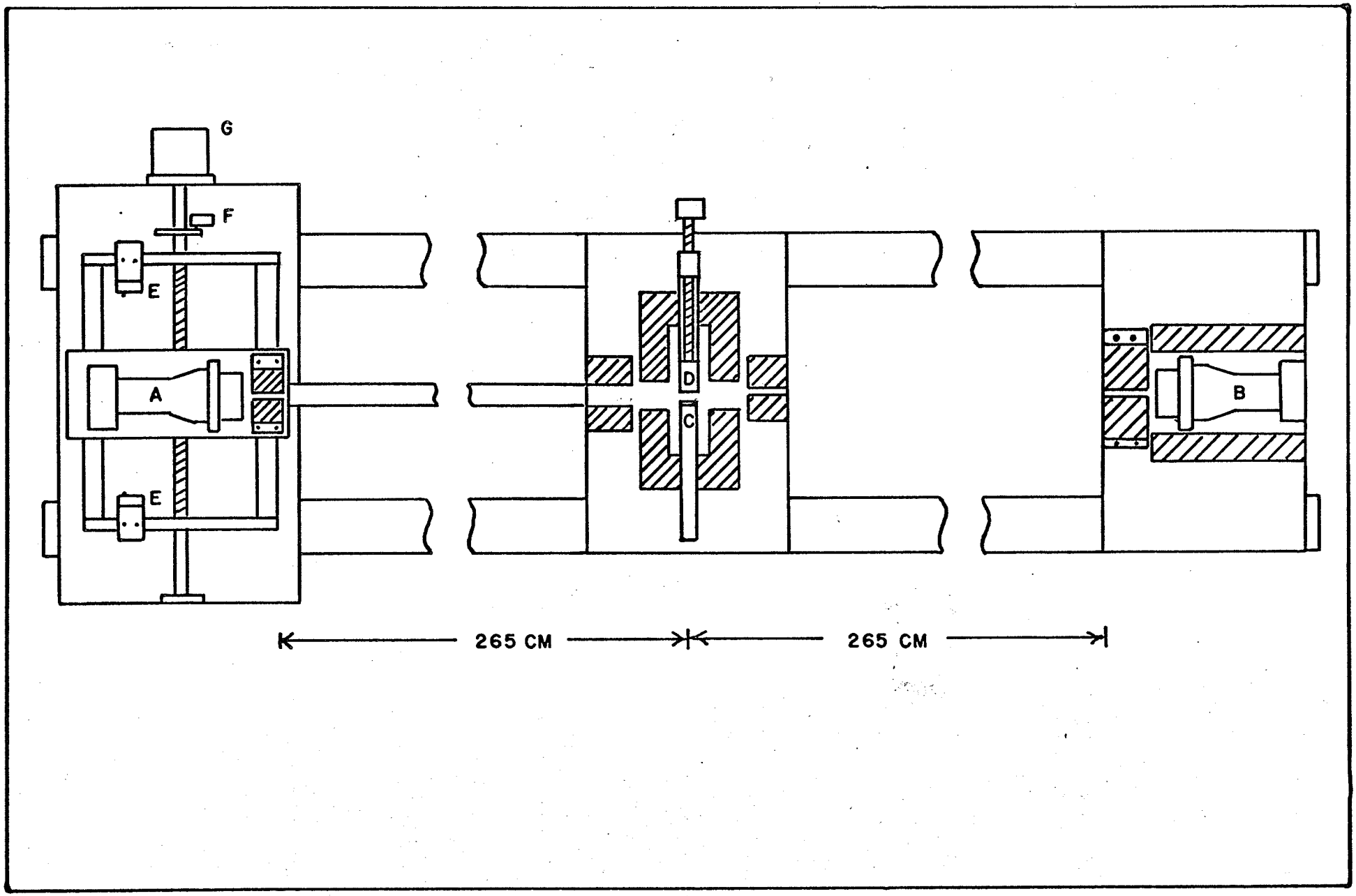
G
F
E
A
E
D
C
B
265 CM
265 CM

The positron source and sample under investigation were housed in a lead castle with collimating slits facing each detector. On the side of the fixed detector, the slit width was 0.1" and on the side of the movable detector it was 0.2". Each of these slit systems was fixed and therefore it was necessary to have the one on the side of the movable detector wide enough to permit the detector to see the sample from a variety of positions. The purpose of these crude collimating slits was only to reduce the amount of scattered radiation reaching the detectors, and to shield the detectors from the positron source itself.

The final collimating slits at each detector were constructed from $2\frac{1}{2}$" thick blocks of babbitt. This thickness was sufficient to stop more than 99% of the .511 Mev gamma rays and about 95% of the 1.28 Mev gamma rays. Each block of babbitt for a particular set of slits was mounted on a 3/16" metal plate about twice the width of the block itself. Slots were machined in the section of the plate which protruded from underneath the babbitt block for mounting screws to facilitate alignment and to allow the slit width to be changed when desired. The slots were wide enough to permit a small amount of rotation about a vertical axis for alignment purposes. When a particular slit width was chosen, metal shims of the appropriate thickness were inserted between the blocks at the top and bottom and the assembly was secured by bolts passing

through the two blocks and the shims.

To keep the collimating slits of the movable detector aligned on the sample as the detector moved to different positions, a 1" diameter aluminum tube was extended from the front of the rotatable steel plate to a pivot point directly beneath the sample. The aluminum tube was reinforced by means of a set of three steel cables attached to either end of the tube and offset from its axis at the centre as shown in Plate 2. The desired degree of rigidity was obtained by adjusting line tighteners in the three cables. To allow for the slight increase in the distance from the detector to the pivot point as the detector was moved off the 180 degree line, the end of the aluminum tube was permitted to slide freely in a hole in the pivot shaft.

For alignment purposes a pin was extended from the centre of the pivot shaft into the source and sample housing. The collimating slits for the fixed detector were then put in place and a sight was taken through these slits and through the pivot point with a horizontal cathetometer to locate the slits for the movable detector when it was in its position on the 180 degree line. The position of the platform was then marked on the rails with a fine scratch. Using the same sight, the crude collimating slits on the other side of the source castle were put in place. The slits on the detectors were adjusted so that a horizontal line parallel to the slit surface actually passed

through the sample simply by looking through the slits at the sample and rotating the slit system about a vertical axis to what appeared to be the proper position. As will be seen in section 3.5, this setting is not critical. If the slits are not pointing directly at the sample, the angular resolution will be improved slightly but the coincidence counting rate will decrease. Finally, a check was made with a level to ensure that all the slits were vertical.

To position each new sample properly it was found most convenient to place the movable detector on the 180 degree line (defined by the fine scratch mark) and to stretch a fine wire between the slits of the two detectors. The position of the new sample was adjusted so that its face was just in contact with the wire. The use of the horizontal cathetometer was awkward since this entailed the removal of the detectors each time to allow a sight to be taken.

The alignment of the apparatus was checked periodically (about every month) but little, if any readjustment was ever necessary. Even if the slits were shifted slightly out of line, the only effect would be a change in the peak position of the angular correlation curves. Such a change would not affect the final experimental results.

It was also necessary to periodically ensure that the slits in front of the movable detector were in line with the sample face i.e. to ensure that the top steel plate described

previously was turning freely on the ball races and the central shaft. If any binding were to occur, the effective slit width would be reduced resulting in an artificial decrease in the coincidence counting rate. This check was made using a travelling microscope to observe the distance that the corner of the upper plate moved relative to the lower plate on which it rotated as the system moved from one position to the next. The angle through which the upper plate had rotated was then calculated and compared with the angle through which it should have rotated. As expected, it was found that there was always a slight lag which remained essentially constant except at the point where the direction of motion was reversed. This lag was such as to reduce the counting rate by about 2% everywhere except at the reversal points. Here the counting rate was so low that the correction did not have to be applied.

A check was also made on the constancy of the pitch of the worm screw by measuring the distance the whole slit system moved with each rotation of the screw. The slit system moved 2.54 mm. with each rotation with a maximum variation of .03 mm. A deviation of this magnitude would not affect the experimental results noticeably.

However, the backlash in the screw resulted in a displacement of the slits by 0.2 mm. at a given station on a reverse run. A correction for this was made by simply reducing the slit width on the movable detector by 0.2 mm. so that the

effective slit width on the average of two opposite runs resulted in the desired value.

3.2 Electronics.

A block diagram of the electronics is shown in Figure 3.2. The detector heads including the cathode followers are of a standard design and have been described elsewhere.[51] A positive high voltage (1100 volts) was provided for each of the photomultipliers by a Hamner Model N401 high voltage supply. Suitable decoupling was employed in each of the detector heads to eliminate cross talk between them.

Negative pulses from the cathode followers in the detector heads were fed to amplifiers through 1059 Amphenol coaxial cable. The demands on the amplifiers as far as linearity and non-overload features are concerned were not too great and therefore two simple amplifiers were designed and built, the circuit diagram for which is shown in Figure 3.3. The input is a cascode arrangement employing the two triodes in a 6DJ8. This is followed by two stages of amplification with negative feedback to improve the linearity and stability. The output is a cathode follower. The pulses from the detector heads which are negative and of the order of one volt in amplitude, are amplified about twenty times and shortened to approximately 1 microsecond.

The power for the amplifiers and the cathode followers in the detector heads was provided by a highly regulated 250

FIGURE 3.2

BLOCK DIAGRAM OF THE ANGULAR CORRELATION APPARATUS

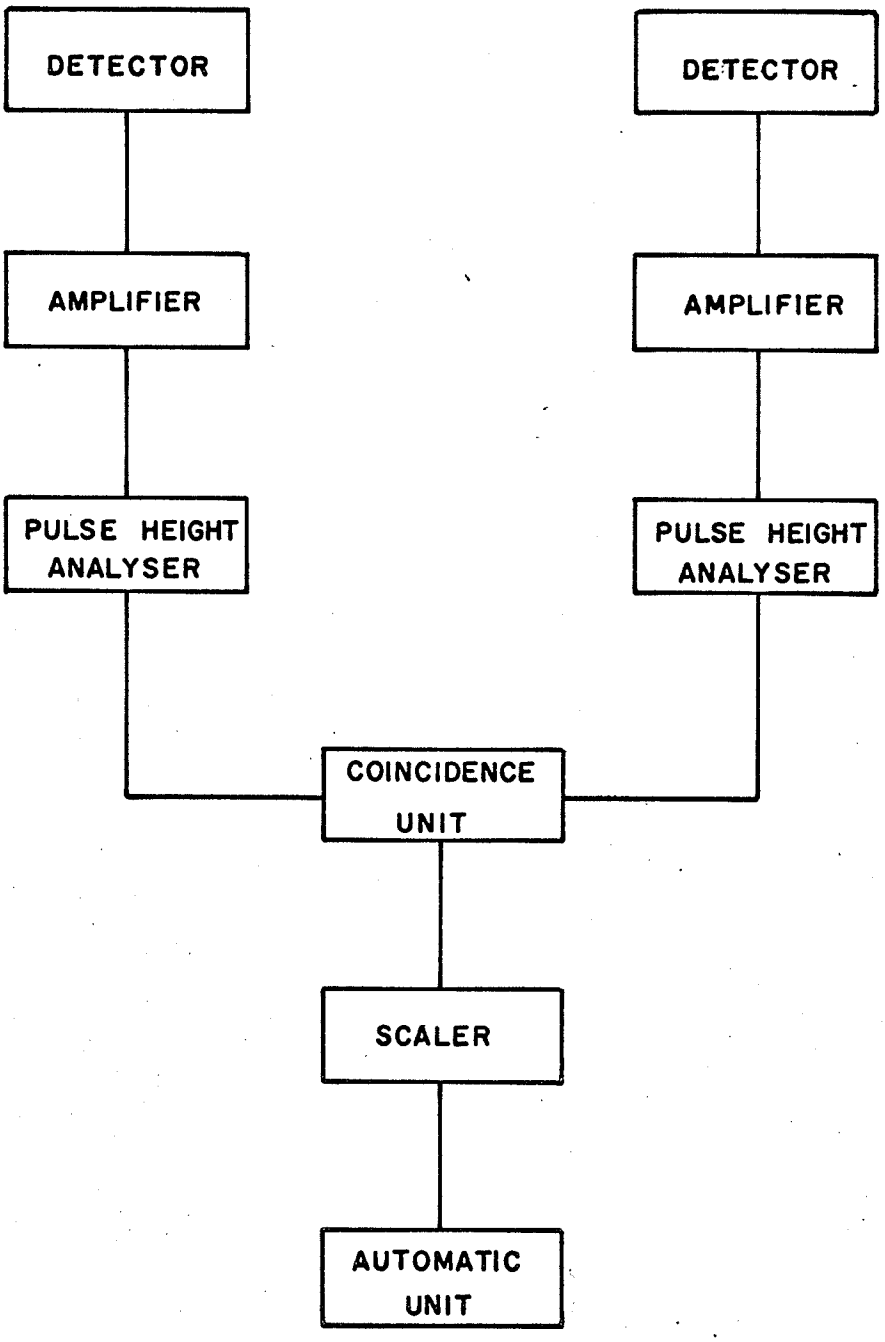
DETECTOR
DETECTOR
AMPLIFIER
AMPLIFIER
PULSE HEIGHT ANALYSER
PULSE HEIGHT ANALYSER
COINCIDENCE UNIT
SCALER
AUTOMATIC UNIT

FIGURE 3.3

AMPLIFIER CIRCUIT DIAGRAM

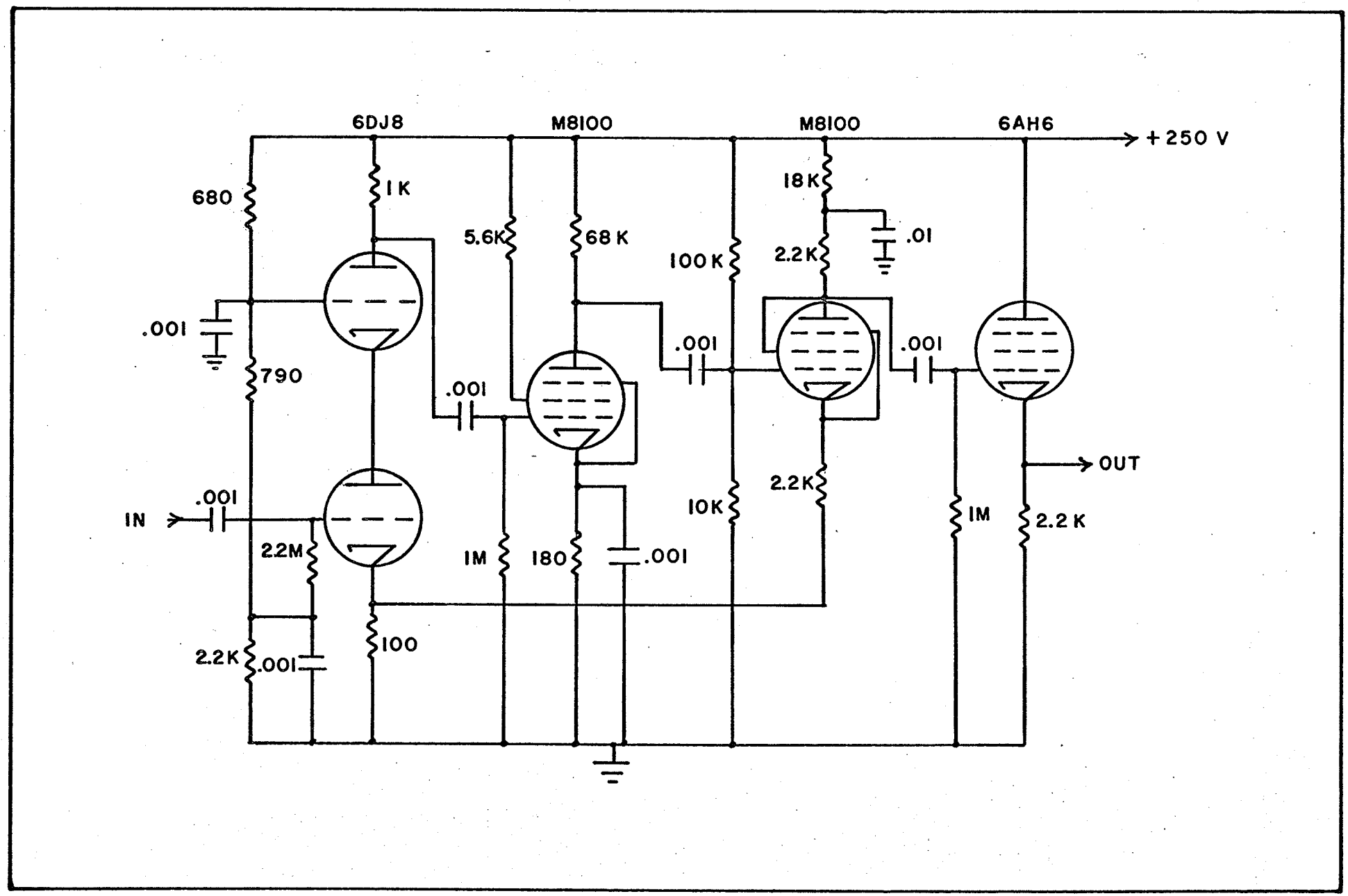
6DJ8
M8100
M8100
6AH6
+250 V
680
1K
5.6K
68K
18K
.01
100K
2.2K
.001
.001
790
.001
.001
.001
OUT
2.2K
IN
.001
10K
IM
2.2K
2.2M
IM
180
.001
2.2K
.001
100

volt supply based on a National Bureau of Standards design.

Pulses from the amplifiers were fed to single channel pulse height analysers set to select gamma rays in the energy range between 0.1 and 0.5 Mev. The resulting fast rising narrow pulses (0.2 microseconds) were sent to a coincidence unit which had a resolving time of less than 0.5 microseconds. The pulse height analysers and coincidence unit have been described previously.[51] A Technical Measurement Corporation Model SG-3A scaler was used to record the number of coincidences.

The detectors were Integral Assembly Model 16MB4/A-X obtained from the Harshaw Chemical Company. These consisted of 4" diameter, 1" thick NaI(Tl) crystals mounted on 5018 HB photomultipliers with mu-metal shields. The measured pulse height resolution of the combination was 11% at 661 Kev.

All the electronic instruments were powered by a Model 2000 S Sorensen A. C. voltage regulator. Stability in the complete system was excellent. A check for electronic drifts was made every few days but adjustment was seldom necessary.

3.3 Automation of the Apparatus.

The process of accumulating data was made automatic by the mechanism shown in Figure 3.4. In this diagram, the position of each of the switches is that for counting. The operation of the system is as follows. When 1000 counts have

FIGURE 3.4

AUTOMATION UNIT

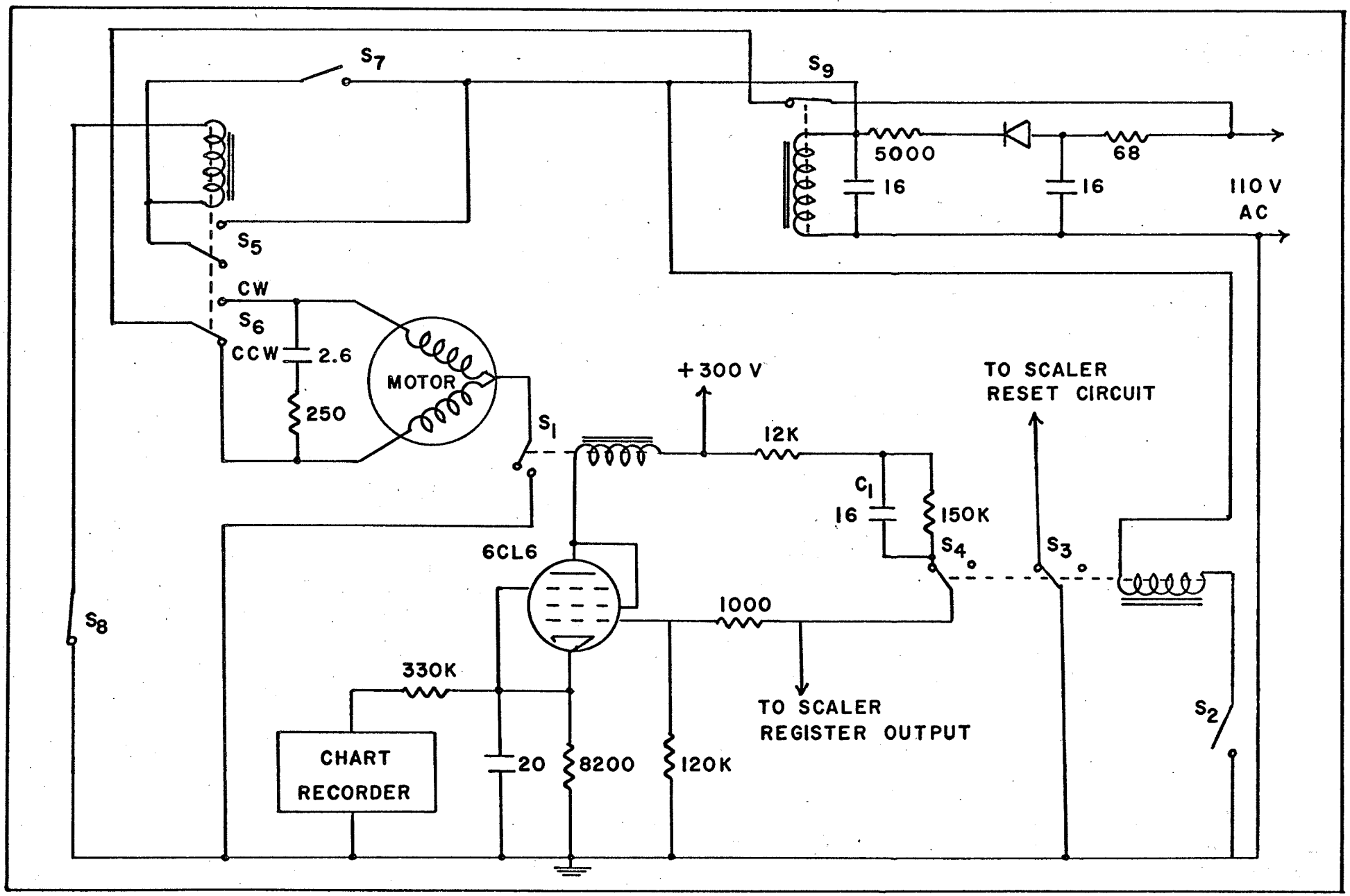
S7
S9
5000
68
16
16
110 V
AC
S5
CW
S6
CCW
2.6
250
MOTOR
+300 V
TO SCALER
RESET CIRCUIT
S1
12K
C1
16
150K
S4
S3
6CL6
S8
1000
330K
TO SCALER
REGISTER OUTPUT
S2
CHART
RECORDER
20
8200
120K

been accumulated on the scaler, its last decade strip produces a pulse to activate the mechanical register. This pulse is passed to a power amplifier employing a 6CL6 tube. The resulting pulse activates the stepping relay S_1 thereby supplying power to the Slo-Syn driving motor which moves the detector to its next position. The cam operated switch S_2 is closed activating the relay comprising switches S_3 and S_4. S_3 operates the reset mechanism in the scaler so that no counts can be registered while the detector is moving. S_4 is opened allowing condenser C_1 to discharge through the 150 K resistor. After one complete revolution of the drive shaft, S_2 is opened returning S_3 to its original position thus allowing the scaler to begin accumulating again. At the same time, S_4 is closed applying a pulse to the power amplifier which again operates the stepping switch turning off the motor. This pulse is maintained for a sufficient length of time by the charging action of condenser C_1. Each time a pulse is produced by the power amplifier, a small voltage is applied across an Esterline-Angus chart recorder which then gives the time for the accumulation of 1000 counts.

As the detector moves to the predetermined end of its run in either direction, one of the switches S_7 or S_8 is operated. This reverses the direction of rotation of the driving motor in the following way. Consider the switches S_5, S_6, S_7, and S_8 in the positions shown. The motor is then running

counterclockwise moving the detector toward S_7. When S_7 is closed momentarily, it activates a relay closing S_5 and S_6. The closing of S_6 causes the motor to reverse and the closing of S_5 provides an alternate circuit through the relay coil to hold the relay in its present position. The alternate circuit is necessary since S_7 opens again as the detector moves away. When the detector reaches the other end of its run, S_8 is opened momentarily. This opens the circuit through the relay coil causing S_5 and S_6 to return to their original positions, thus reversing the direction of rotation of the motor again.

S_9 is incorporated to protect the apparatus against damage in the event that the power supply for the reversing relay should fail. In this case S_9 would open (since it is powered by the same supply) thereby shutting off the motor.

3.4 The Positron Source and Samples.

A positron source of 7 millicuries of Na^{22} in the form of an aqueous solution of NaCl was obtained from the Radiochemical Centre, Amersham, England. A number of requirements had to be met in the preparation of the source. It was necessary to enclose it in such a manner that it could be handled and moved safely, but at the same time the source covering had to be thin enough to obtain a reasonable yield of positrons. It was desirable to restrict the source to as small an area as possible from the standpoint of good geometry,

but to again obtain a high positron yield, self absorption in the source had to be minimized by spreading the source material in a thin layer. For this reason a source of high specific activity (1.97 mc/mg) was used.

Since the source was to be eventually mounted with its face vertical, the surface onto which the activity was to be deposited was first prepared by machining shallow, concentric circular grooves on it. This was done to prevent the salt crystals from flaking off and accumulating in one area.

Initially, the source was evaporated a few drops at a time onto a 3/16" diameter stainless steel button. This was rather a tedious process since the NaCl had been dissolved originally in 4.5 ml. of water. After the evaporation process was complete, it was estimated that approximately 6 mc. of the source had been deposited on the stainless steel button. The remainder was left on the walls of the original container, in syringes and in hypodermic needles. It was necessary to leave the source open under a low heat for about two weeks, and in spite of the precautions taken some of the source was lost in the evaporation process.

The stainless steel button was fixed to the end of a 10" long, $\frac{1}{2}$" diameter aluminum rod, and a 0.00004" nickel foil obtained from the Chromium Corporation of America was cemented over the source with an epoxy resin glue. After approximately one month some leakage developed due to the corrosive action

of the salt on the nickel. The source was opened and it was found that even the stainless steel had been attacked. The source was redissolved in a small amount of water and then deposited on the end of a 3/4" diameter plastic rod which had been prepared in the same manner as the stainless steel surface. Approximately 1 mc of activity was lost in this process. In this case the source was spread over a circular area of 3/8" diameter since, with the smaller source, there had appeared to be a considerable thickness of salt crystals. A thin piece of mica (3 mg/cm^2) was then attached over the end of the plastic rod with epoxy resin cement. This source has remained intact for more than two years.

The plastic rod was inserted into a brass tube in the side of the source castle as indicated in Figure 3.1 and was held in place by a locking screw. To achieve the maximum counting rate, the source was placed as near to the sample as possible (~0.5 cm) without the source becoming directly visible to both detectors through the crude collimating slits.

Most of the samples investigated were highly volatile organic liquids. These were contained originally in a small brass tank with a 3/4" vertical face made of 0.00004" nickel foil. The walls of the tank that were to be perpendicular to the source were tapered to a .002" thickness to reduce the number of annihilations in the tank itself. The container was fitted with a chimney through which it was filled and

which acted as a reservoir against evaporation. The nickel foil was attached with an epoxy resin cement but the seal broke periodically, particularly under the action of benzene compounds. Repairs could be made only once or twice and then the foil had to be replaced.

The brass tank was used for about one half the experiment but then it was decided to change to a glass container to ensure that no metallic impurities were being intoduced into the sample. Since positrons annihilating in metals give rise to quite broad distributions, a small impurity could affect the results considerably. Also, impurities were almost certainly being introduced from the epoxy resin cement which is slightly soluble in organic liquids.

The glass tank consisted of a $1\frac{1}{2}$" long, $\frac{1}{2}$" diameter glass tube sealed at one end and flared at the other to a diameter of 3/4" to give a wall thickness at the end of .002". A thin piece of mica (1.5 mg/cm^2) was attached to this end with Eastman's 910 Adhesive and then the edges were further sealed with an epoxy resin cement. With this method, the Eastman's adhesive was the only cement in contact with the organic liquids, in which it is almost completely insoluble. The epoxy resin cement which is attacked by benzene compounds served only to prevent the edge of the mica from being accidentally lifted off the glass during handling. This seal would normally last a number of months before any leak developed.

Both sample tanks were mounted similarly on the end of a 12" threaded rod to facilitate accurate placement on the 180 degree line. The tanks were guided into the source castle through a metal tube.

3.5 Angular Resolution of the Apparatus.

The following discussion parallels one by de Zafra[41] except that the effect of a non-uniform source has been taken into account.

For the purpose of discussing the angular resolution we define a coordinate system with its origin at the centre of the apparatus, the z axis vertical, the y axis along the horizontal line joining the sample and the fixed detector and the x axis parallel to the direction of motion of the movable detector. First we shall consider the resolution function in the x direction assuming that the detectors extend to infinity in the z direction. This resolution function is the angular distribution that would be observed viewing a source which emitted gamma rays correlated only at exactly 180 degrees. Since we are attempting to measure the x component of the total momentum of the annihilating positron electron pair, it is clearly desirable to have this resolution function as narrow as possible.

Consider two sets of slits of width s at a distance r on either side of an infinitely thin source. (In this

discussion, "source" refers to the origin of the gamma rays being observed i.e. the portion of the sample in which the positrons annihilate.) If one of the slit systems is moved in the x direction, the coincidence counting rate for photons correlated at 180 degrees will increase linearly from zero at $x = x_o - s$ to a maximum at x_o and then decrease again to zero at $x = x_o + s$. x_o is the position of the movable slit system when it is on the line defined by the infinitely thin source and the fixed slit system. Thus, we have a triangular resolution function for an infinitely thin source.

In practice, the source has a finite thickness due to the various penetration depths of the positrons. It is due to this fact that the distance from the source to the detector must be as large as it is in this type of apparatus. (In this particular case the distance is 2.65 meters.) If the source were infinitely thin it would be possible to achieve the desired angular resolution with the detectors much closer by simply making the slit width smaller. However, since the source has a finite thickness, the most convenient method of minimizing its angular width is to make the source to detector distance large.

To calculate the resolution function it is necessary to know the source thickness and the intensity of the source as a function of depth. A short digression will be made here to consider this problem.

Since the annihilation cross section for positrons becomes significant only at quite low energies, we shall apply the results of electron penetration studies to examine the behaviour of the positrons during most of the slowing down process. On the basis of available data, Katz and Penfold[52] have proposed the empirical relationship

$$R_o = 412E^n$$
$$n = 1.265 - 0.0954 \ln E \qquad (3.1)$$

where R_o is the extrapolated or practical range[53] in mg/cm^2 of monoenergetic electrons, and E is the electron energy in Mev. This formula applies in the energy interval .01 Mev to 3 Mev. It was seen that the maximum range for electrons with a continuous energy spectrum was indistinguishable from the practical range of monoenergetic electrons with the same energy as the maximum energy of the continuous spectrum. Thus, the above formula may be applied to determine the maximum penetration depth of positrons from Na^{22}.

The transmission curve for a continuous electron spectrum is very nearly exponential[53] except where the transmission is less than 1%. Thus, the number of positrons N reaching a depth x is approximately

$$N = e^{-4.5\, x/d} \qquad (3.2)$$

where d is the maximum penetration depth in cm and the coefficient -4.5 has been chosen so that N = .01 when x = d.

The positron spectrum for Na^{22} has a maximum energy

of 0.54 Mev. Substitution of this value for E into equation 3.1 yields R_o = 180 mg/cm^2. We estimate that the positrons pass through an average of 22 mg/cm^2 of NaCl (corresponding to a thickness of .01 cm) and 3 mg/cm^2 of mica before entering the sample. Thus, the maximum penetration into the sample itself will be 155 mg/cm^2. In the case of hexane, the least dense material studied, this corresponds to a depth of .24 cm. We need not consider the diffusion of thermal positrons further into the sample since their lifetime against annihilation is too short to allow them to travel an appreciable distance.

Now, a single isosceles triangle of unit height centred at x_o is given by

$$f(x,x_o) = 1 - \frac{|x - x_o|}{s} \quad \text{for } |x - x_o| < s$$
$$= 0 \quad \text{for } |x - x_o| > s$$

Each infinitesimal slice of the source will give rise to such a triangular resolution function weighted by the appropriate exponential term to account for the decrease in source intensity with increasing depth. Consider a source of thickness d centred over the pivot point of the movable detector. Then the triangular resolution functions must be weighted by the factor $e^{-4.5(x_o + d)/2d}$ as x_o varies from -d to d. Therefore, the total resolution function is

$$F(x) = \int_{-d}^{d} f(x,x_o) e^{k(x_o + d)} dx_o$$

where k = -4.5/2d. For d $\geqslant$ s (which is true in this case) the

integration must be performed in six steps in the following way.

$$F_1(x) = \int_{-d}^{s+x} \left(1 - \frac{x_o - x}{s}\right) e^{k(x_o + d)} dx_o \quad \text{for } -(d + s) \leq x \leq -d$$

$$= (e^{k(s + d + x)} - kd - ks - kx - 1)/k^2 s.$$

$$F_2(x) = \int_{x}^{s-x} \left(1 - \frac{x_o - x}{s}\right) e^{k(x_o + d)} dx_o \quad \text{for } -d \leq x \leq (d - s)$$

$$= e^{k(x + d)}(e^{-ks} + ks - 1)/k^2 s.$$

$$F_3(x) = \int_{x}^{d} \left(1 - \frac{x_o - x}{s}\right) e^{k(x_o + d)} dx_o \quad \text{for } (d - s) \leq x \leq d$$

$$= \left[e^{2kd}(ks - kd + kx + 1) - e^{k(x + d)}(ks + 1)\right]/k^2 s.$$

$$F_4(x) = \int_{-d}^{x} \left(1 - \frac{x - x_o}{s}\right) e^{k(x_o + d)} dx_o \quad \text{for } -d \leq x \leq (s - d)$$

$$= \left[e^{k(s + d)}(ks - 1) + kx + kd - ks + 1\right]/k^2 s.$$

$$F_5(x) = \int_{x-s}^{x} \left(1 - \frac{x - x_o}{s}\right) e^{k(x_o + d)} dx_o \quad \text{for } (s - d) \leq x \leq d$$

$$= e^{k(x + d)}(e^{-ks} + ks - 1)/k^2 s.$$

$$F_6(x) = \int_{x-s}^{d} \left(1 - \frac{x - x_o}{s}\right) e^{k(x_o + d)} dx_o \quad \text{for } d \leq x \leq (d + s)$$

$$= \left[e^{2kd}(ks - kx + kd - 1) + e^{k(x + d - s)}\right]/k^2 s.$$

Combining the appropriate terms were the ranges of x overlap we have finally

$$F_A(x) = (e^{k(s + d + x)} - kd - ks - kx - 1)/k^2s$$

$$\text{for } -(d + s) \leq x \leq -d$$

$$F_B(x) = \left[e^{k(x + d)}(e^{ks} - 2) + kx - ks + kd + 1\right]/k^2s$$

$$\text{for } -d \leq x \leq (s - d)$$

$$F_C(x) = e^{k(x + d)}(e^{ks} + e^{-ks} - 2)/k^2s$$

$$\text{for } (s - d) \leq x \leq (d - s)$$

$$F_D(x) = \left[e^{2kd}(ks - kd + kx + 1) + e^{k(x + d - s)} - 2e^{k(x + d)}\right]/k^2s$$

$$\text{for } (d - s) \leq x \leq d$$

$$F_E(x) = \left[e^{2kd}(ks + kd - kx - 1) + e^{k(d + x - s)}\right]/k^2s$$

$$\text{for } d \leq x \leq (d + s)$$

The slit width used throughout the experiment was .16 cm or in terms of the angle subtended at the source, .60 milliradians. Substituting this value for s and the value for d in hexane (.24 cm) into the above equations yields the resolution function shown in Figure 3.5. The full width at half maximum is .82 milliradians.

To correct the angular distribution curves for the finite resolution in the x direction, we use the method of Eckhart[54]. The counting rate $I_c(\theta_n)$ that would be observed

FIGURE 3.5

THE ANGULAR RESOLUTION FUNCTION

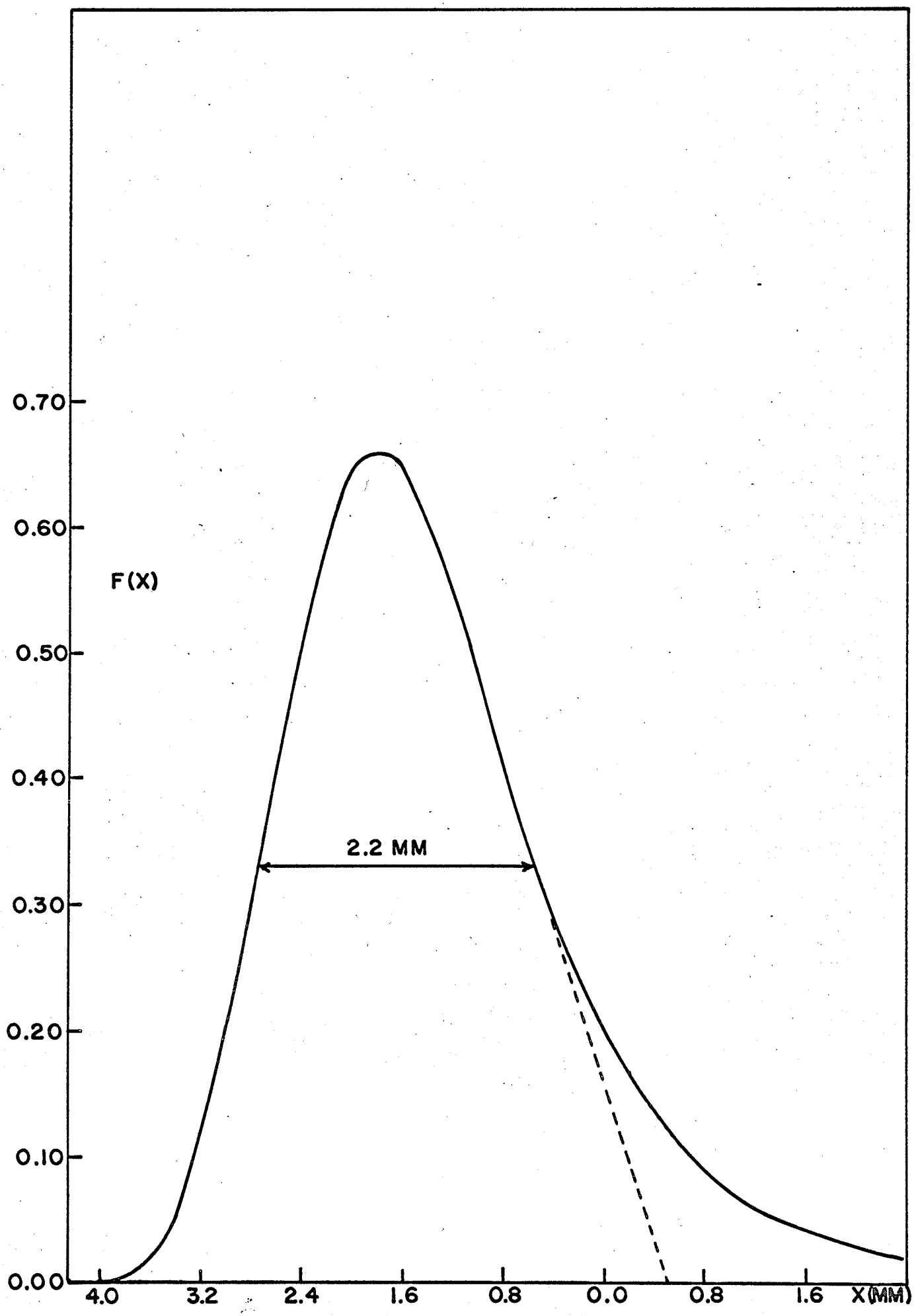
0.70
0.60
F(X)
0.50
0.40
2.2 MM
0.30
0.20
0.10
0.00
4.0
3.2
2.4
1.6
0.8
0.0
0.8
1.6
X(MM)

if the resolution function had zero width is given by

$$I_c(\theta_n) = I(\theta_n) - \left[I(\theta_{n+1}) - 2I(\theta_n) + I(\theta_{n-1})\right] a^2/b^2$$

where $I(\theta_n)$ is the experimental counting rate at θ_n ,

$$b = \theta_{n+1} - \theta_n$$

and $a^2 = \frac{1}{2}\int_{\theta_L}^{\theta_R} \theta^2 F(\theta)d\theta$ where $\int_{\theta_L}^{\theta_R} F(\theta)d\theta$ has been normalized to unity. $F(\theta)$ is the resolution function in terms of θ rather than x, where $\theta = x/r$. θ_R and θ_L are the points on the right and left sides of the resolution curve where $F(\theta) = 0$.

$F(\theta)$ should be a symmetric function for Eckhart's method to be applicable. To approach this condition we have neglected the tail on the right side of the resolution function as indicated by the dotted line in Figure 3.5. The resulting curve is still not perfectly symmetric but the error intoduced by this and by neglecting the tail on the curve is not significant.

The value of a^2 is obtained by numerical integration, and the value of b was .907 milliradians throughout the experiment. For the resolution function shown i.e. the resolution function for hexane, $a^2/b^2 = .051$. The resulting correction to the angular distribution for hexane is shown in Figure 3.6. The correction is only applied in this case and in the case of decane since both give rise to quite narrow distributions. In all other cases the distributions are broader and the compounds are more dense resulting in a small positron penetration depth

FIGURE 3.6

ANGULAR DISTRIBUTION FOR HEXANE

CORRECTED FOR FINITE ANGULAR RESOLUTION

1. Full width at half maximum of angular resolution function = 0.82 milliradians.

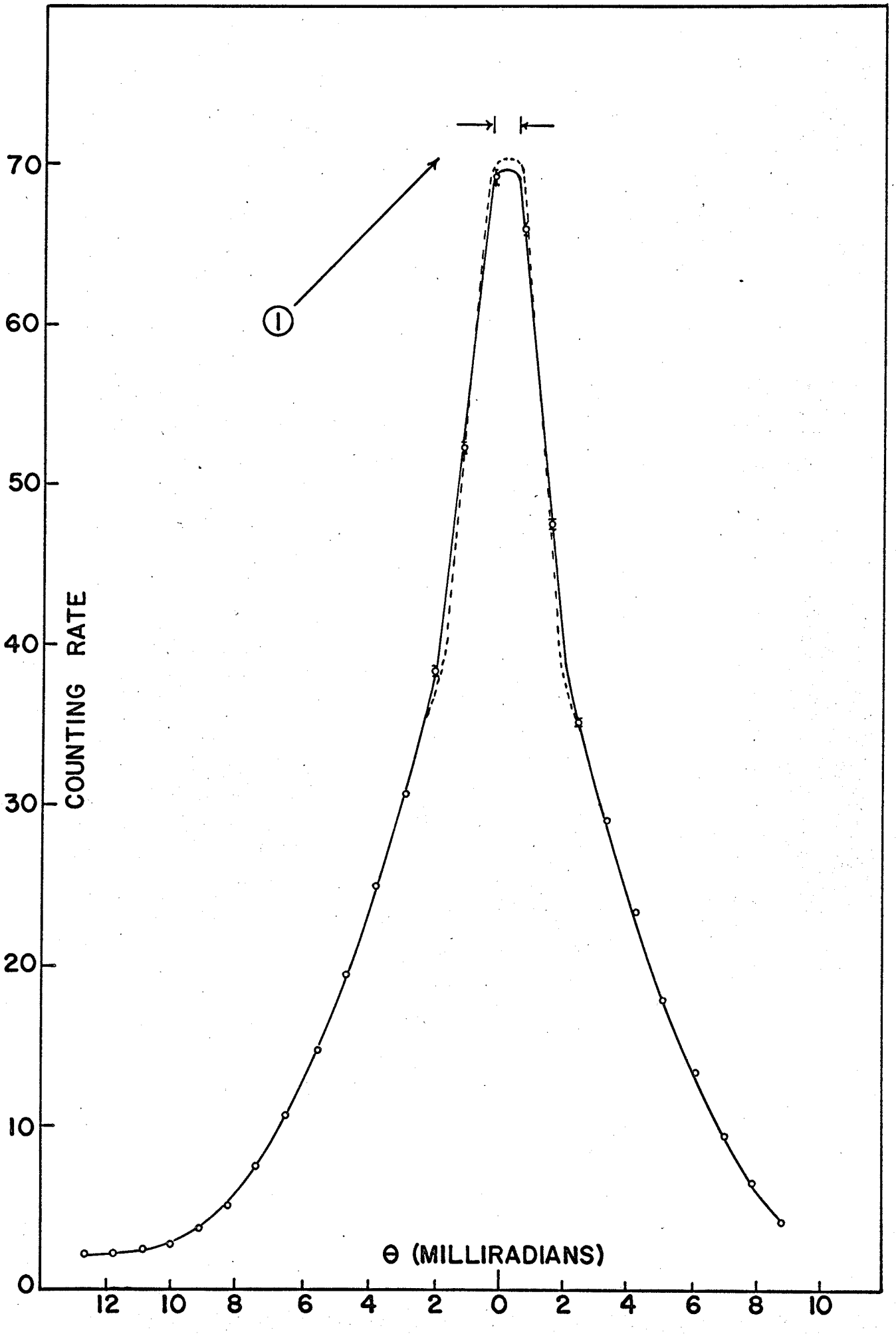
70
60
50
40
30
20
10
0
COUNTING RATE
(1)
12
10
8
6
4
2
0
2
4
6
8
10
θ (MILLIRADIANS)

and a narrower resolution function. Therefore, the correction becomes unimportant.

It was assumed at the beginning of this section that the detectors extended to infinity in the z direction. The fact that the detectors have only a finite extension in this direction causes a slight distortion in the angular distributions, the distortion being the greatest for the broadest distributions. Lang[55] has calculated that the height of the distribution for gold is in error by less than 1% when measured with an apparatus of dimensions similar to those reported here. All the distributions obtained here are narrower than that for gold and therefore no correction has been applied.

3.6 Data Accumulation and Analysis.

A single complete run consisted of accumulating 1000 counts at each of 25 points on an angular distribution curve ranging from 13 milliradians on the left side of the centre to 9 milliradians on the right side. The positions of the reversing switches could be adjusted for runs covering a smaller range. The interval between the points was .907 milliradians.

The method of analysis to be described involves obtaining the slopes of the angular distribution curves and therefore, very good statistics are required, particularly close to the peaks of the curves. In the regions from 0 to 6 milliradians and from 7 to 9 milliradians on both sides of the distributions approximately 40,000 and 10,000 counts respectively were accumulated at each point. In the interval from

9 to 13 milliradians the counting rate was very small (~5 counts per minute) and therefore only one side of the curve was investigated in this region. In the central part of the distribution the counting rate was still only 50 to 70 counts per minute and therefore a month or more was usually required to complete the investigation of one sample.

Each run was examined for any obvious irregularities which might be caused by electronic drifts. If any irregularities were apparent, the whole run was discarded. After a complete set of data had been obtained, an average was taken of the time required for the accumulation of 1000 counts at each point.

In view of the type of analysis to be done on the angular distributions, it was important to determine the background distribution as accurately as possible. Due to the nature of the sources of background counts, this distribution would be expected to be quite broad. Since we shall later be comparing the relative intensities of the broad and narrow portions of the angular distributions, a significant error could be introduced by the background.

There were three main sources of background counts in the angular distributions. The first was due to chance coincidences which contributed a flat background of approximately 3 counts per minute. This was determined by moving detector A 20 milliradians off the 180 degree line so that coincidences from annihilations in the sample or metal parts near the source

would not be registered.

The second source was the radiation resulting from annihilations in any part of the source castle or sample tank holder visible to both detectors through the crude collimating slits. This background was determined by measuring the distribution with no sample tank inserted. This resulted in a broad distribution with a peak counting rate of ~2 counts per minute.

The third source was due to annihilations in the mica covering the face of the sample tank and in the walls of the sample tank itself. This background could not be determined by simply performing a run with an empty sample tank since some positrons that would normally be stopped by, and annihilate in the sample would be able to reach the walls of the tank and annihilate there. This would then indicate a higher background counting rate than would actually be present if the sample tank were full. An attempt was made to simulate the actual experimental conditions by cementing a piece of mica of the same thickness originally used to a plastic ring with the same dimensions as the sample tank (i.e. the same diameter and wall thickness) except that its depth was only .1 cm. Using this arrangement in place of the sample tank, the resulting background distribution was fairly broad with a peak counting rate of 3 counts per minute. Its area was approximately 6% of the area of an average complete angular distribution curve. As a

further check, substitution of the value of the mica thickness for x in equation 3.2 yields the result that 4% of the positrons incident on the sample tank should annihilate in the mica. From the dimensions of the tank it was found that 1% of the incident positrons should annihilate in its walls. The total calculated background is then 6%, in good agreement with the experimental value.

Every angular distribution was corrected for these three contributions to the background. The resulting distributions were then plotted as counting rate vs angle on semi-transparent graph paper. This was placed over a light box and folded to bring the points on either side of the distribution into as close ageement as possible thus determining the centre of the distribution. A curve was then drawn to fit both sides of the distribution simultaneously.

Since the samples had an appreciable thickness along the direction of gamma ray observation, the gamma rays were subject to various types of scattering, particularly Compton and Rayleigh scattering. However, the angular distribution of Compton scattered photons with an initial energy of .5 Mev is not sufficiently peaked in the forward direction to have a significant effect here other than to add a small uniform background[56]. It has been shown by Moon[57] that Rayleigh scattering may be up to one hundred times as great as Compton scattering at small angles but the correction becomes significant only for

high atomic number and therefore it has not been applied.

A method has been described by Stewart[35] whereby the momentum distribution of the annihilating positron-electron pairs may be derived from the angular correlation data obtained with an apparatus having parallel slit geometry. The following is based on Stewart's derivation.

If p_x is the x component of the total momentum $\underline{p}$ of the centre of mass of the positron-electron pair at the time of annihilation, then in the laboratory system the annihilation quanta are emitted at a relative angle which deviates from 180 degrees in the x-y plane by the amount $\theta = p_x/mc$. (The coordinate system described in section 3.5 is being used here.)

Let $\rho(\underline{p})$ be the density of momenta of the annihilating pairs i.e. the number of vector end points per unit area on the surface of a sphere of radius p in momentum space. Here we make the reasonable assumption that for liquids $\rho(\underline{p})$ is isotropic i.e. $\rho(\underline{p}) = \rho(p)$. If $N(p)$ is the number of pairs with momentum p then $N(p) = 4\pi p^2 \rho(p)$.

Now, for a given value of θ, the coincidence counting rate $C(\theta)$ is proportional to the total number of annihilating pairs whose x component of momentum is $p_x = mc\theta$. The total number of such pairs is obtained by integrating the momentum space density over a plane of constant p_x. Thus,

$$C(\theta) = K\int\int\rho(p)dp_y dp_z$$

where K is a constant. If we now set $p' = (p_y^2 - p_z^2)^{\frac{1}{2}}$ this becomes

$$C(\theta) = 2\pi K \int_0^\infty p' \rho(p) dp'$$

Differentiating with respect to p_x we get

$$\frac{dC(\theta)}{dp_x} = 2\pi K \int_0^\infty p' \frac{d\rho(p)}{dp_x} dp'$$

After rearranging and integrating this becomes

$$\frac{dC(\theta)}{dp_x} = -2\pi K p_x \rho(p)$$

Therefore, $\rho(p) = -\frac{2\pi K}{p_x} \frac{dC(\theta)}{dp_x} = -\frac{2\pi K}{mc\theta} \frac{dC(\theta)}{d\theta} \frac{1}{mc}$

Finally, combining the constants we get

$$\rho(p) = \frac{K'}{\theta} \frac{dC(\theta)}{d\theta}$$

and $$N(p) = K'' \theta \frac{dC(\theta)}{d\theta}$$

In the following chapters the data will be presented in three forms: (1) the angular distribution $C(\theta)$ vs θ

(2) the slope of the angular distribution $\frac{dC(\theta)}{d\theta}$ vs θ

(3) the momentum distribution $N(p)$ vs p.

Chapter 4.

EXPERIMENTAL RESULTS

In this chapter, the results of the time studies of positron annihilations are given and most of the angular correlation data are presented in the form of angular distributions. From these results certain implications are drawn which will be discussed in detail in Chapter 5.

4.1 The Time Spectra of Positron Annihilations.

The results from time spectra studies that are of interest here are listed in Table 4.1. Some of these results have been reported previously[58,59].

Figure 4.1 shows the time spectra of positrons annihilating in hexane and its halogen derivatives. For the sake of clarity, no errors are shown but the actual number of counts is indicated from which the standard deviation may be computed. It is clear that as the size of the halogen atom increases, the intensity I_2 of the long lived component decreases indicating that the halogen atom has a considerable influence on the positron. The same situation is evident in the case of benzene and its halogen derivatives as can be seen from an examination of Table 4.1.

4.2 The Angular Correlation of the Annihilation Radiation.

(i) Hexane and its Halogen Derivatives: The angular distributions

Table 4.1

I_2 and τ_2 for Some Organic Compounds

Compound	I_2(%)	τ_2(nsec)
Hexane	38 ± 2	2.25 ± .05
Fluorohexane	26 "	2.03 ± .05
Chlorohexane	16 "	1.93 ± .05
Bromohexane	10 "	1.9 ± .1
Iodohexane	4 "	1.8 ± .1
Benzene	34 "	2.20 ± .05
Fluorobenzene	26 "	1.90 ± .05
Chlorobenzene	15 "	1.50 ± .05
Bromobenzene	9 "	1.6 ± .1
Iodobenzene	4 "	1.6 ± .1
Decane	35 "	2.30 ± .05
Chlorodecane	17 "	1.94 ± .05
M-xylene	39 "	2.27 ± .05
Chloropropane	16 "	1.97 ± .05
Chlorobutane	17 "	1.98 ± .05
Difluorobenzene	31 "	2.25 ± .05

FIGURE 4.1

TIME SPECTRA FOR HEXANE AND ITS HALOGEN DERIVATIVES

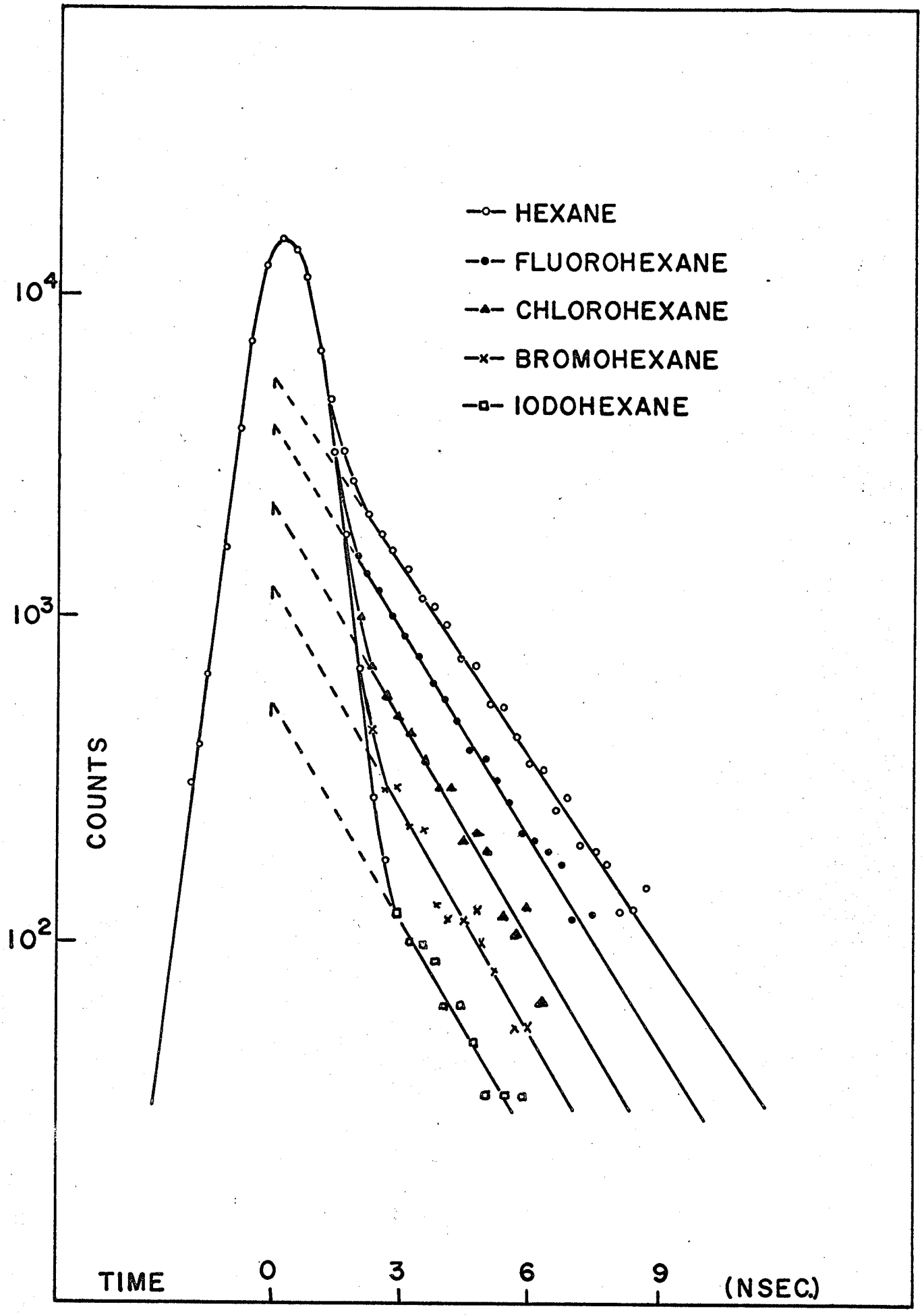
HEXANE
FLUOROHEXANE
CHLOROHEXANE
BROMOHEXANE
IODOHEXANE
10^4
10^3
10^2
COUNTS
TIME
0
3
6
9
(NSEC)

of the annihilation photons from hexane and its halogen derivatives are shown in Figure 4.2. Again for the sake of clarity, no errors are shown here. They may be computed from the actual number of counts accumulated at each point as indicated in section 3.6. All the angular distributions have been normalized to equal areas. Neglecting iodohexane for the moment, the correlation between the intensity of the long lived component and the shape of the angular distribution is apparent. As the amount of positronium formed decreases, the angular distribution becomes less peaked. Thus, there is qualitative agreement with the hypothesis that the angular distributions consist of a broad and a narrow component, the latter being due to the annihilation of singlet positronium. The result for iodohexane which shows an increase in the height of the angular distribution over that found for bromohexane, even though the amount of positronium formed decreases, is not necessarily contradictory. The shape of the broad component could be varying as the halogen atom is changed resulting in a more peaked distribution for iodohexane in spite of a decrease in the narrow component intensity. In Chapter 5 this will be shown to be a correct interpretation.

(ii) Test for Oxygen Contamination of Samples; Electric Field Experiment: It has been noted[60] that the introduction of oxygen into a sample induces a triplet to singlet conversion. This conversion is not due to the exchange of electrons but is

FIGURE 4.2

ANGULAR DISTRIBUTIONS FOR HEXANE

AND ITS HALOGEN DERIVATIVES

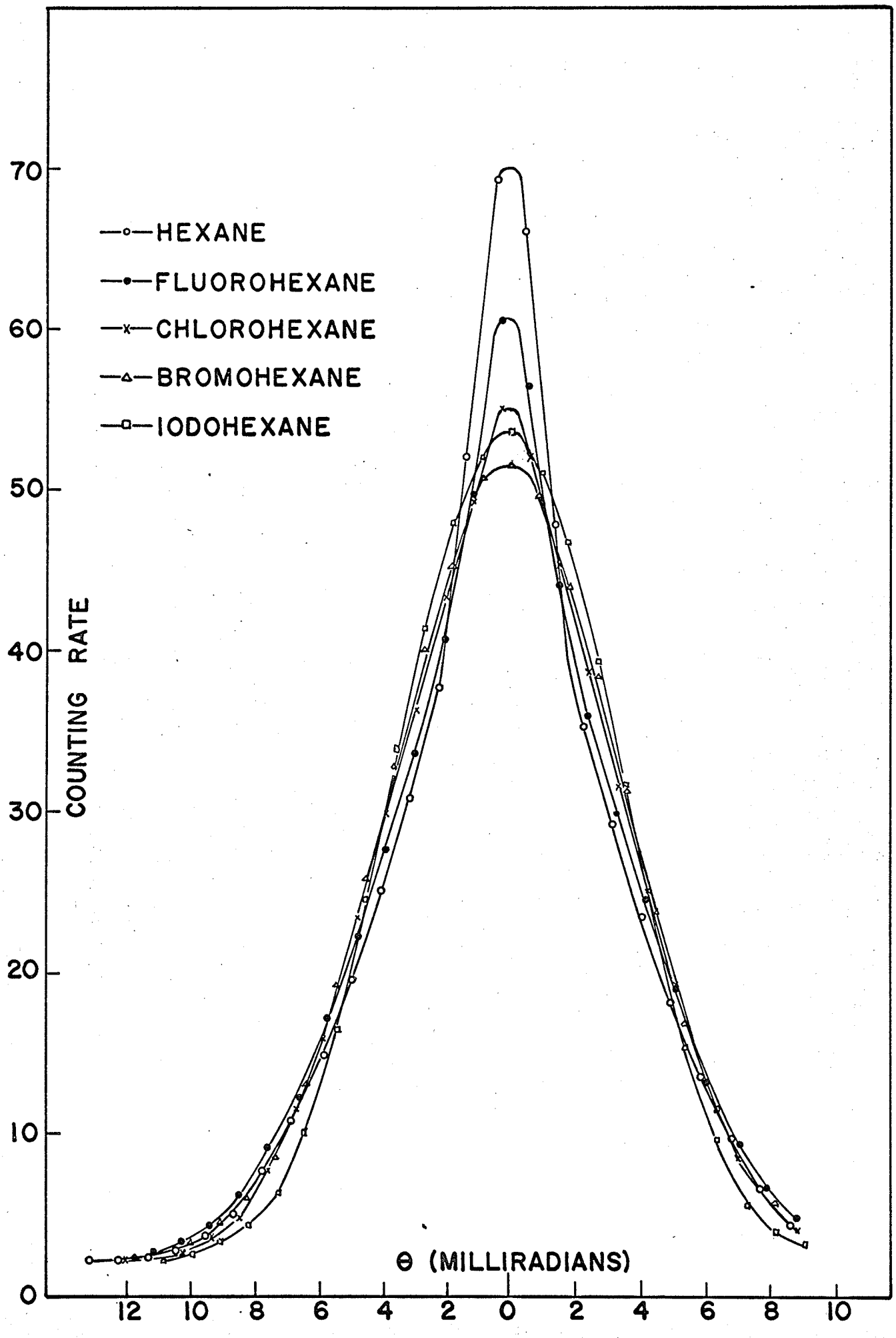
HEXANE
FLUOROHEXANE
CHLOROHEXANE
BROMOHEXANE
IODOHEXANE
COUNTING RATE
θ (MILLIRADIANS)
0
10
20
30
40
50
60
70
12
10
8
6
4
2
0
2
4
6
8
10

caused by the magnetic field of the oxygen molecule. To ensure that the present results were not being affected by oxygen contamination of the sample, angular distributions for hexane were determined first with a sample that had been boiled to expel any dissolved gases, and then with a sample through which oxygen was bubbled. Hexane was chosen for this test since a relatively large amount of positronium is formed in it. Therefore, any triplet-singlet conversion would be more easily detected. Within the experimental error, no difference was noted in the angular distributions from the samples under the two different conditions.

In an attempt to change the amount of positronium being formed and thus perhaps obtain information regarding the shapes of the individual broad and narrow components, an angular distribution for hexane was measured while the sample was in an electric field of 1000 volts per cm. The application of an electric field to some gaseous samples has been found to increase the amount of positronium formed due to the recycling of positrons through the Ore gap. The result in this case was negative however, as was expected, since most molecules have low lying rotational and vibrational states which allow inelastic scattering processes to operate, preventing the positron from gaining sufficient energy to reenter the Ore gap.

(iii) Benzene and its Halogen Derivatives: Figure 4.3 shows the angular distributions (normalized to equal areas) for benzene

FIGURE 4.3

ANGULAR DISTRIBUTIONS FOR BENZENE

AND ITS HALOGEN DERIVATIVES

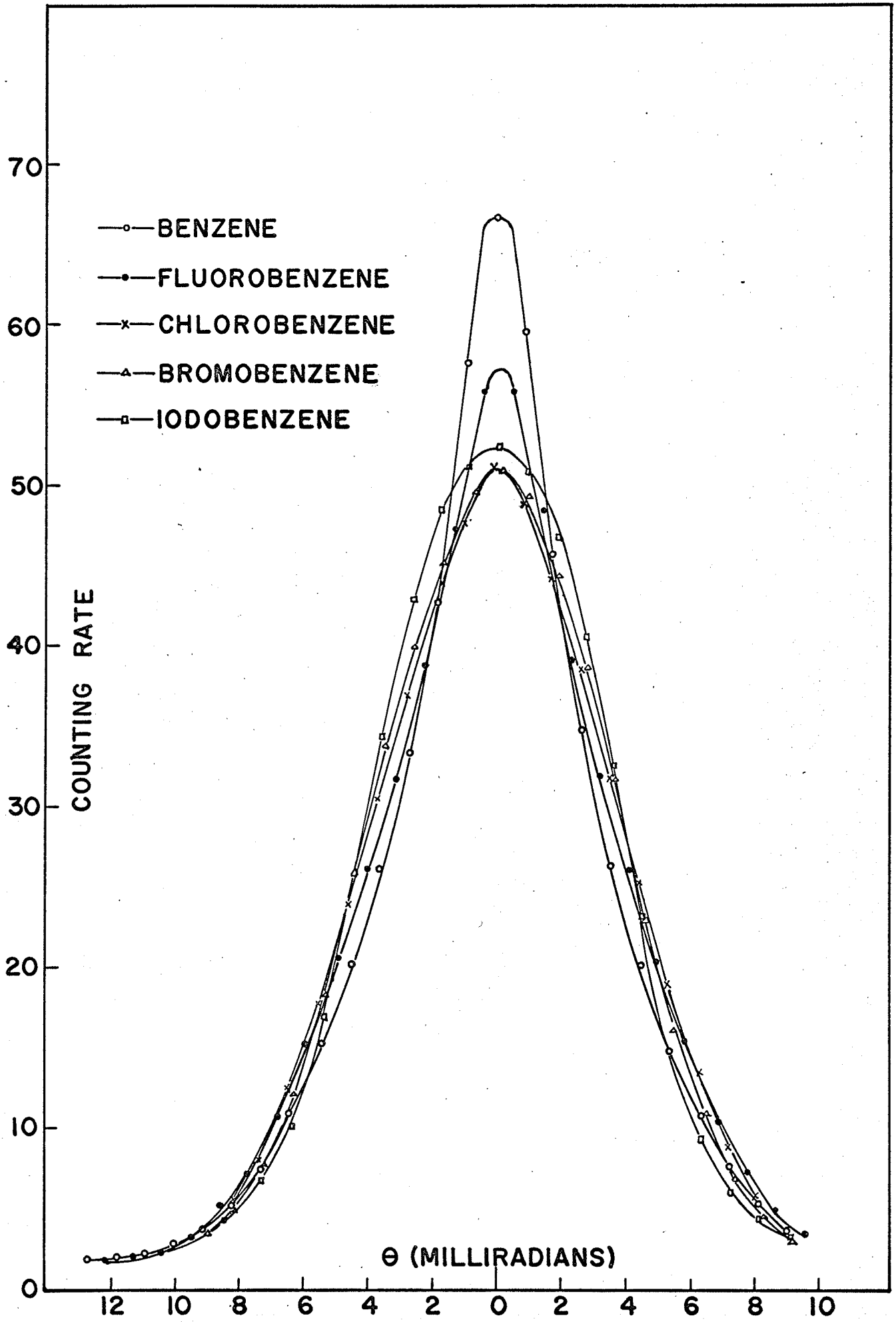
BENZENE
FLUOROBENZENE
CHLOROBENZENE
BROMOBENZENE
IODOBENZENE
COUNTING RATE
θ (MILLIRADIANS)
0
10
20
30
40
50
60
70
12
10
8
6
4
2
0
2
4
6
8
10

and its halogen derivatives. As I_2 decreases in this group, the peak values of the angular distributions decrease only from benzene to chlorobenzene suggesting, as did the result for iodohexane, that the broad component shape is changing. The narrow component shape may also be changing, but the intensity of this component should be small when the heavier halogens are present. Therefore, in this case the change in the total distribution resulting from a variation in the shape of the narrow component alone would be smaller than that observed.

From Table 4.1 it can be seen that the values of I_2 for the benzene compounds correspond very closely to those for the hexane compounds. However, the angular distributions for benzene and its halogen derivatives are generally less peaked than the corresponding distributions for hexane and its halogen derivatives. If the intensity of the narrow component is to bear a constant relationship to I_2, then the difference in angular distributions for compounds with the same I_2 again suggests that the shape of the broad or narrow component is changing.

(iv) Chlorine Compounds; Decane and M-xylene: In Table 4.1 is listed a number of chlorine compounds all of which exhibit a long lived component of approximately the same intensity. To further investigate the possible change in shape of the components comprising the total angular distribution, the

angular correlations of the annihilation photons were measured for these compounds. The results for 1-chloropropane and chlorobenzene are shown in Figure 4.4. The angular distributions for the other chlorine compounds studied, namely 1-chlorobutane, 1-chlorohexane and 1-chlorodecane have shapes intermediate to those shown here. The marked difference between the peaks of the angular distributions for chloropropane and chlorobenzene suggests that it is the narrow component that is changing in this case i.e. the narrow component for chloropropane appears sharper than the narrow component for chlorobenzene.

If the narrow component is subject to change then it is clearly desirable to investigate this effect using compounds in which a large amount of positronium is formed since these compounds will exhibit the largest narrow components. Unfortunately, a large number of compounds that would be expected to exhibit large I_2 values are gases at room temperature. However, decane and m-xylene have similar large I_2 values (see Table 4.1) and are liquid at room temperature. The angular distributions for these compounds shown in Figure 4.5 exhibit significant differences in shape. It appears here that both the broad and narrow component shapes are varying.

With the data in the present form it is not possible to make any statements of a quantitative nature regarding the two components, but in the next chapter the data are analysed in a manner which allows direct measurements to be made on the

FIGURE 4.4

ANGULAR DISTRIBUTIONS FOR CHLOROBENZENE AND CHLOROPROPANE

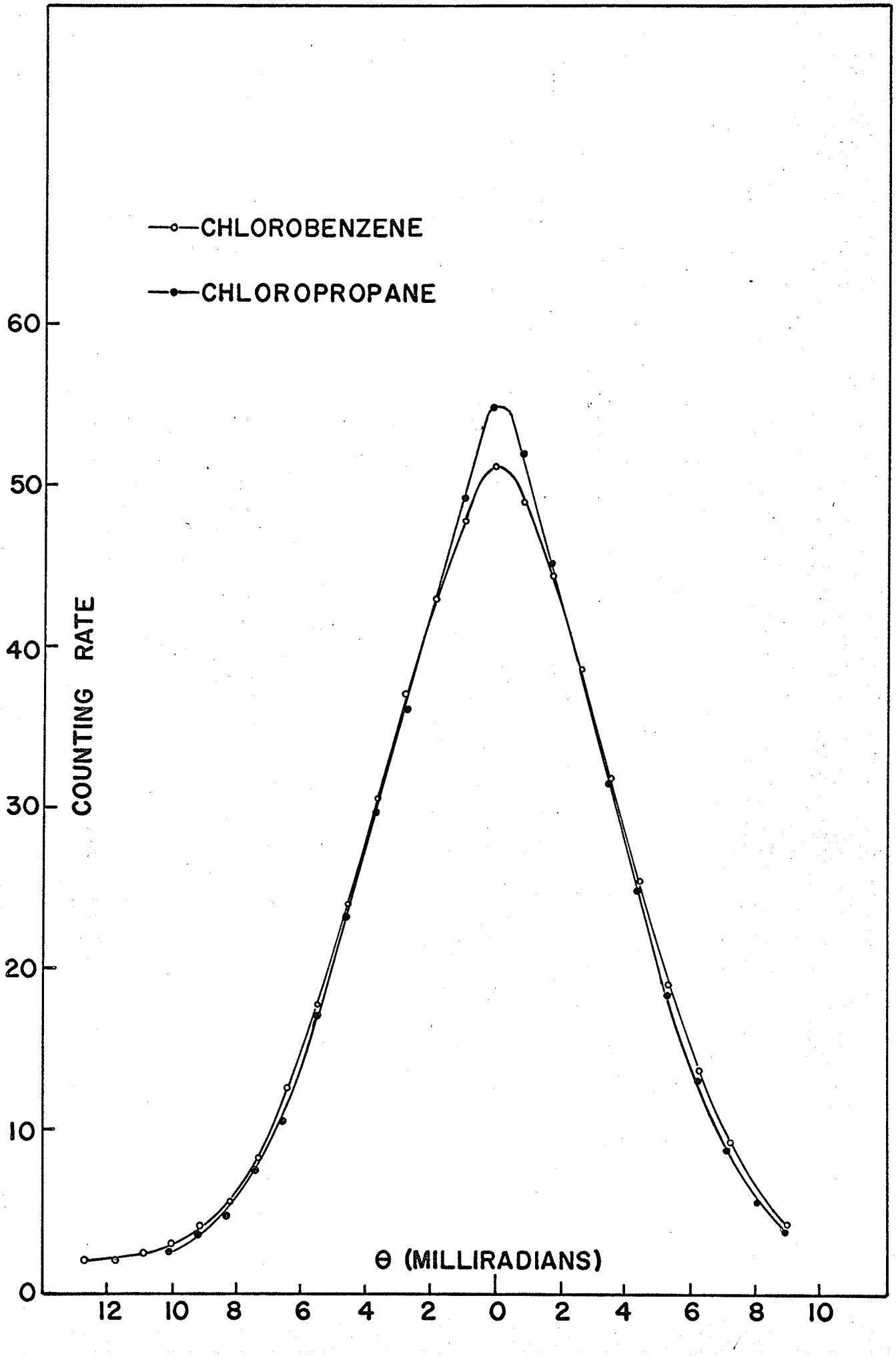
—o—CHLOROBENZENE
—•—CHLOROPROPANE
COUNTING RATE
60
50
40
30
20
10
0
12
10
8
6
4
2
0
2
4
6
8
10
θ (MILLIRADIANS)

FIGURE 4.5

ANGULAR DISTRIBUTIONS FOR M-XYLENE AND DECANE

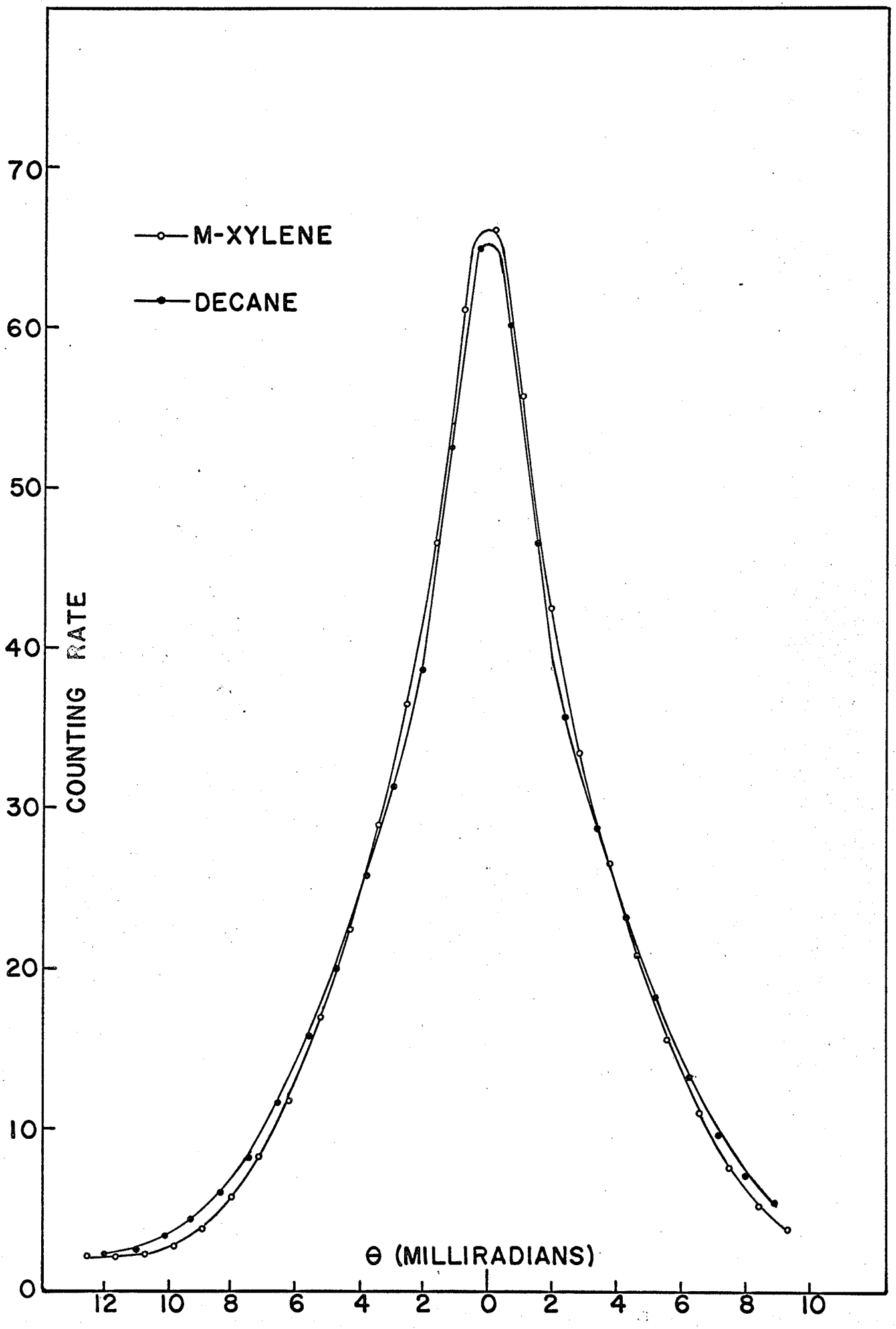
M-XYLENE
DECANE
COUNTING RATE
θ (MILLIRADIANS)
0
10
20
30
40
50
60
70
12
10
8
6
4
2
0
2
4
6
8
10

broad and narrow components.

(v) Dichlorobenzene and Difluorobenzene: In the type of compounds with which we are dealing the presence of more than one halogen atom per molecule normally quenches or removes the long lived component completely. For this reason, the angular distribution for *p*dichlorobenzene was measured with a view to comparing the resulting pure broad component with the angular distribution for chlorobenzene. It might be expected that the broad component would be the same in both cases since the halogen atom, which appears to have the greatest influence on the positron, is the same in both cases. If such were the case, a direct separation of the broad and narrow components would be possible. These results will be presented in Chapter 5 in the form of momentum distributions which most clearly indicate the presence of two distinct components.

It was thought to use *p*difluorobenzene for the same purpose i.e to compare its angular distribution with that for fluorobenzene, but the resulting angular distribution indicated the presence of a strong narrow component. The results from the time studies of positron annihilation in difluorobenzene (Table 4.1) verify that a large amount of positronium is formed in this compound. Surprisingly, I_2 for difluorobenzene is even larger than that for fluorobenzene. At present, no explanation for this can be offered. The angular correlation results for difluorobenzene are presented in their final form in Chapter 5.

(vi) Polyethylene: Reference was made in section 1.5 to recent experiments[24,25] which have indicated the presence of three lifetime components in the time spectra of positrons annihilating in polyethylene and other plastics where it was thought previously that only two lifetime components existed. The angular distribution of the annihilation radiation from polyethylene was measured but it exhibited no irregularities. Further comments will be made in Chapter 5 where these results are presented in their analysed form.

Chapter 5.

DISCUSSION AND INTERPRETATION

5.1 General.

In this chapter the data are presented in the forms obtained by the method described in section 3.6. All the angular distributions are converted to momentum distributions, N(p) vs p, of the annihilating positron-electron pairs. In some cases the slopes of the angular distributions vs angle ($dC/d\theta$ vs θ) are also shown, since in this form some details are apparent that do not exhibit themselves in the momentum distributions. Both of these forms lend themselves more easily to interpretation than do the original angular distributions.

In previous experiments[41] on the angular correlation of the annihilation photons from materials exhibiting a narrow component, the statistical accuracy was not sufficient to permit the conversion of the angular correlation data into momentum distributions. The statistical errors on the angular distributions here are a factor of seven less than the errors in previous work. The errors on the $dC/d\theta$ vs θ curves to be shown are derived in the usual manner i.e. the standard deviation for each point on the angular distribution curve is obtained from the square root of the total number of counts accumulated at that point. The error in the difference between two neighbouring points i.e. the error in the slope of the curve midway

between the points is then the square root of the sum of the squares of the individual errors. The error in N(p), which is proportional to the product $\theta dC/d\theta$ may then be obtained.

It was seen in the introduction that if some fraction of the positrons entering a material form positronium, then three different types of decay are expected to occur. Free positrons will annihilate with bound electrons and therefore the centre of mass of the positron-electron pair will have some appreciable momentum at the time of annihilation even if the positron is virtually at rest. Similarly, positrons that form triplet positronium will also annihilate with bound atomic electrons via the pickoff process. Positrons that form singlet positronium, however, will annihilate with their own electrons and the momentum of such annihilating pairs will be quite small. Therefore, the total momentum distribution of the annihilating pairs would be expected to exhibit two components, a high momentum component resulting from the annihilation of triplet positronium and free positrons, and a low momentum component resulting from the self-annihilation of singlet positronium. The high and low momentum components in the momentum distributions correspond to the broad and narrow components respectively in the angular distributions.

Since one quarter of the positronium is formed in the singlet state and three quarters is formed in the triplet state, and since I_2, the intensity of the long lived component in time spectra is a measure of the amount of triplet positronium formed,

the intensity of the low momentum component should be equal to $I_2/3$.

5.2 The Separation of the High and Low Momentum Components.

The momentum distributions for all the materials studied are shown in Figures 5.1 to 5.13. The momentum distribution for hexane (Figure 5.1) shows most clearly the presence of two distinct momentum components. To measure the relative intensities of the two components one must have some knowledge of the shape of the high momentum component in the region where it is obscured by the low momentum component. Unfortunately, it is not possible to separate the two experimentally, and therefore one must turn to an investigation of materials for which the momentum distributions have little or no low momentum component i.e. materials in which little or no positronium is formed. Two such momentum distributions, those for iodohexane and carbon tetrachloride, are shown in Figure 5.14. Examination of these distributions reveals some useful information. The first and most obvious point is that the low momentum sides of the high momentum components have no irregularities and fall smoothly to zero at zero momentum. The second point is that the portions of the distributions above half maximum are very nearly symmetric. This is shown by the dotted line on the left side of each curve which is a reflection of the solid line on the right side of each curve.

FIGURE 5.1

N(p) VS p AND $dC/d\theta$ VS θ FOR HEXANE

The dotted line on the low momentum component indicates the correction for the finite angular resolution of the apparatus.

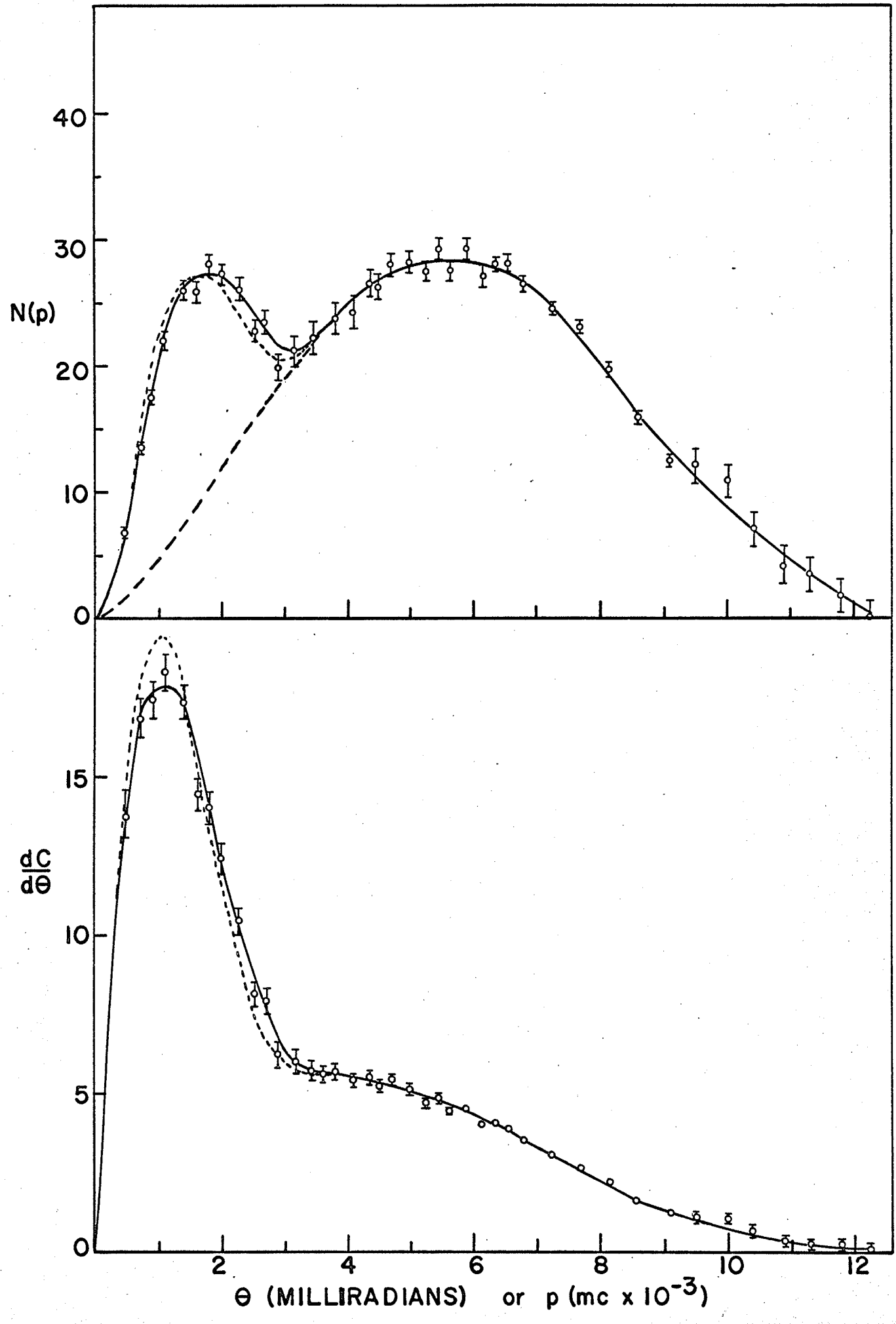
40
30
20
10
0
N(p)
15
10
5
0
dC/dθ
2
4
6
8
10
12
θ (MILLIRADIANS) or p (mc x 10^-3)

FIGURE 5.2

N(p) VS p AND $dC/d\theta$ VS θ FOR FLUOROHEXANE

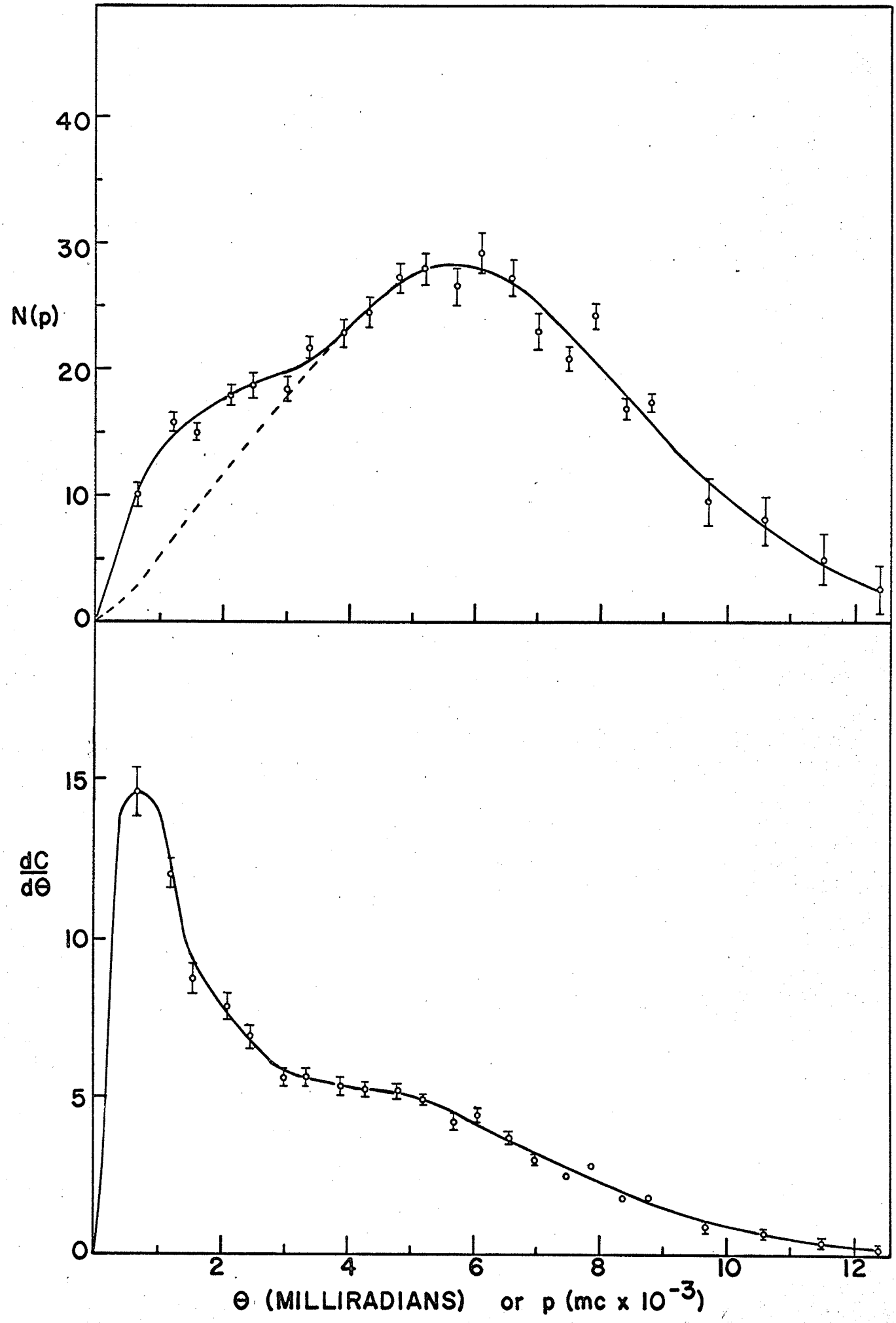
40
30
N(p)
20
10
0
15
dC/dθ
10
5
0
2
4
6
8
10
12
θ (MILLIRADIANS) or p (mc x 10^-3)

FIGURE 5.3

N(p) VS p AND $dC/d\theta$ VS θ FOR CHLOROHEXANE

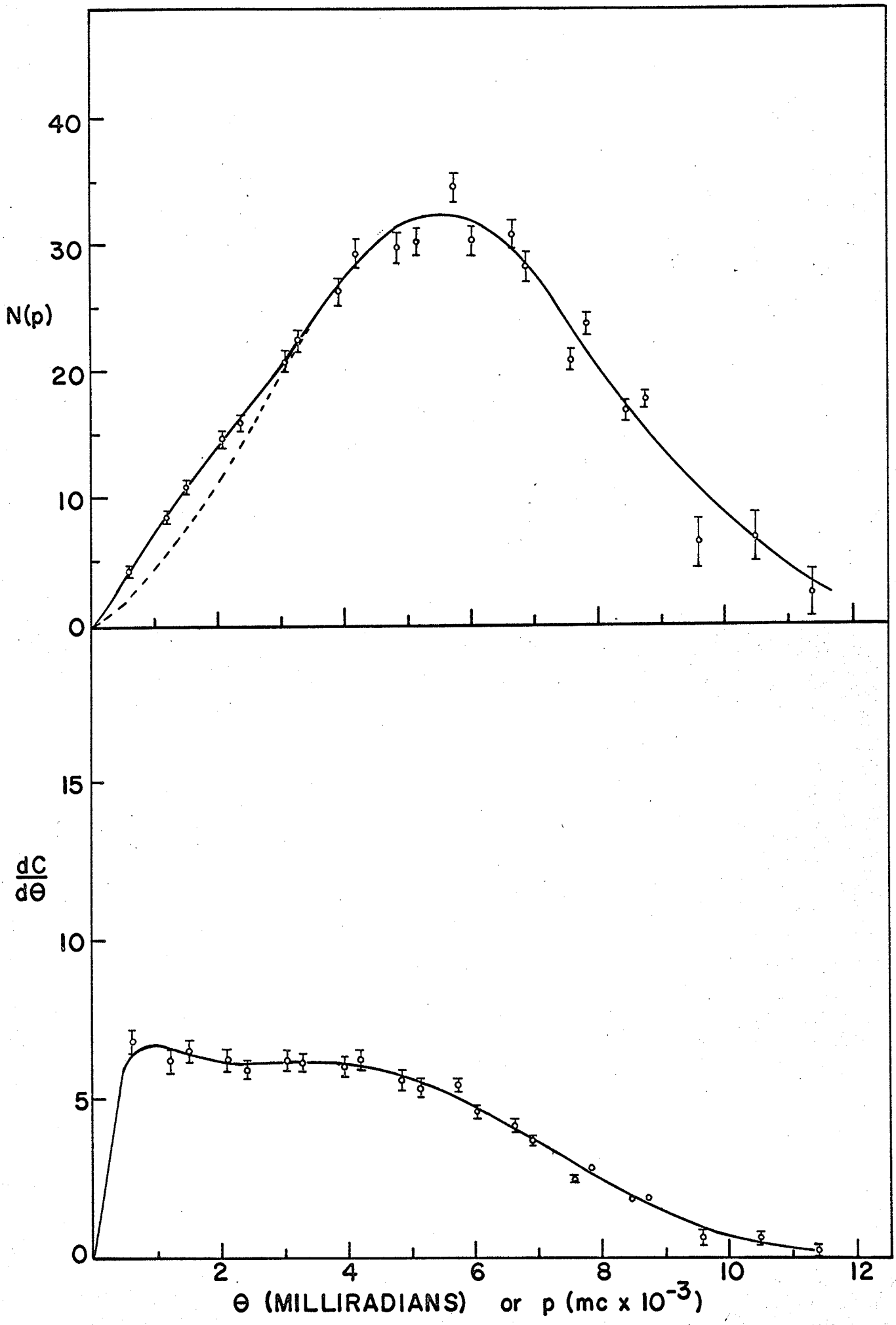
40
30
N(p)
20
10
0
15
dC/dθ
10
5
0
2
4
6
8
10
12
θ (MILLIRADIANS) or p (mc x 10^-3)

FIGURE 5.4

N(p) VS p AND $dC/d\theta$ VS θ FOR BROMOHEXANE

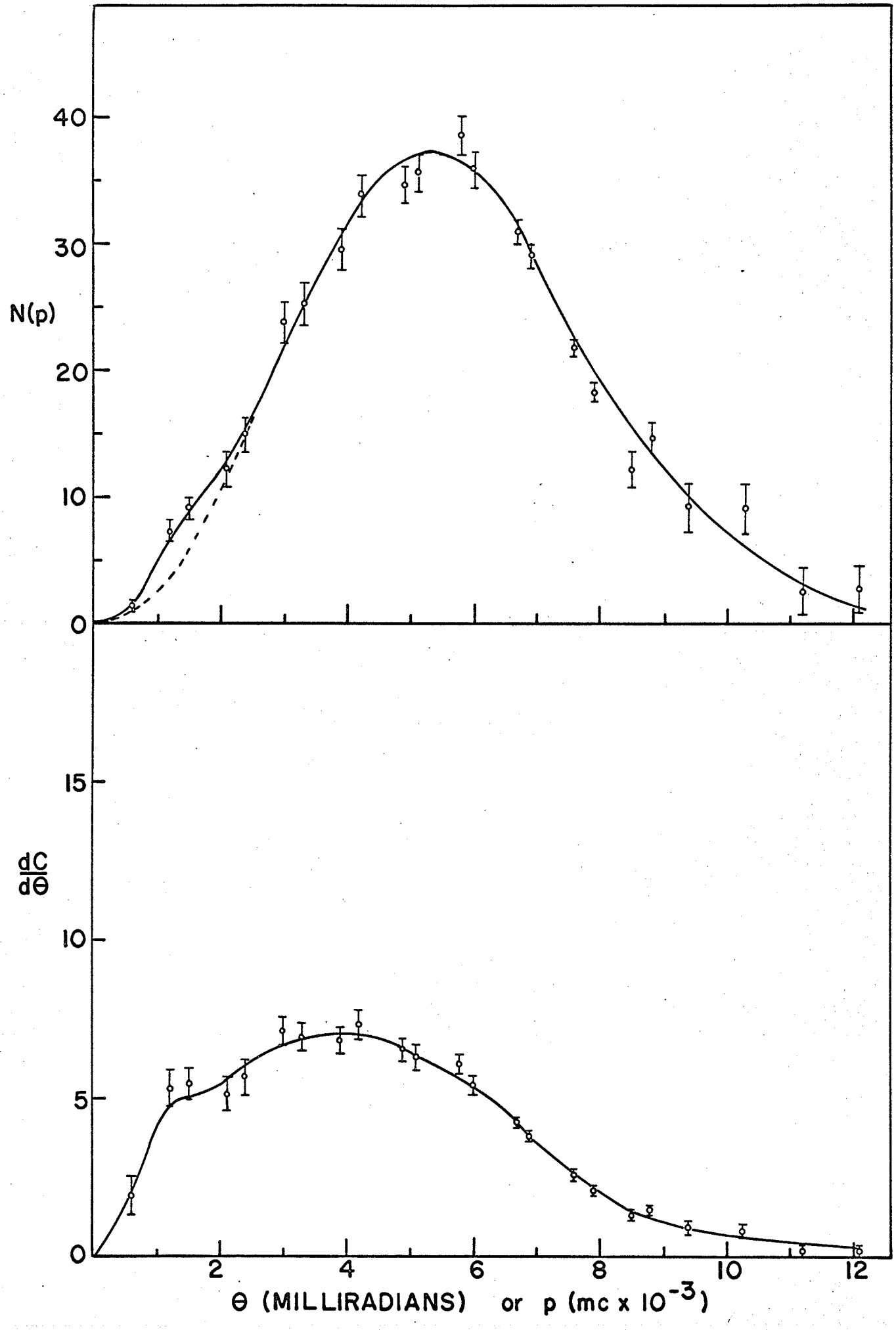
40
30
N(p)
20
10
0
15
dC/dθ
10
5
0
2
4
6
8
10
12
θ (MILLIRADIANS) or p (mc x 10^-3)

FIGURE 5.5

N(p) VS p AND $dC/d\theta$ VS θ FOR IODOHEXANE

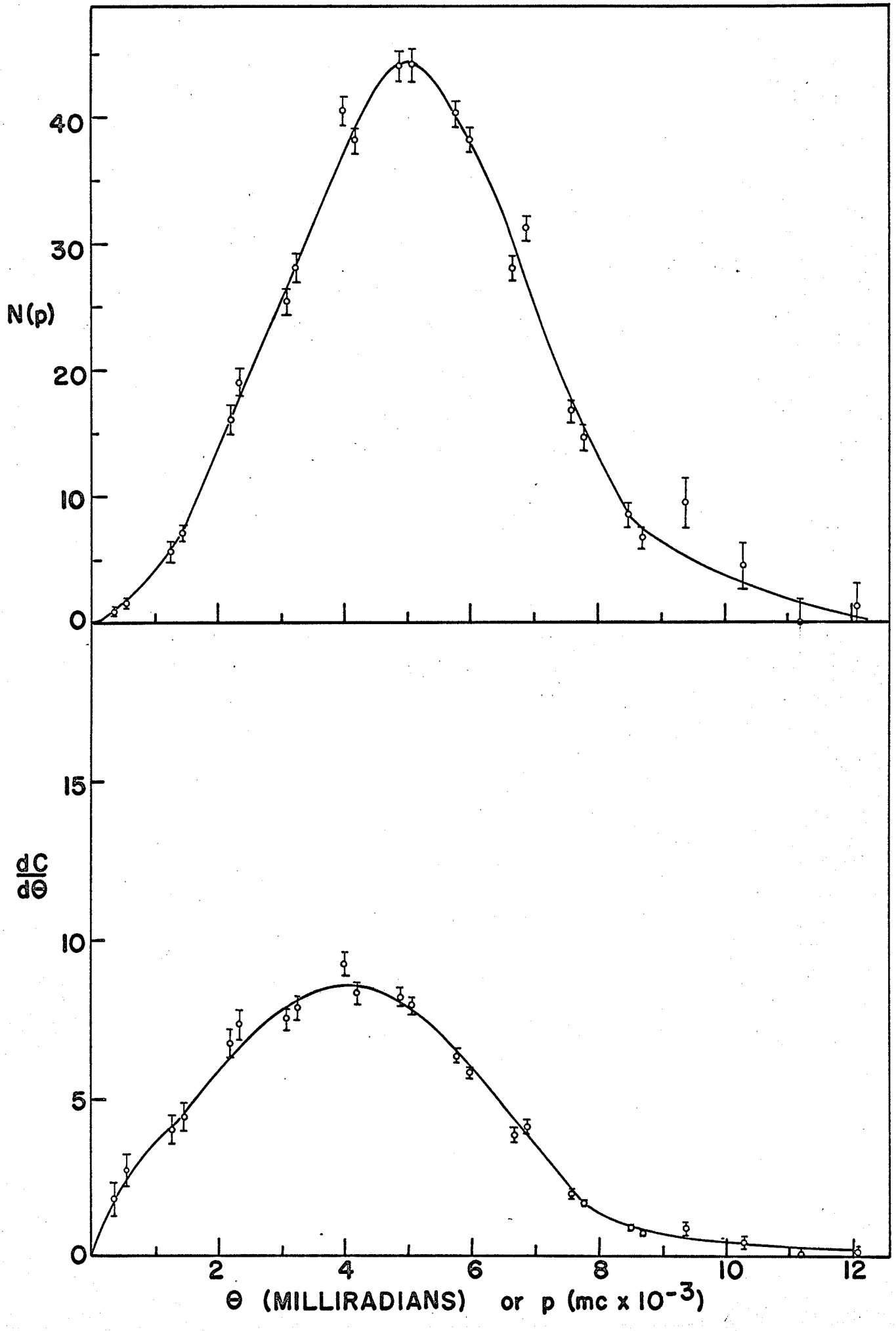
40
30
N(p)
20
10
0
15
dC/dΘ
10
5
0
2
4
6
8
10
12
Θ (MILLIRADIANS) or p (mc x 10⁻³)

FIGURE 5.6

N(p) VS p AND $dC/d\theta$ VS θ FOR BENZENE

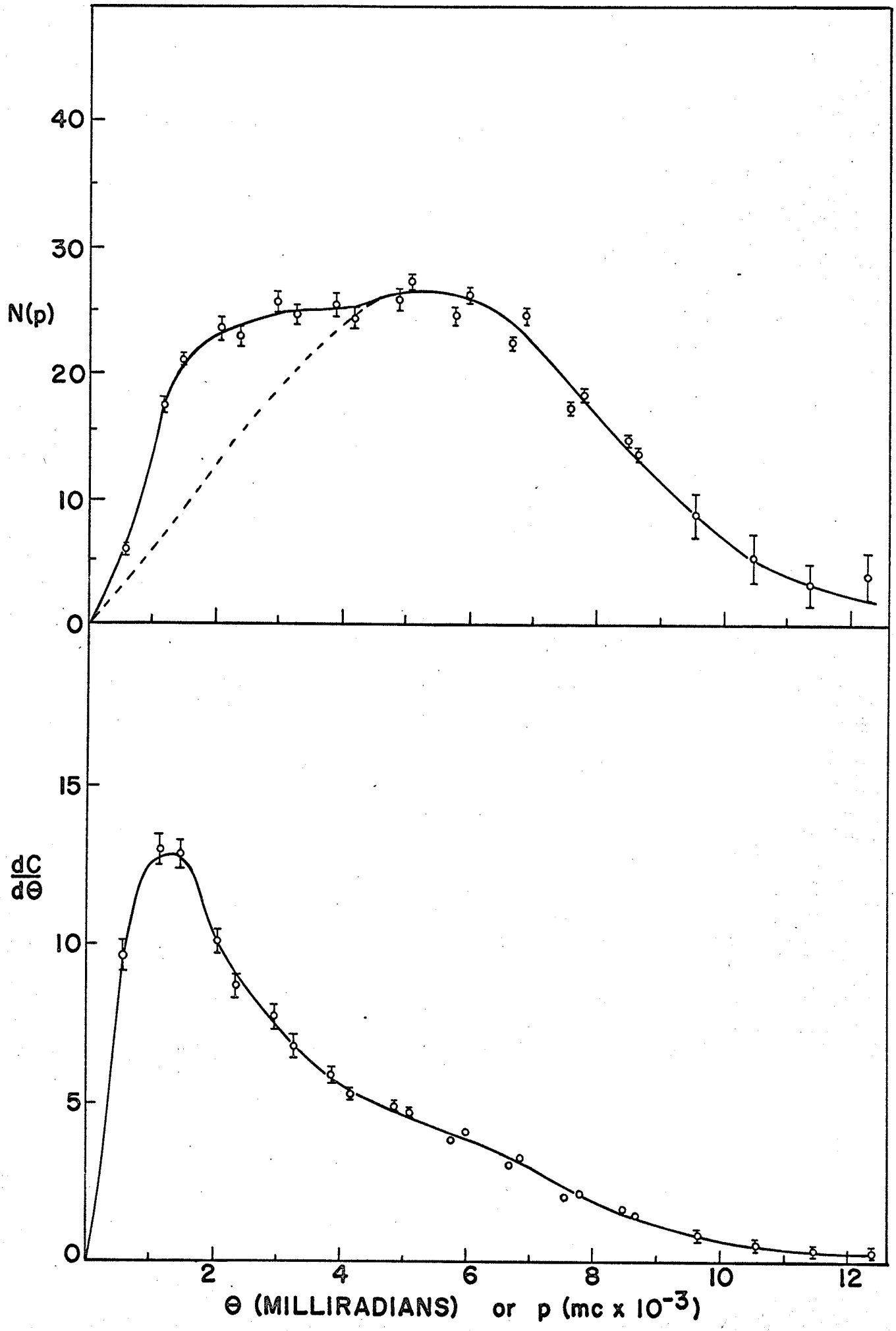
40
30
N(p)
20
10
0
15
dC/dθ
10
5
0
2
4
6
8
10
12
θ (MILLIRADIANS) or p (mc x 10^-3)

FIGURE 5.7

$N(p)$ VS p AND $dC/d\theta$ VS θ FOR FLUOROBENZENE

A. Low momentum component end point.
B. Mean momentum in high momentum component.
C. Full width at half maximum of high momentum component.

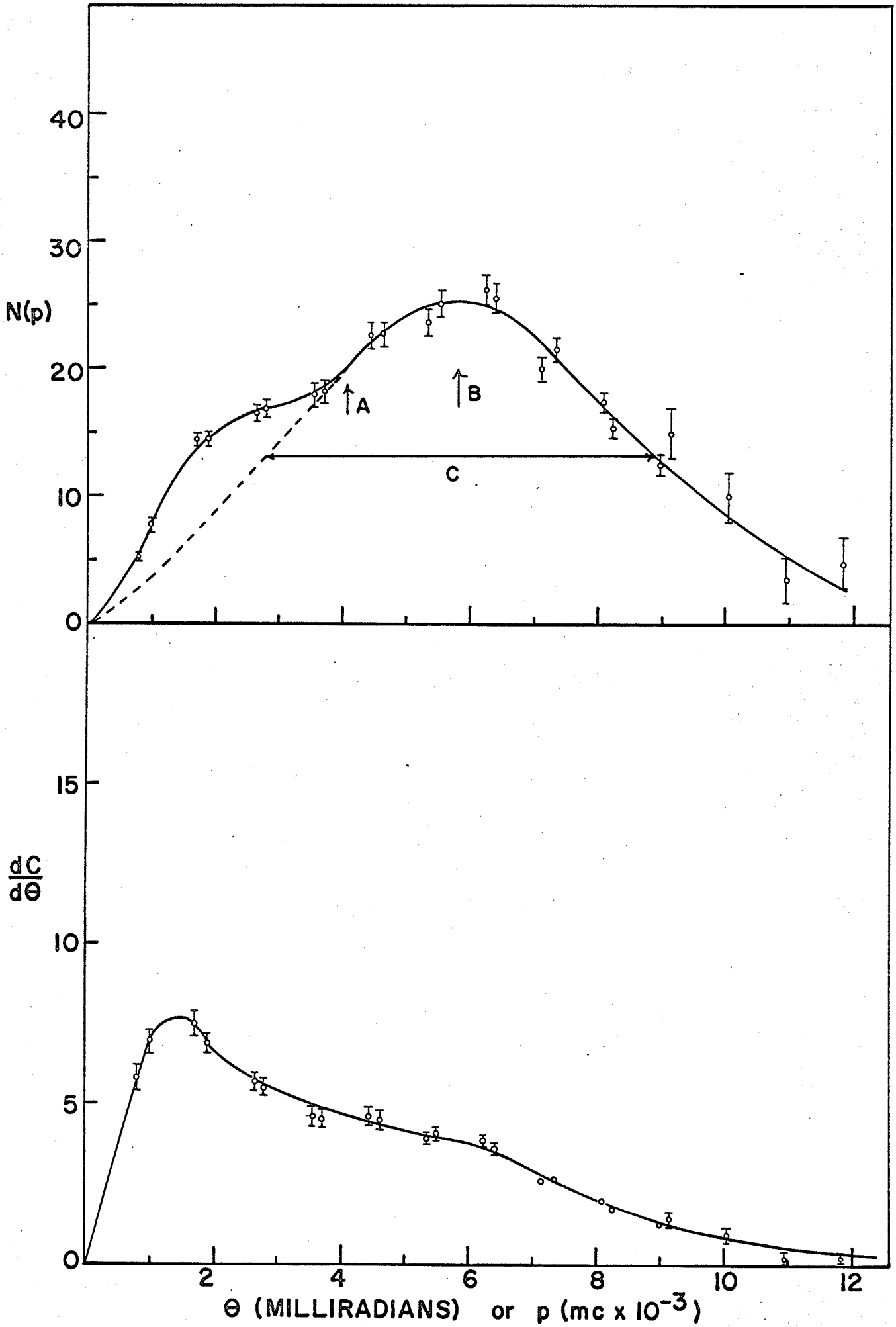
40
30
N(p)
20
10
0
A
B
C
15
dC/dΘ
10
5
0
2
4
6
8
10
12
Θ (MILLIRADIANS) or p (mc x 10^-3)

FIGURE 5.8

N(p) VS p AND $dC/d\theta$ VS θ FOR CHLOROBENZENE
AND N(p) VS p FOR DICHLOROBENZENE

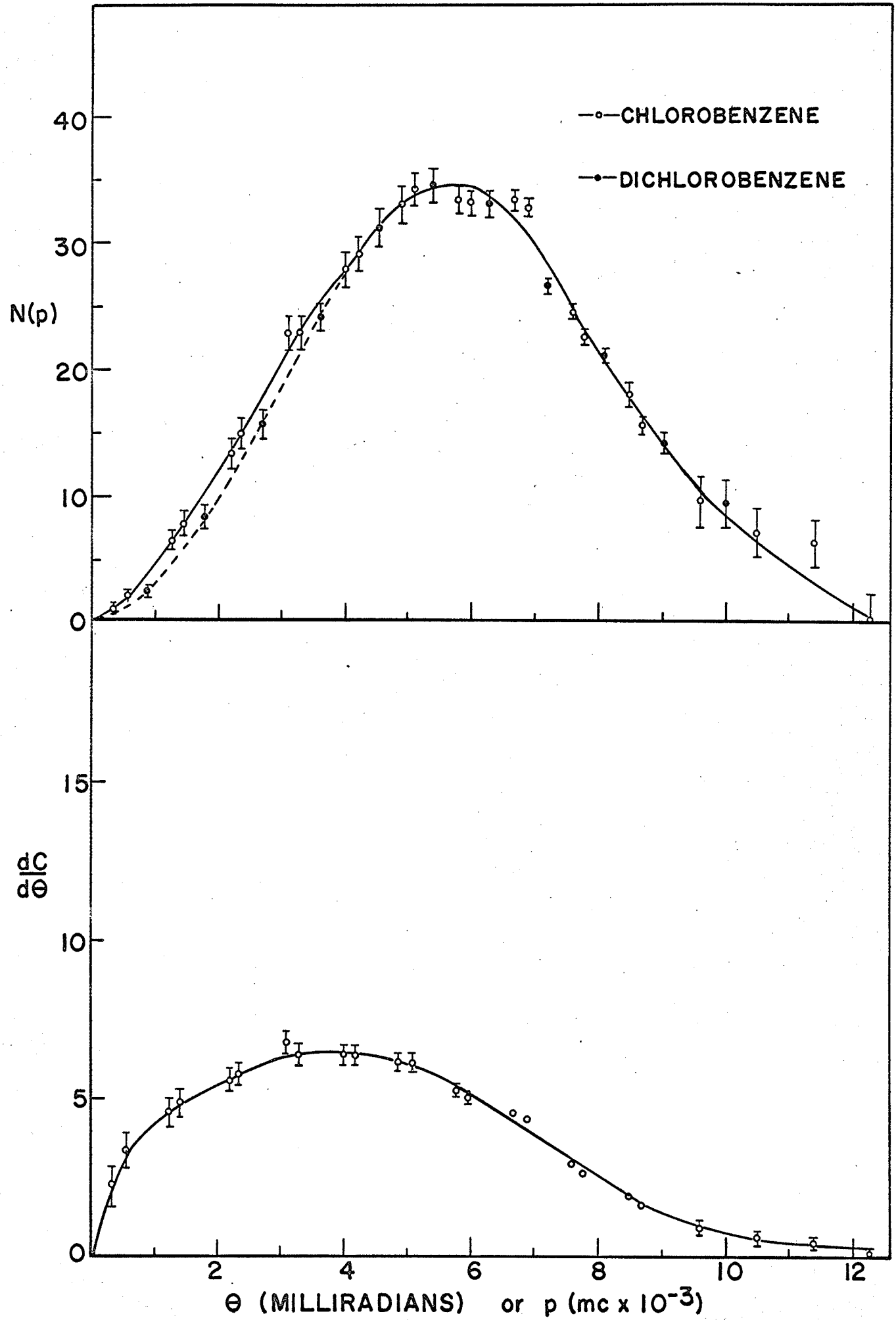
—o—CHLOROBENZENE
—•—DICHLOROBENZENE
N(p)
40
30
20
10
0
dC/dΘ
15
10
5
0
2
4
6
8
10
12
Θ (MILLIRADIANS) or p (mc x 10⁻³)

FIGURE 5.9

N(p) VS p AND $dC/d\theta$ VS θ FOR BROMOBENZENE

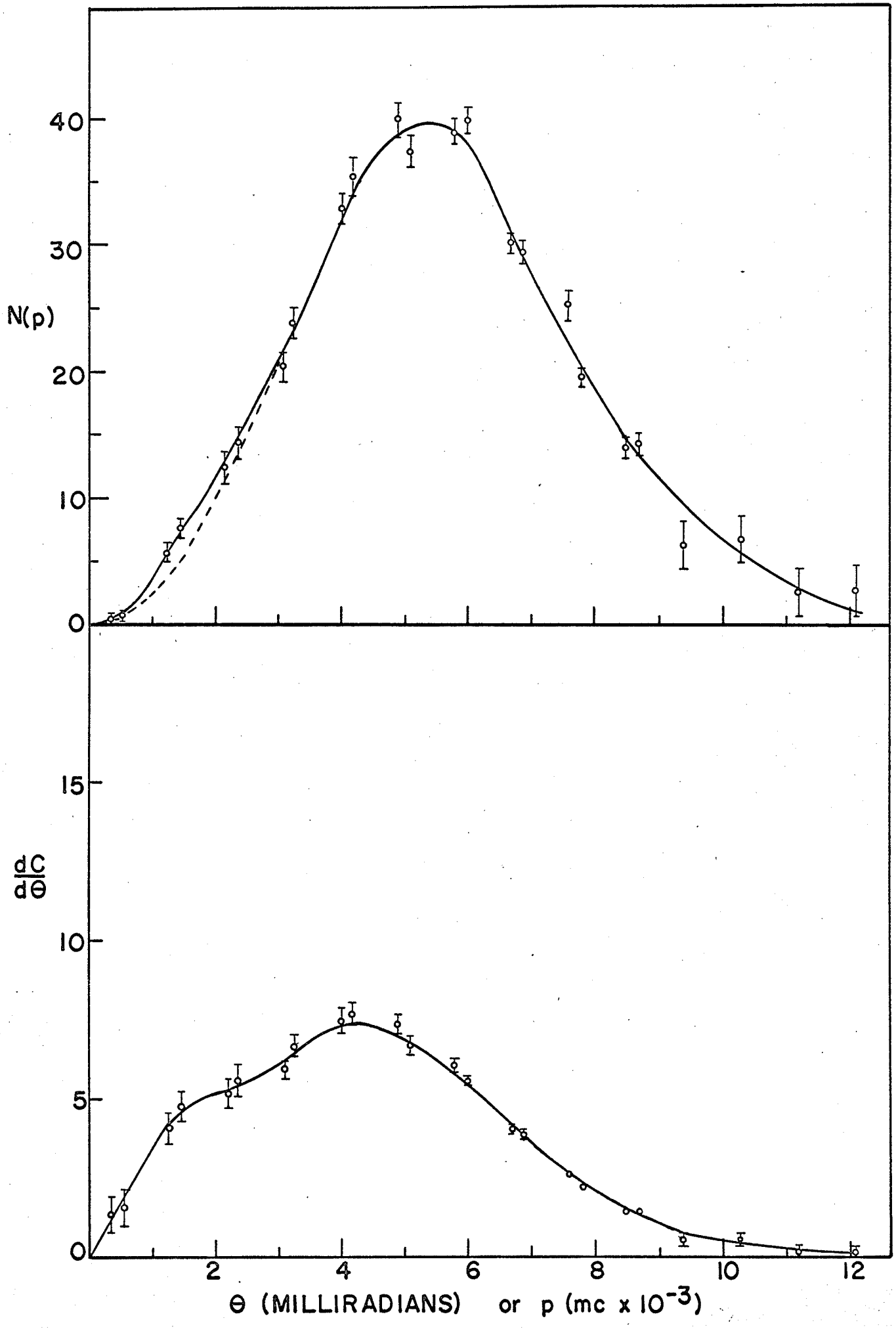
40
30
N(p)
20
10
0
15
dC/dθ
10
5
0
2
4
6
8
10
12
θ (MILLIRADIANS) or p (mc x 10^-3)

FIGURE 5.10

N(p) VS p AND $dC/d\theta$ VS θ FOR IODOBENZENE

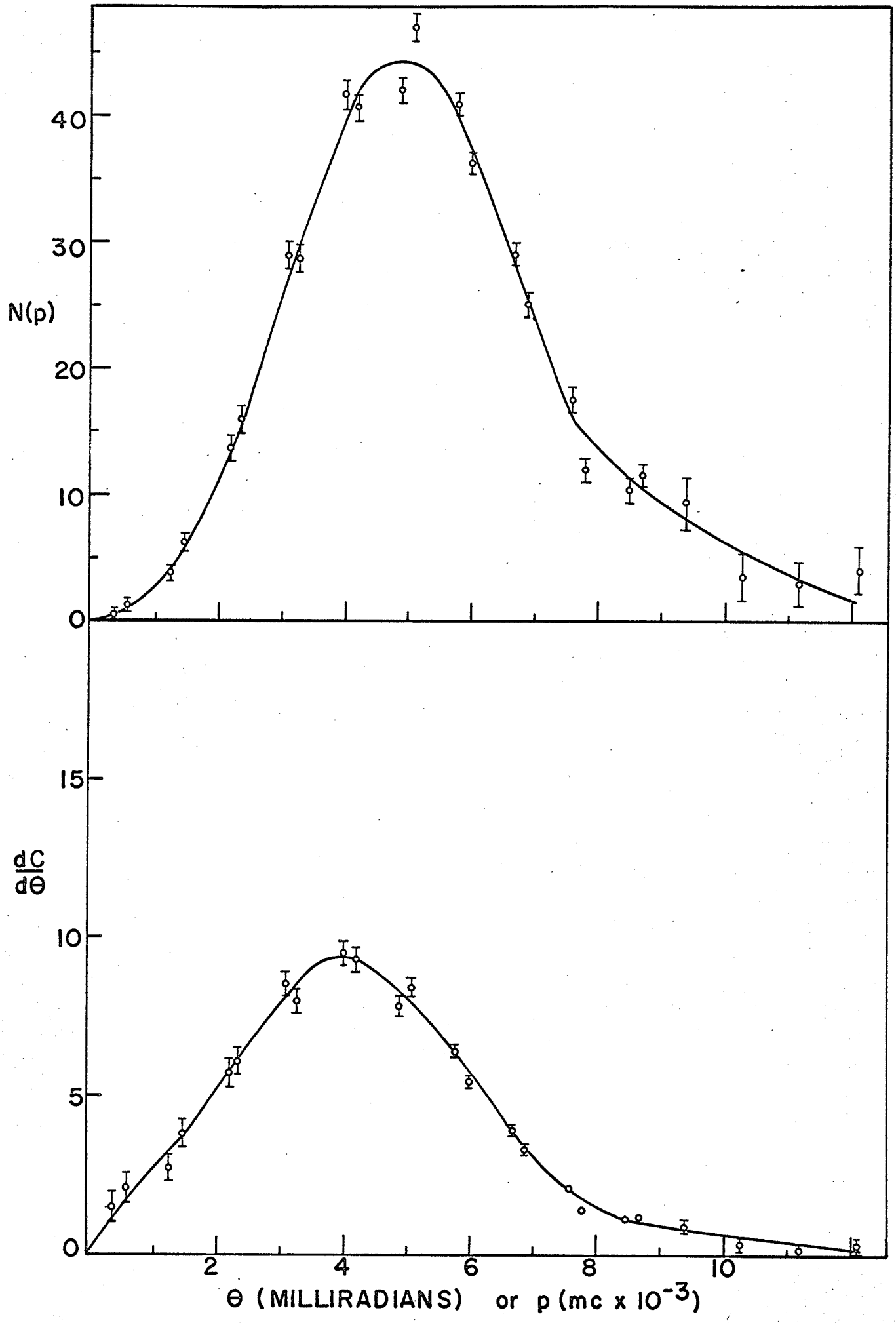
40
30
N(p)
20
10
0
15
dC/dθ
10
5
0
2
4
6
8
10
θ (MILLIRADIANS) or p (mc x 10^-3)

FIGURE 5.11

(a) N(p) VS p FOR DECANE

The dotted line on the low momentum component indicates the correction for the finite angular resolution of the apparatus.

(b) N(p) VS p FOR M-XYLENE

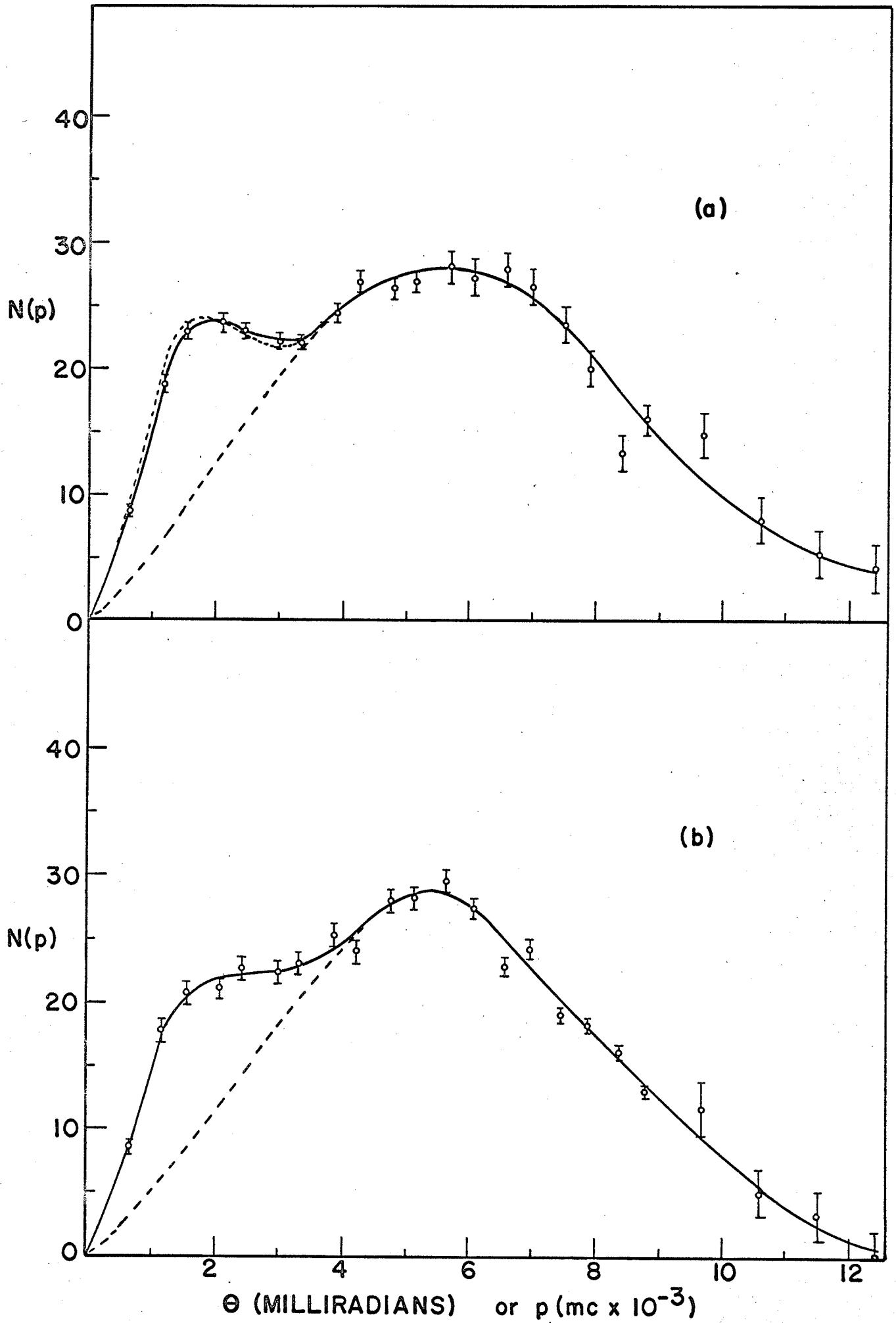
(a)
(b)
N(p)
N(p)
0
10
20
30
40
2
4
6
8
10
12
Θ (MILLIRADIANS) or p (mc x 10^-3)

FIGURE 5.12

(a) N(p) VS p FOR CHLOROPROPANE

(b) N(p) VS p FOR CHLORODECANE

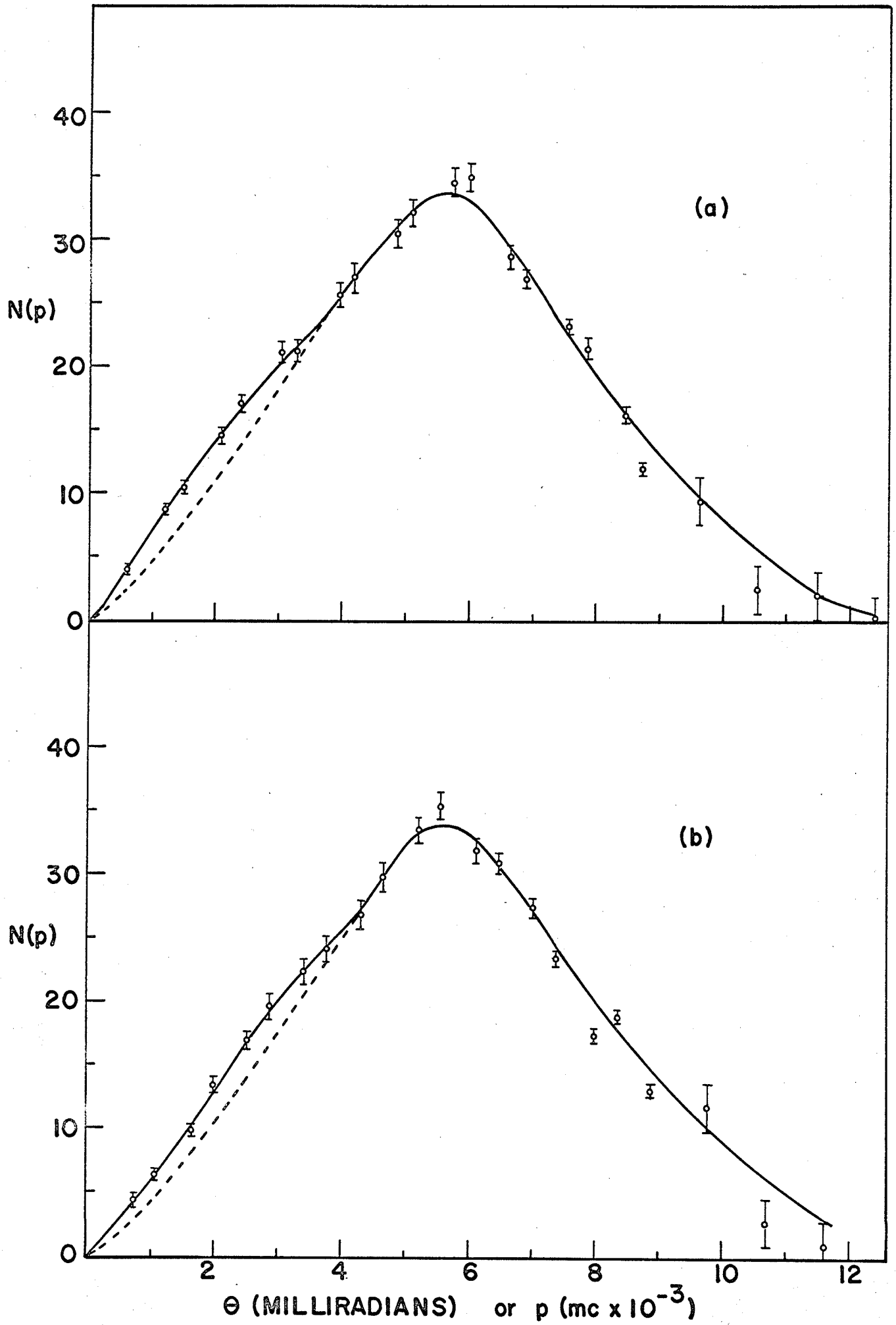
40
30
20
10
0
N(p)
(a)
40
30
20
10
0
N(p)
(b)
2
4
6
8
10
12
Θ (MILLIRADIANS) or p (mc x 10^-3)

FIGURE 5.13

(a) N(p) VS p FOR CHLOROBUTANE

(b) N(p) VS p FOR DIFLUOROBENZENE

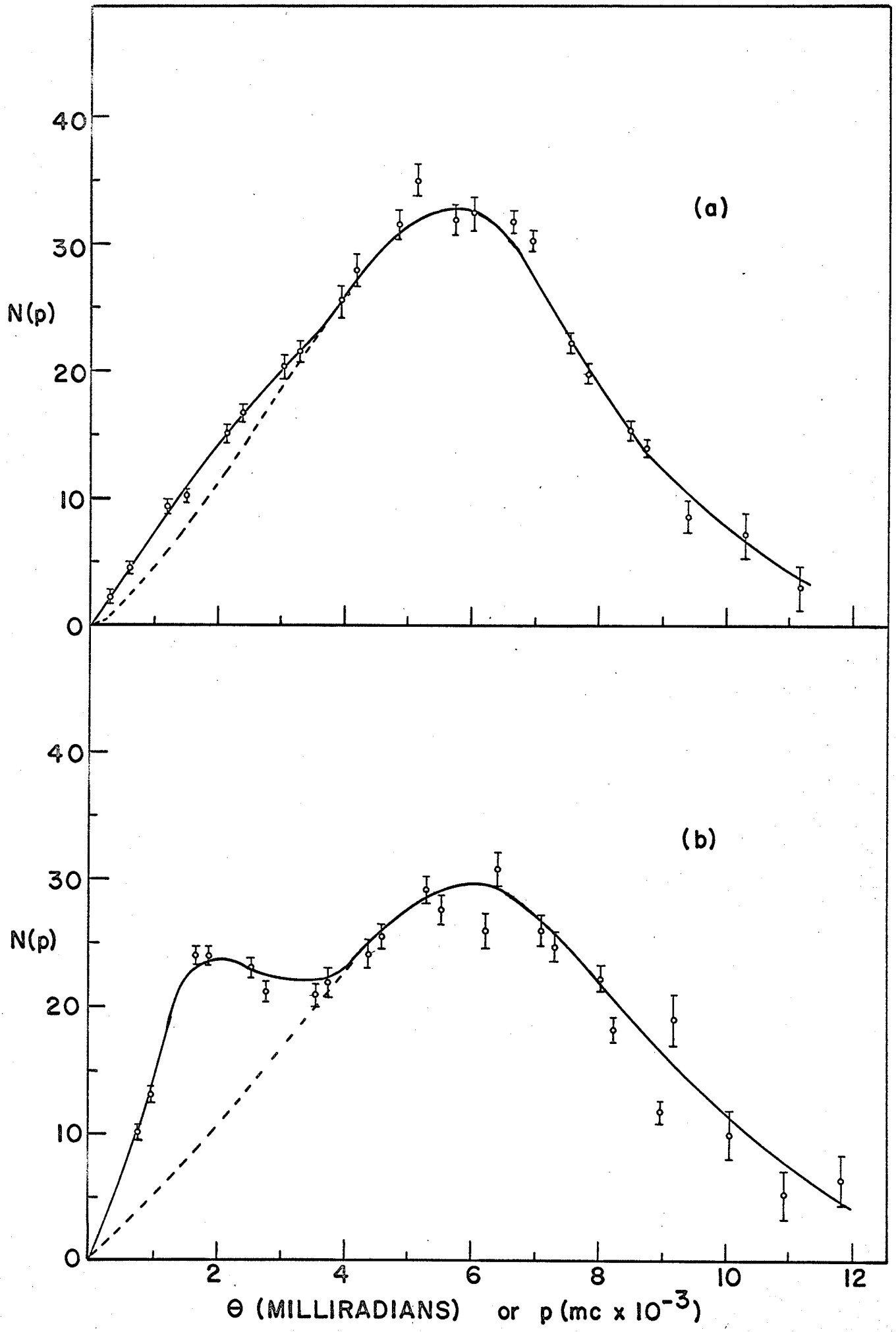
(a)
(b)
N(p)
N(p)
0
10
20
30
40
2
4
6
8
10
12
Θ (MILLIRADIANS) or p (mc x 10⁻³)

FIGURE 5.14

THE HIGH MOMENTUM COMPONENT IN
(a) IODOHEXANE AND (b) CARBON TETRACHLORIDE

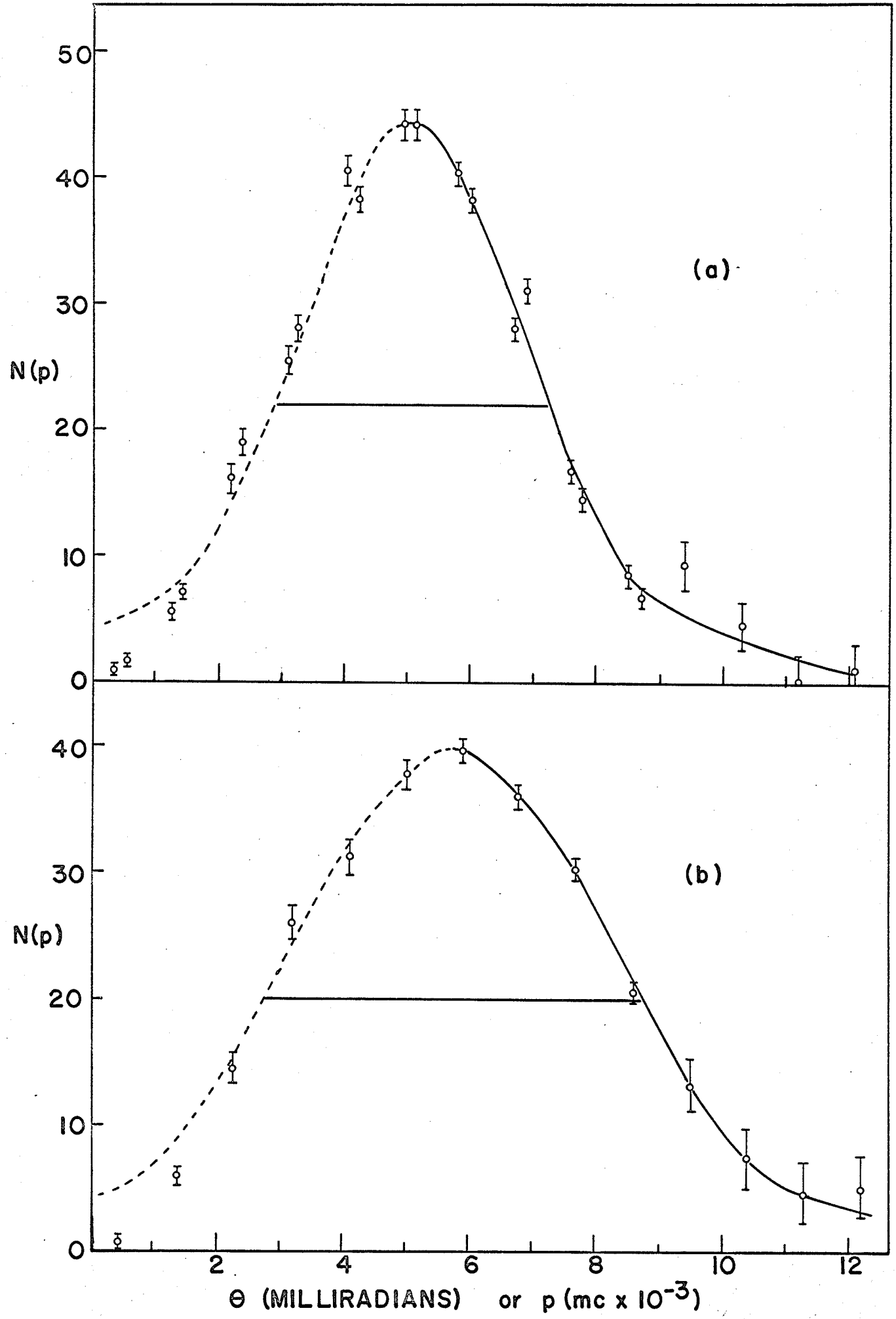
50
40
30
20
10
0
N(p)
(a)
40
30
20
10
0
N(p)
(b)
2
4
6
8
10
12
θ (MILLIRADIANS) or p (mc x 10^-3)

When no positronium is formed, the high momentum component is due only to the annihilation of free positrons, but when positronium is formed, the high momentum component also results from the annihilation of triplet positronium. Arguments will be presented in section 5.4 to show that essentially the same distribution should arise from both types of annihilation. Therefore, the method used to separate the high and low momentum components was to fold the distributions about the peaks of the high momentum components and thus obtain a shape for the hidden part of the high momentum components down to half maximum. From half maximum to zero, a shape was assumed bearing in mind that the total curve must be smooth. Determinations of the low momentum component intensity using the two extreme high momentum component shapes meeting the above conditions differed by only one or two percent.

This method could not be applied to the momentum distributions for the bromine and iodine compounds where the low momentum component is very small. As a result, no attempt was made to measure the intensity of the low momentum component in the iodine compounds and only estimates were made for the bromine compounds. Although low momentum components cannot be seen on the momentum distributions for the iodine compounds, their existence is indicated by the slight irregularities on the low momentum sides of the $dC/d\theta$ vs θ curves.

The separation of the momentum distribution for

chlorobenzene into two components was also attempted by the method described in the previous chapter using the pure high momentum component from dichlorobenzene. The two distributions normalized to the same peak value are shown in Figure 5.8. The agreement is excellent except where the low momentum component is expected to add to the chlorobenzene distribution. Therefore, it is reasonable to assume that the high momentum components are the same in both cases and that the difference in the total distributions is due only to the low momentum component in chlorobenzene. It is encouraging to note that the shapes of the high momentum component for chlorobenzene determined by this method and by the method first mentioned are the same.

In the momentum distributions where it has been possible to separate the two components, the shape of the high momentum component as determined by the first described method is indicated by the dotted curve. Qualitatively, the momentum distributions for hexane and its halogen derivatives clearly show the decrease in intensity of the low momentum component as I_2 decreases. Also, as mentioned in the previous chapter, it can be seen that the shape of the high momentum component varies as the halogen atom is changed. As the halogen atom increases in size, the peak of the high momentum component shifts to a lower momentum and at the same time the width of this component decreases. This fact explains the apparent contradiction which arose when the height of the angular distributions for iodohexane,

bromobenzene and iodobenzene did not decrease with decreasing I_2. Although the intensity of the low momentum component decreases, the shift in position of the high momentum component causes the total distributions in these cases to become more peaked. It is also evident from an examination of the momentum distributions that the shape of the narrow or low momentum component is changing. The changes in shape of the components will be discussed further in sections 5.3 and 5.4.

In Table 5.1 the intensity of the low momentum component I_L, and one third the intensity of the long lived component $I_2/3$ are compared for all the compounds investigated. In each case the values agree within the experimental error. The errors assigned to I_L were estimated on the basis of the uncertainty in the shape of the high momentum component coupled with the uncertainty in shape of the overall momentum distribution. The agreement between I_L and $I_2/3$ is conclusive experimental evidence supporting the view that the narrow or low momentum component results from the self-annihilation of singlet positronium.

5.3 The Ore Model of Positronium Formation.

Hatcher[61] has shown that the intensity of the long lived component in the halogen derivatives of benzene may be explained on the basis of the Ore model of positronium formation assuming that the upper bound of the Ore gap is equal to the dissociation potential of the carbon halogen bond.[62] Referring

Table 5.1

Comparison of I_L and $I_2/3$

Compound	I_L(%)	$I_2/3$(%)
Hexane	14 ± 2	12.7 ± .7
Fluorohexane	8 ± 1	8.7 "
Chlorohexane	3 ± 1	5.3 "
Bromohexane	2 ± 1	3.3 "
Iodohexane	-	1.3 "
Benzene	13 ± 2	11.3 "
Fluorobenzene	8 ± 1	8.7 "
Chlorobenzene	5 ± 1	5.0 "
Bromobenzene	2 ± 1	3.0 "
Iodobenzene	-	1.3 "
Decane	12 ± 2	11.6 "
Chlorodecane	4 ± 1	5.7 "
M-xylene	13 ± 2	13.0 "
Chloropropane	4 ± 1	5.3 "
Chlorobutane	4 ± 1	5.7 "
Difluorobenzene	12 ± 2	10.7 "

to Figure 1.1 where V is the kinetic energy of the free positron, V_i is the ionization potential of the molecule, and V_p is the binding energy of the positronium atom (~6.8ev), V_1 now becomes the dissociation potential of the carbon-halogen bond.

Hatcher makes the following assumptions: (1) for $V > V_i$ positron annihilation may be neglected; (2) if a positron is scattered into the energy interval $0 < V < V_i$ it is equally likely to have any energy in the interval; (3) when the positron has an energy in the range $V_1 < V < V_i$ competing processes (most likely the dissociation of the carbon-halogen bond) are much more probable than the formation of positronium; (4) in these processes the positron loses sufficient energy so that scattering into the Ore gap may be neglected; and (5) all positrons in the Ore gap $V_i - V_p < V < V_1$ form positronium. With these assumptions, the fraction of positrons that form positronium is given by $\left[V_1 - (V_i - V_p)\right]/V_i$ since positronium cannot be formed for $V < V_i - V_p$. Then, since three quarters of the positronium is formed in the triplet state, the intensity of the long lived component is given by

$$I_2 = \frac{3}{4}\frac{\left[V_1 - (V_i - V_p)\right]}{V_i}$$

On this basis Hatcher calculates I_2 for the halogen derivatives of benzene. In his calculations however, he employs

the spectroscopic values[63] of the ionization potentials for these compounds. It would seem more likely that electron impact ionization potentials should be used since we are concerned with ionization which is accomplished by positron impact. The electron impact values are generally higher than the corresponding spectroscopic values as a result of the requirement of the Franck-Condon principle, namely, that when ionization is caused by electron impact, the transition must be vertical and the ion may be left in an excited state. On the other hand, spectroscopic ionization potentials correspond to adiabatic transitions to the ground state of the ionized molecule.

Table 5.2 includes the results for the halogen derivatives of benzene calculated on the basis of both types of ionization potentials. Those figures appearing in brackets correspond to spectroscopic ionization potentials being used, and it is seen in this case the agreement between theory and experiment is reasonable. (We have listed the experimental values of I_2 obtained in the present work which differ slightly from Hatcher's values.) The calculated values of I_2 not enclosed in brackets have been obtained on the basis of electron impact data.[64] In this case the agreement with the experimental results is poor, the calculated values being too small in each case.

To further test Hatcher's model, I_2 was calculated for the halogen derivatives of hexane and for some chlorine compounds. These results are also shown in Table 5.2.

Table 5.2

Measured and Calculated Values of I_2

Compound	V_i (ev)	V_1 (ev)	Calculated I_2(%)	Measured I_2(%)
Fluorobenzene	9.67 (9.19)†	4.98	16.0 (21.0)†	26 ± 2
Chlorobenzene	9.42 (9.07)	3.72	8.8 (12.0)	15 "
Bromobenzene	9.41 (8.98)	3.07	4.0 (7.4)	10 "
Iodobenzene	9.10 (8.73)	2.47	2.0 (4.6)	4 "
Fluorohexane	10.2*	4.6*	8.8	26 "
Chlorohexane	10.1*	3.6*	2.2	16 "
Bromohexane	9.9*	2.8*	0.0	10 "
Iodohexane	9.3*	2.2*	0.0	4 "
Chlorodecane	9.8*	3.6*	4.6	16 "
Chlorobutane	10.3*	3.6*	0.7	17 "
Chloropropane	10.7*	3.6*	0.0	16 "

† The ionization potentials appearing in brackets are spectroscopic values[63] and the bracketed calculated I_2's have been obtained on the basis of these values. All other ionization potentials have been obtained from electron impact data[64].

*All figures marked with an asterisk have been estimated as described in Appendix 1.

Unfortunately, few ionization potentials or carbon-halogen bond dissociation potentials are available for these compounds. All the values in Table 5.2 marked with an asterisk were estimated by comparison with known values as described in Appendix 1. In all cases electron impact ionization potentials have been employed.

It is evident from these results that the model is not successful beyond the particular case of the benzene halogen derivatives, and it is successful there only if spectroscopic ionization potentials are employed. In some cases, for example in chloropropane, it is predicted that no Ore gap exists, but it is found experimentally that a considerable amount of positronium is formed. Without exception the model predicts a smaller value of I_2 than is found experimentally. Even if one reduces the electron impact ionization potentials by $\sim$0.5 ev to approximate the spectroscopic ionization potentials, the calculated values of I_2 are still in poor agreement with experiment. Hatcher states that he has neglected the effect of positron attachment to the molecules and therefore his model would be expected to work only for compounds in which the dissociation cross section is considerably higher than the positron attachment cross section. However, if positron compounds were formed, one would expect the yield of positronium to decrease. Thus, a higher, rather than lower value of I_2 would be predicted. From the point of view of the amount of positronium formed, therefore,

the designation of the dissociation potential of the carbon-halogen bond as the upper bound of the Ore gap does not appear to be correct.

Hatcher also points out that this model of positronium formation implies that singlet positronium atoms should annihilate while they posses a kinetic energy between zero and the width of the Ore gap. Again, this would not be the case for triplet positronium since its positron normally annihilates with an electron bound to a molecule. Hatcher therefore suggests that a comparison be made between the experimentally determined width of the low momentum component and the width of the Ore gap $\left[V_l - (V_i - V_p)\right]$ for the halogen derivatives of benzene.

On the momentum distribution for fluorobenzene in Figure 5.7, the estimated end of the low momentum component is marked by the arrow "A". It is very difficult to determine the absolute end points of the low momentum components, and therefore the error in such determinations is quite large. However, it should be possible to at least make qualitative comparisons among the results.

Table 5.3 lists the estimated end points for all the halogen derivatives of benzene. It becomes progressively more difficult to determine these end points from the momentum distributions as I_L decreases, and therefore, in the case of bromobenzene, use was made of the $dC/d\Theta$ vs Θ curve as well as the momentum distribution. As can be seen in Figure 5.9, the

Table 5.3

Measured and Calculated Ore Gaps

Compound	Low Momentum Component End Point ($mc \times 10^{-3}$)	Measured Ore Gap (ev)	Calculated Ore Gap (ev)
Fluorobenzene	4.1 ± 0.3	2.1 ± 0.3	2.1 (2.6)*
Chlorobenzene	4.0 ± 0.4	2.0 ± 0.4	1.1 (1.4)
Bromobenzene	3.0 ± 0.5	1.1 ± 0.4	0.5 (0.9)
Iodobenzene	2 ± 1	$0.5 \begin{smallmatrix}+0.6\\-0.4\end{smallmatrix}$	0.2 (0.6)
Fluorohexane	3.8 ± 0.3	1.8 ± 0.3	1.2
Chlorohexane	3.5 ± 0.4	1.5 ± 0.4	0.3
Bromohexane	2.5 ± 0.5	0.8 ± 0.3	0.0
Iodohexane	2 ± 1	$0.5 \begin{smallmatrix}+0.6\\-0.4\end{smallmatrix}$	0.0
Chloropropane	3.7 ± 0.4	1.7 ± 0.4	0.0
Chlorobutane	3.7 ± 0.4	1.7 ± 0.4	0.1
Chlorodecane	4.3 ± 0.4	2.3 ± 0.4	0.6
Hexane	3.3 ± 0.4	1.4 ± 0.2	0.8
Decane	3.7 ± 0.4	1.7 ± 0.3	1.0
Benzene	4.5 ± 0.4	2.5 ± 0.4	2.0
M-xylene	4.4 ± 0.4	2.4 ± 0.4	2.2

*The values in brackets have been calculated using spectroscopic ionization potentials.

same end point (3.0 ± 0.5 milliradians) is indicated by both curves. The momentum distribution for iodobenzene does not show a low momentum component, but, as pointed out above, there is an irregularity on the low momentum side of the $dC/d\theta$ vs θ curve indicating its presence. From this curve an end point of 2 ± 1 milliradians is suggested. One could also apply the following argument. If it is accepted that $I_L = I_2/3$, as is certainly indicated by the other results, then in this case I_L should be approximately 1%. To obtain this value of I_L from the momentum distribution for iodobenzene without assuming an unreasonable shape for the high momentum component, the end point of the low momentum component should be at approximately 2.5 milliradians which agrees within the error with the above mentioned value.

Turning again to Table 5.3, the "measured Ore gaps" in electron volts have been derived from the low momentum component end point through the relation $E = p^2/2M$ where M is the mass of the positronium atom i.e. we are assuming that the positron and the electron have equal momenta. The calculated Ore gaps have been obtained from the expression $V_1 - (V_i - V_p)$. In this column, the figures in brackets have been obtained using spectroscopic ionization potentials, whereas those not in brackets have been obtained using electron impact ionization potentials. The agreement between the measured and calculated Ore gaps is better when the spectroscopic ionization potentials

are employed, just as the values of I_2 calculated using these ionization potentials were in better agreement with experiment. However, since there are generally large errors in the determination of ionization potentials (see Appendix 1), the agreement between the measured Ore gaps and those calculated using electron impact data is not unreasonable. Certainly the same trend is apparent in both cases. As the experimentally determined Ore gap decreases, so do both the calculated Ore gaps. Therefore, these results for the halogen derivatives of benzene lend some support to Hatcher's hypothesis concerning the width of the Ore gap.

Table 5.3 also summarizes the results for the low momentum component end points in the halogen derivatives of hexane. For this group of compounds, the theoretically determined Ore gaps do not agree with the experimental values as was the case for the calculated values of I_2. No Ore gap, as Hatcher defines it, exists in bromohexane or iodohexane, yet a low momentum component is present. However, the trend in the width of the Ore gap is the same in the experimental and theoretical values i.e. the gap becomes narrower as the size of the halogen increases.

These results indicate, therefore, that in the halogen derivatives of hexane, the carbon-halogen dissociation potential is not the upper bound of the Ore gap. If a strict upper bound actually exists, then we are forced to conclude that there is

some excited level above V_1 which acts as this upper bound. It is more probable, however, that no strict upper bound for the Ore gap exists, but that when the positron has an energy above V_1, there is still some appreciable probability of positronium formation. In the energy range above V_1, the dissociation of the carbon-halogen bond or electronic excitation of the molecule will certainly compete with positronium formation, but not to the extent that the possibility of such an occurrence is excluded. Also, the higher that the positron energy is above the lowest excitation or dissociation potential, the less likely is the formation of positronium, since, at higher energies, there are greater numbers of competing processes.

The absence of a definite upper bound for the Ore gap could account for the measured Ore gaps being larger than the calculated ones in the hexane compounds. In the benzene compounds, even though there is reasonable agreement between experimental and theoretical values, the experimental values are as large or larger than the values calculated using electron impact ionization potentials. This again indicates the absence of an absolute upper bound on the Ore gap.

Now, even if we use the experimentally determined Ore gap to calculate I_2 according to

$$I_2 = \frac{3}{4}(\text{Ore gap}),$$

then the resulting values of I_2 for fluorohexane, chlorohexane,

bromohexane and iodohexane (13%, 10%, 6%, and 3% respectively) are still considerably smaller than the experimental values. This discrepancy can be explained as follows. One of the initial assumptions for the model stated that when the positron has an energy between the top of the Ore gap and the ionization potential, then in any subsequent collision, it loses sufficient energy so that scattering into the Ore gap may be neglected. In practice, this is probably an unrealistic assumption. If scattering into the Ore gap is taken into account, then the calculated values of I_2 will become larger as required. Notice that when I_2 is calculated for the benzene halogen derivatives employing electron impact ionization potentials, the values are consistently too small, again suggesting that scattering into the Ore gap should be considered.

The amount by which such scattering would increase I_2 is difficult to determine. Consider for example the specific case of fluorobenzene where $V_i = 9.2$ ev, $V_1 = 5.0$ ev, and $V_i - V_p = 2.4$ ev, and let us assume for the sake of argument that V_1 is the upper bound of the Ore gap which would then have a width of 2.6 ev. If the dissociation of the carbon-halogen bond were the only process competing with positronium formation in the energy interval $V_1 < V < V_i$, then each positron in this energy interval would lose at least 5.0 ev. Therefore, the positrons with energies between $2.4 + 5.0 = 7.4$ ev and 9.2 ev could be scattered into the Ore gap. Not all of these

positrons will be scattered into the Ore gap since some will lose an energy greater than 5.0 ev in a collision causing the dissociation of the carbon-halogen bond. Some of these positrons may suffer greater energy losses for another reason. Electronic spectra of benzene[65] indicate that there are excited states 4.5 ev, 5.7 ev, and 6.9 ev above the ground state energy. These energies are probably typical of those that would be found in the molecules with which we are dealing. Therefore, some positrons in the energy range between 7.4 ev and 9.2 ev may lose more energy than 5.0 ev as a result of electronic excitation and thus not be scattered into the Ore gap. The maximum total fraction of positrons forming positronium would be the fraction originally in the Ore gap, $[V_1 - (V_i - V_p)]/V_i = 0.28$, plus the fraction eligible for scattering into the Ore gap, $(9.2 - 7.4)/V_i = 0.20$. It can be seen that the process of scattering into the Ore gap does not have to be very efficient to appreciably increase the yield of positronium. A knowledge of the relative cross sections for all the possible processes is necessary before any detailed calculations can be made.

Finally, we turn to an examination of the results for all the chlorine compounds investigated and the results for hexane, decane, benzene and m-xylene to obtain further support for the above arguments. These results are also shown in Table 5.3. Unfortunately, there are large error limits on the experimental determination of the low momentum component end points

for the chlorine compounds. However, it may be significant that chloropropane, chlorobutane and chlorohexane which have the smallest calculated Ore gaps, also have the smallest measured Ore gaps as compared with chlorodecane and chlorobenzene for which the calculated and experimental Ore gaps are larger.

For the parent compounds, a logical choice for the "upper limit" of the Ore gap (or rather the energy at which positronium formation is no longer the only possible process) is the dissociation potential of the carbon-hydrogen bond which is about 4.4 ev[62] in all cases. This value has been substituted for V_1 in the Ore gap calculations. It is apparent again that, although there is no absolute agreement between the calculated and experimental values, the trend is the same for both, and also that the calculated values are smaller than the experimental values.

In summary therefore, the results from the low momentum components indicate that a simple explanation of positronium formation on the basis of energy considerations is not possible. It appears that a type of Ore gap exists having a definite lower bound, $(V_i - V_p)$, but without a precise upper bound. The particular model suggested by Hatcher requires modification to allow for positronium formation by positrons whose energies are above that at which competing processes may occur. Allowance must also be made for the scattering into the Ore gap of positrons

having energies between V_1 and V_i as well as those that have been initially scattered into it from the energy range above V_i.

5.4 The High Momentum Component.

If all the positrons contributing to the high momentum component are thermalized at the time of their annihilation, and if the annihilation probability is independent of the relative velocity of the positron and electron with which annihilation occurs, then the high momentum component represents the momentum distribution of the electrons that the positrons are annihilating. These electrons would most probably be the ones occupying the highest molecular orbitals i.e. the outermost electrons of the molecule.

It is unlikely that the above conditions are completely satisfied in practice, but there is some evidence that they are closely approximated under actual experimental conditions. We shall consider first the degree of thermalization of the free positron at the time of its annihilation. It was seen in section 1.4 that a positron is thermalized in metals in approximately 3×10^{-12} seconds, where less than 0.1% of this time is required to slow the positron from its initial energy of several Kev to an energy of 1 ev, and only 6% of the total time is required to further reduce the positron's energy to 0.1 ev. In other words, the positron spends approximately 94% of its time before thermalization between the energies 0.1 ev and 0.25 ev. The time

required for thermalization in insulators is considerably longer. The calculation by de Benedetti et al[29] for the thermalization of positrons in gold by the excitation of lattice vibrations yields a time of 3×10^{-10} seconds. Wallace[5] has stated that this calculation may be considered to give an indication of the thermalization time in insulators. In an insulator, however, the positron will spend an even greater percentage of the total thermalization time in the low energy range since, below the lowest excitation potential of the molecules, inelastic processes are no longer possible and the positron must lose energy by the relatively slow process of elastic collisions. Therefore, on the basis of de Benedetti's estimate of the thermalization time, the positron should require less than 2×10^{-11} seconds to reach an energy of 0.1 ev. The lifetime of free positrons in insulators is at least 10^{-10} seconds, and therefore we are justified in assuming that the positron's energy is approximately 0.1 ev at the time of its annihilation.

It is also possible to estimate the degree of thermalization of free positrons from experimental evidence. From the momentum distributions shown in Figures 5.1 to 5.13 it is seen that a typical mean momentum of singlet positronium is $2mc \times 10^{-3}$ corresponding to an energy of 0.5 ev. Singlet positronium, due to its electric neutrality, will be attenuated more slowly than free positrons. Therefore, since free positrons and singlet positronium have approximately the same lifetime,

the mean energy of free positrons will be less than 0.5 ev when annihilation occurs.

The same experimental evidence implies that the energy of triplet positronium, whose positrons also contribute to the high momentum component, is small at the time of annihilation. Triplet positronium will undergo the same attenuating processes as does singlet positronium, but since its mean lifetime is at least a factor of ten longer than the mean lifetime of singlet positronium, its energy will also be less than 0.5 ev when annihilation occurs.

Now, the outer electrons with which annihilation occurs have typical mean momenta of 5 to 6 mc x 10^{-3} corresponding to mean energies of 6 to 9 ev. The distribution of momenta would be expected to have a shape similar to the high momentum components in the present momentum distributions. If we assume an electron momentum distribution as indicated by the solid curve in Figure 5.15, and consider annihilations with positrons having an energy of 0.5 ev, then the resulting momentum distribution of the annihilating positron-electron pairs is as indicated by the dotted curve in the same figure. The only significant difference between the two distributions is that the full width at half maximum of the momentum distribution of the annihilating pairs is about 5% larger than that for the original electron momentum distribution. This figure can be taken as an upper limit since we have shown that the positrons

FIGURE 5.15

(a) THE EFFECT OF THE POSITRON'S FINITE MOMENTUM ON THE ORIGINAL ELECTRON MOMENTUM DISTRIBUTION

1. Assumed electron momentum distribution.
2. Momentum distribution of annihilating pairs when positron has energy of 0.5 ev.

(b) EXPERIMENTAL AND THEORETICAL SHAPES FOR THE HIGH MOMENTUM COMPONENT IN HEXANE

Closed circles indicate the theoretical distribution.

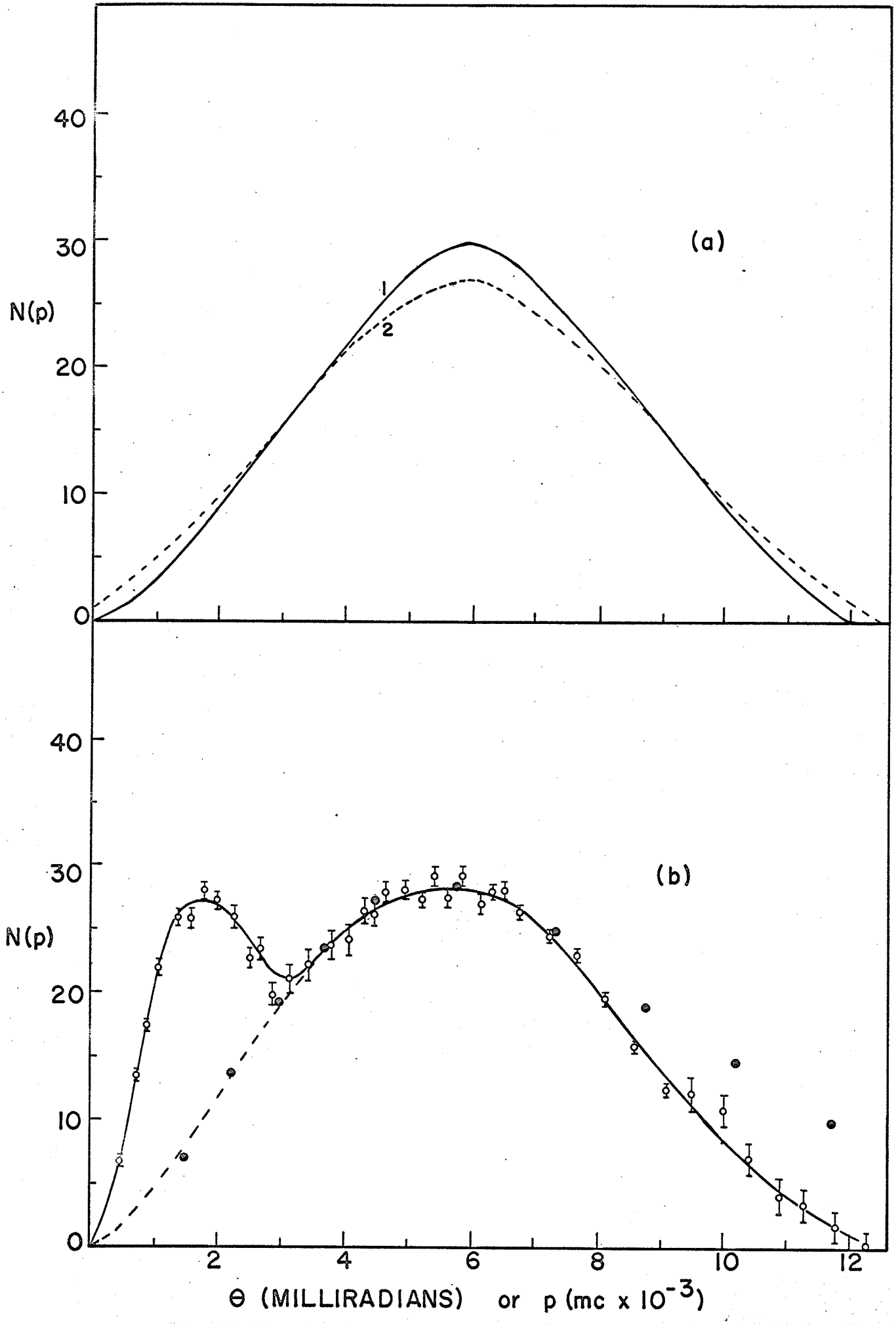
(a)
N(p)
40
30
20
10
0
1
2
(b)
N(p)
40
30
20
10
0
2
4
6
8
10
12
θ (MILLIRADIANS) or p (mc x 10⁻³)

have energies less than 0.5 ev when annihilation occurs. Since the error in the experimental determination of the width of the high momentum component is approximately 3%, we may say that the effect of the positron's finite velocity on the momentum distribution is negligible. Furthermore, the small effect that it does have will be very nearly the same in all cases, and therefore we are certainly justified in making comparisons among the results.

We must now consider the dependence of the annihilation probability on the relative velocity of the positron and the electron. In Stewart's original work[35] in metals, the agreement between his experimentally determined Fermi energies and those obtained in soft x-ray emission experiments allow one to exclude an annihilation probability which varies as strongly as $1/v$, where v is the relative velocity of the positron and the electron. Within his experimental error, one may assume a velocity independent annihilation probability. More recently, Kahana[66] has performed calculations which indicate that the dependence is very small, and Stewart's results[67] in Li and Li-Mg alloys agree very well with the assumption of a velocity independent annihilation probability. In the present work, therefore, we are justified in assuming that the variation of the annihilation probability with momentum will not affect the results significantly.

Since the two conditions mentioned at the beginning

of this section are reasonably satisfied, the measured momentum distributions of the annihilating positron-electron pairs represent the distributions in momenta of the annihilating electrons. The only problem remaining is to determine to what extent the momentum distribution of the electrons is perturbed by the presence of the positron before annihilation. In the various organic liquids investigated here, the perturbation should be very nearly the same so that we may at least make comparisons among our results. Very little work of a theoretical nature has been done on this problem, and therefore we turn again to the experimental work of Stewart.[35,67] Since his experimentally determined Fermi energies are in good agreement with those obtained by other methods, it appears that the effect of the positron on the electronic configuration is small. If such is the case, then our high momentum components should be good approximations to the original momentum distributions of the electrons with which annihilation occurs.

In 1939 Hughes and Starr[68] attempted to determine experimentally the momentum distribution of the electrons in methane by the inelastic scattering of fast (4000 ev) electrons by the methane molecules. Their results indicate that the electrons have a mean momentum of roughly $10mc \times 10^{-3}$ whereas the present results show that for hexane, belonging to the same chemical family as methane, the electrons have a mean momentum of $6mc \times 10^{-3}$. One would not expect hexane and methane to have identical electron momentum distributions, but neither would

one expect them to differ by such a large amount.

In 1941, Coulson and Duncanson[69] calculated the electron momentum distributions in several hydrocarbons, among them methane and ethane. Their results indicate mean electron momenta approximately the same as are indicated in the present work. They suggested that the momentum distributions of Hughes and Starr were in error due to an incorrect interpretation of the experimental results. For their method of analysis to be correct, only single scattering can occur but it is probable that, at the energies involved, some multiple scattering also takes place.

Very briefly, the method of Coulson and Duncanson was to calculate separately the momentum distributions of the electrons in the carbon-hydrogen and carbon-carbon bonds and the momentum distribution of the carbon 1s electrons, and to then take a weighted mean of the individual distributions. Employing their results for the separate momentum distributions, we have performed a similar calculation for the momentum distribution of the electrons in hexane according to

$$N(p) = \frac{1}{n_1 + n_2}\left[n_1 N_{CH}(p) + n_2 N_{CC}(p)\right] \qquad (5.1)$$

where n_1 and n_2 are the total numbers of electrons involved in the carbon-hydrogen and carbon-carbon bonds respectively, and $N_{CH}(p)$ and $N_{CC}(p)$ are the respective momentum distributions of these electrons. Since positron annihilation with the 1s

electrons is unlikely, their contribution to the momentum distribution is neglected. The result of this calculation is shown in Figure 5.15(b) where a comparison is made with the high momentum component in hexane. The agreement is suprisingly good considering the fact that the shape of the calculated distribution is highly dependent upon the initial choice of the molecular wave function.[70] A significant disagreement occurs only in the high momentum region where the main contribution to the theoretical curve arises from the electrons in the carbon-carbon bond. It is quite probable that positrons annihilate predominantly with the outer electrons of the carbon-hydrogen bond, and therefore, in equation 5.1, $N_{CH}(p)$ should be weighted more heavily. This would have the effect of reducing N(p) in the high momentum region on the theoretical curve bringing it into closer agreement with experiment. The rather good agreement between theory and experiment here gives some support to the view that the high momentum component is a direct measure of the momentum distribution of the electrons involved in the annihilating process.

Table 5.4 summarizes the high momentum component results for all the compounds investigated in terms of the mean momentum and the full width at half maximum of the momentum distributions. These measurements are made as indicated in Figure 5.7 for fluorobenzene.

Considering first the compounds hexane, decane, benzene and m-xylene, it is seen that the mean momentum decreases with

Table 5.4

Summary of the High Momentum Component Results

Compound	Mean Electron Momentum ($mc \times 10^{-3}$)	Full Width at Half Maximum of High Momentum Component ($mc \times 10^{-3}$)
Hexane (10.43 ev)*	5.7 ± .2	6.5 ± .3
Fluorohexane	5.7 "	6.7 "
Chlorohexane	5.6 "	6.2 "
Bromohexane	5.4 "	5.1 "
Iodohexane	5.0 "	4.5 "
Benzene (9.21 ev)	5.4 "	6.6 "
Fluorobenzene	5.8 "	6.2 "
Chlorobenzene	5.6 "	5.6 "
Bromobenzene	5.4 "	5.0 "
Iodobenzene	4.9 "	4.4 "
Decane (10.19 ev)	5.6 "	6.6 "
Chlorodecane	5.7 "	5.5 "
Chloropropane	5.6 "	5.4 "
Chlorobutane	5.5 "	5.8 "
Difluorobenzene	5.9 "	6.4 "
M-xylene (8.97 ev)	5.3 "	6.2 "

* Ionization potentials.

decreasing ionization potential. (See brackets in Table 5.4) This result is expected since the ionization potential corresponds approximately to the total energy of the highest occupied molecular orbital of the system.[71] Therefore, a lower ionization potential should result in a lower mean energy or momentum of the outer electrons. It is not possible to correlate directly the ionization potential with the mean momentum since it is not known to what extent the electrons' kinetic energies change as the ionization potential changes.

The results for the halogen derivatives of hexane and benzene clearly indicate a trend to a lower mean momentum as the size of the halogen atom increases. This trend is also expected since, as the halogen atom increases in size, its outer electrons are more weakly bound, and therefore their momentum will have a lower mean value. It is of interest to compare these results with those of Stewart[36] for the alkali halides. In the series NaF, NaCl, NaBr, and NaI where most annihilations occur with the negative halogen ion, the mean momentum of the electrons decreases more rapidly than it does here. It would be expected that, in the halogen derivatives of hexane and benzene, the trend to a lower mean momentum would be present, but to a lesser degree, since many annihilations must still occur with electrons in the carbon-hydrogen and carbon-carbon bonds which have higher mean momenta. It may also be noted that the decrease in the full width at half maximum of the

momentum distributions for the halogen derivatives of hexane and benzene as the halogen atom increases in size is in qualitative agreement with Stewart's results for the sodium halides, although the decrease in the latter case is again more rapid.

In summary therefore, evidence has been presented which indicates that the high momentum component is a direct measure of the momentum distribution of the "outer" electrons of the molecule. It is difficult to determine precisely which electrons are involved in the annihilation process, but qualitative agreement is obtained with both theory and experiment on the basis that annihilation is occurring predominantly with electrons in the carbon-hydrogen bonds in the case of the parent molecules, and with electrons in the carbon-hydrogen and carbon-halogen bonds in the case of the halogen derivatives of the parent molecules.

5.5 Polyethylene.

As was mentioned in the introduction, improved fast coincidence techniques have allowed the time spectra of positrons annihilating in amorphous solids and plastics to be resolved into three components instead of the previous two components. It might have been expected that the original short lived component resulting from the annihilation of singlet positronium and free positrons could be resolved into two components corresponding to the two different modes of decay. In that case,

the short lived component corresponding to the decay of singlet positronium should have an intensity equal to $I_2/3$. However, in polyethylene the three components which have lifetimes of 0.25, 0.50 and 2.50 nanoseconds have intensities of 45%, 30% and 25% respectively, where I_2 = 25%. The intermediate component, if due to the annihilation of singlet positronium, should have an intensity of 8%. Thus, the 30% intermediate component does not appear to be due to singlet positronium annihilation.

The angular distribution of the annihilation radiation from polyethylene was measured to determine if any irregularities were present in the resulting momentum distribution which is shown with $dC/d\theta$ vs θ in Figure 5.16. The intensity of the low momentum component is $6 \pm 1\%$ in reasonable agreement with the value $I_2/3$ = 8% indicating that nothing unusual is occurring as far as the relative amounts of singlet and triplet positronium formed are concerned. The only significant difference between the polyethylene results and those for organic liquids is that the mean momentum of the singlet positronium is somewhat higher in the case of polyethylene. This is particularly evident from an examination of the $dC/d\theta$ vs θ curve.

Therefore, no explanation of the intermediate lifetime is apparent from the angular correlation results for polyethylene.

FIGURE 5.16

N(p) VS p AND $\bar{d}C/d\theta$ VS θ FOR POLYETHYLENE

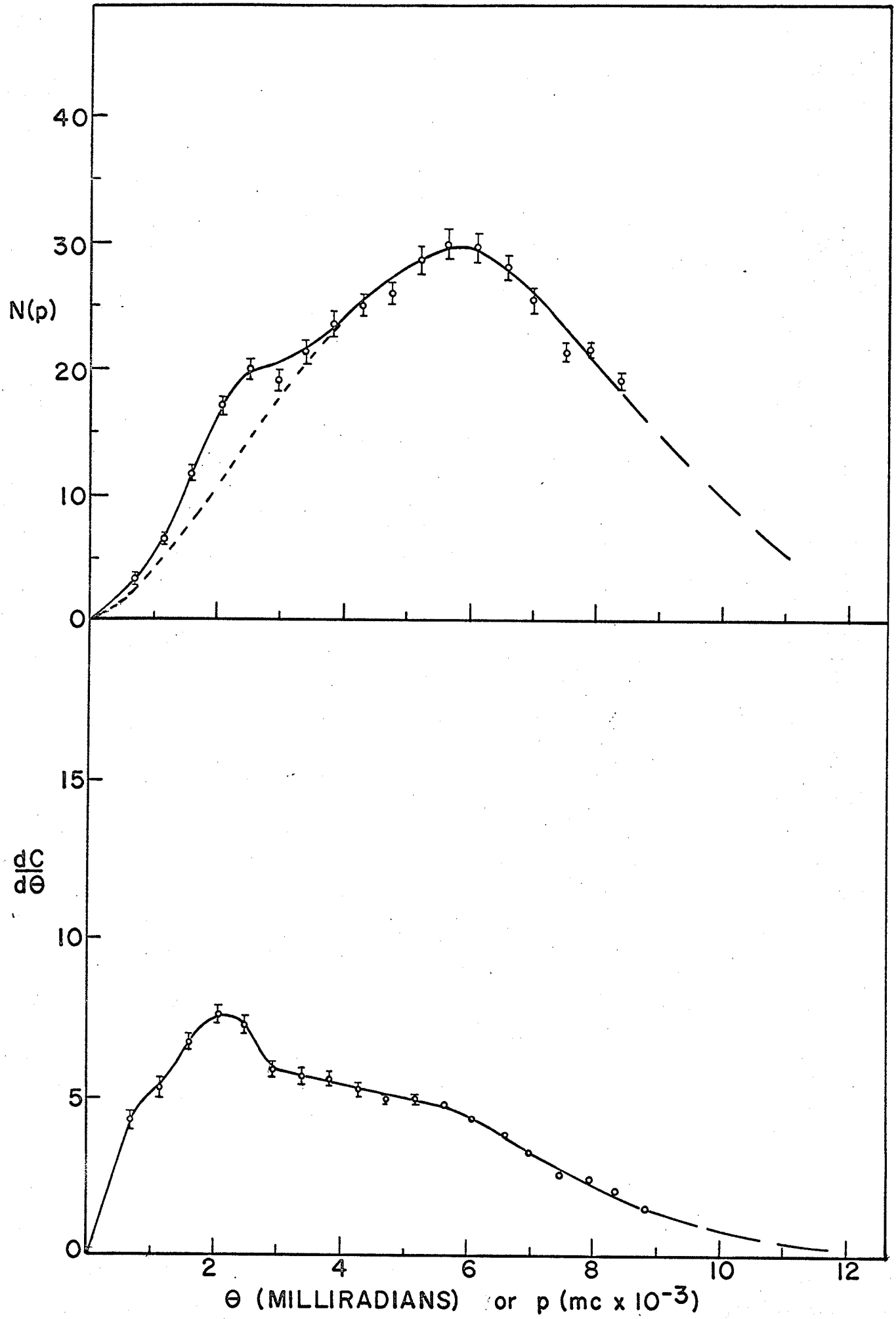
40
30
N(p)
20
10
0
15
dC/dθ
10
5
0
2
4
6
8
10
12
θ (MILLIRADIANS) or p (mc x 10⁻³)

Appendix 1

THE ESTIMATION OF IONIZATION AND DISSOCIATION POTENTIALS

It can be seen from an examination of known ionization potentials that, within any homologous series of compounds, the ionization potential decreases with increasing molecular weight. In Figure A.1 all the known ionization potentials[64] for the paraffins and their halogen derivatives are plotted showing this trend very clearly. The experimental errors for three of these ionization potentials are also shown. Typical errors are approximately 0.2 ev. In any particular group of compounds consisting of the parent molecule and its halogen derivatives, the trend in ionization potential as the size of the halogen atom increases is indicated by the solid lines joining the known values. Where ionization potentials are not known, we assume a trend as indicated by the dotted lines. Thus, for example, the estimated ionization potentials for fluorohexane, chlorohexane, bromohexane and iodohexane are 10.2 ev, 10.1 ev, 9.9 ev and 9.3 ev respectively. It is reasonable to assume that these values are accurate to within 0.3 ev.

Dissociation potentials of the carbon-halogen bond are available only for the following paraffin compounds:[62] CH_3F (4.6 ev), CH_3Cl (3.5 ev), CH_3Br (2.9 ev), CH_3I (2.3 ev), C_2H_5Cl (3.6 ev), C_2H_5Br (2.8 ev), and C_2H_5I (2.2 ev). It is evident, therefore, that in the methane and ethane halogen

ESTIMATION OF IONIZATION POTENTIALS

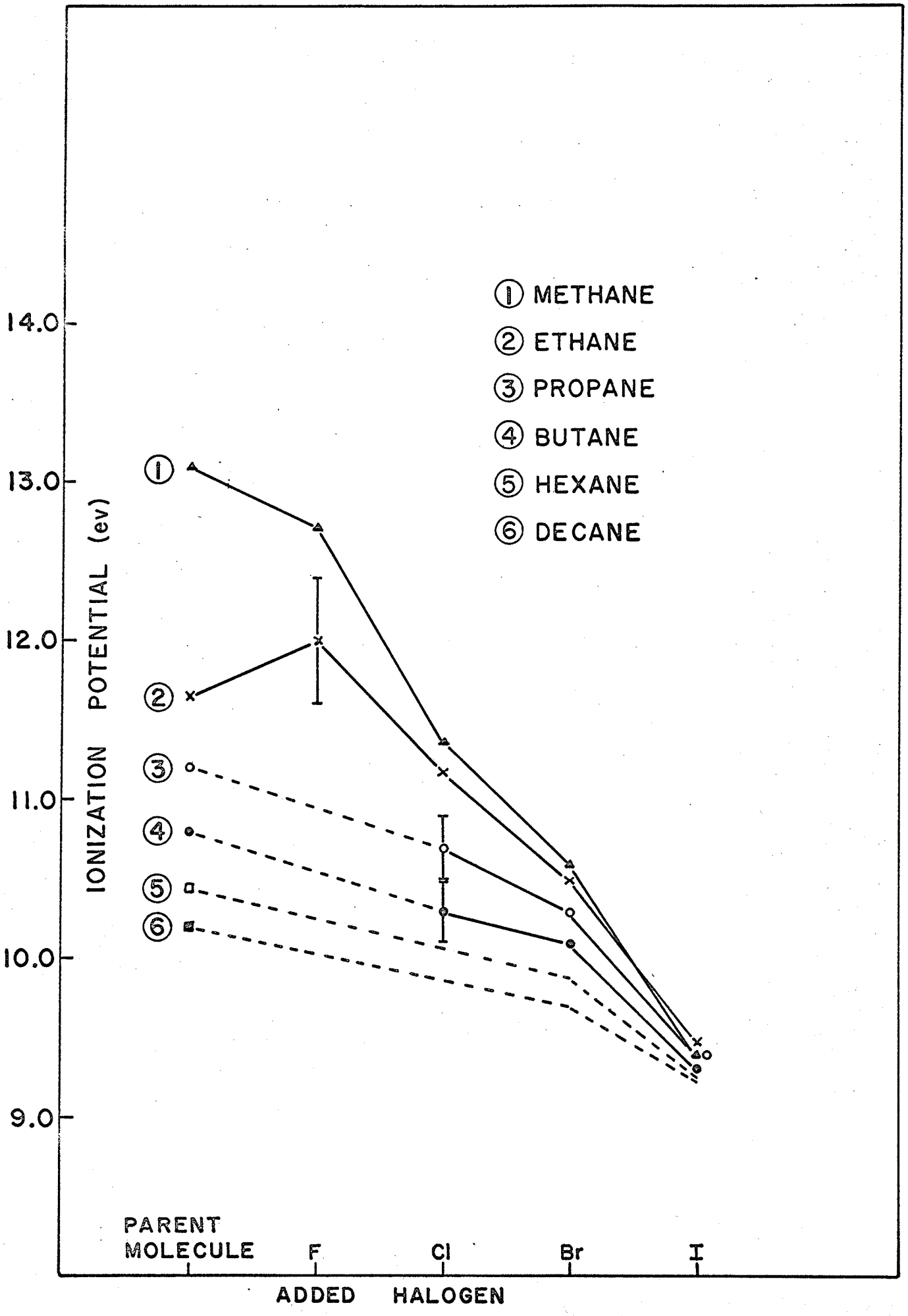
① METHANE
② ETHANE
③ PROPANE
④ BUTANE
⑤ HEXANE
⑥ DECANE
14.0
13.0
12.0
11.0
10.0
9.0
IONIZATION POTENTIAL (ev)
PARENT MOLECULE
F
Cl
Br
I
ADDED HALOGEN

derivatives, the corresponding bond dissociation potentials are very similar. Very little change would be expected as we progress through the propane, butane, hexane and decane compounds since the carbon-halogen bonds are the same in each case. Therefore, we have assumed the carbon-fluorine, carbon-chlorine, carbon-bromine and carbon-iodine bond dissociation potentials to be 4.6 ev, 3.6 ev, 2.8 ev and 2.2 ev.

REFERENCES

1. R. Weinsein, M. Deutsch and S. Brown, Phys. Rev. 94, 758 (1954).
2. M. Deutsch, Prog. in Nuc. Phys. 3, 131 (1953).
3. S. De Benedetti and H. C. Corben, Annual Rev. of Nuc. Science, 4, 191 (1954).
4. R. A. Ferrell, Rev. Mod. Phys. 28, 308 (1956).
5. P. R. Wallace, "Solid State Physics", p. 1, edited by F. Seitz and D. Turnbull, Academic Press (1960).
6. W. Heitler, "Quantum Theory of Radiation", Oxford University Press, London (1944) p. 230 ff.
7. A. Ore and J. L. Powell, Phys. Rev. 75, 1696 (1949).
8. J. A. Wheeler, Ann. N. Y. Acad. Sci. 48, 219 (1946).
9. J. Pirenne, Arch. Sci. Phys. et Nat. 29, 121, 207 (1947).
10. A. Ore, University of Bergen, Arbok No. 9 (1949).
11. A. E. Ruark, Phys. Rev. 68, 278 (1945).
12. P. A. M. Dirac, Proc. Camb. Phil. Soc. 26, 361 (1930).
13. J. W. Shearer and M. Deutsch, Phys. Rev. 76, 642 (1949).
14. M. Deutsch, Phys. Rev. 83, 866 (1951).
15. S. de Benedetti and R. Siegel, Phys. Rev. 85, 371 (1952).
16. M. Deutsch and S. C. Brown, Phys. Rev. 85, 1047 (1952).
17. S. de Benedetti and H. J. Richings, Phys. Rev. 85, 377 (1952).
18. R. E. Bell and R. L. Graham, Phys. Rev. 90, 644 (1953).
19. R. E. Bell and M. H. Jørgensen, Can. J. Phys. 38, 652 (1960).
20. S. Berko and J. S. Plaskett, Phys. Rev. 112, 1877 (1958).

21. A. Ore, University of Bergen, Arbok No. 12, (1949).

22. D. A. L. Paul and R. L. Graham, Phys. Rev. 106, 16 (1957).

23. J. Wackerle and R. Stump, Phys. Rev. 106, 18 (1957).

24. I. Spirn, W. Brandt, G. Present and A. Schwarzchild, Bull. Am. Phys. Soc. 9, 394 (1964).

25. A. W. Sunyar, Bull. Am. Phys. Soc. 9, 394 (1964).

26. G. E. Lee-Whiting, Phys. Rev. 97, 1557 (1955).

27. Page, Heinberg, Wallace and Trout, Phys. Rev. 98, 206 (1955).

28. P. R. Wallace, Phys. Rev. 100, 738 (1955).

29. S. de Benedetti, C. E. Cowan, W. R. Konneker and H. Primakoff, Phys. Rev. 77, 205 (1950).

30. W. E. Millet and R. Castillo-Bahena, Phys. Rev. 108, 257 (1957).

31. S. S. Hannah and R. S. Preston, Phys. Rev. 109, 716 (1958).

32. J. B. Warren and G. M. Griffiths, Can. J. Phys. 29, 325 (1951).

33. R. E. Green and A. T. Stewart, Phys. Rev. 98, 486 (1955).

34. A. T. Stewart, Phys. Rev. 99, 594 (1955).

35. A. T. Stewart, Can. J. Phys. 35, 168 (1957).

36. A. T. Stewart and N. K. Pope, Phys. Rev. 120, 2033 (1960).

37. J. J. Donaghy and A. T. Stewart, Bull. Am. Phys. Soc. 9, 238 (1964).

38. R. A. Ferrell, Rev. Mod. Phys. 28, 308 (1956).

39. L. Page and M. Heinberg, Phys. Rev. 102, 1545 (1956).

40. S. D. Warshaw, Phys. Rev. 108, 713 (1957).

41. R. L. de Zafra, Physics Dept. Technical Report 108, University of Maryland (1958).

42. J. G. Lundholm Jr., J. A. Bjorkland and A. C. Menius Jr., Bull. Am. Phys. Soc. 2, 173 (1957).

43. R. Stump, Bull. Am. Phys. Soc. 2, 173 (1957).

44. H. S. Landes, S. Berko and A. J. Zuchelli, Phys. Rev. 103, 828 (1957).

45. R. A. Ferrell, Physics Dept. Technical Report 98, University of Maryland (1958).

46. R. E. Green and R. E. Bell, Can. J. Phys. 35, 398 (1957).

47. D. P. Kerr, M.Sc. Thesis, University of Manitoba (1961).

48. G. Jones, Ph.D. Thesis, University of British Columbia (1960).

49. R. E. Bell and R. E. Green, Nuclear Instruments 3, 127 (1958).

50. D. P. Kerr and B. G. Hogg, Rev. Sci. Instr. 33, 391 (1962).

51. S. I. H. Naqvi, Ph.D. Thesis, University of Manitoba (1961).

52. L. Katz and A. S. Penfold, Rev. Mod. Phys. 24, 28 (1952).

53. R. D. Evans, "The Atomic Nucleus" p. 263, McGraw-Hill (1955).

54. C. Eckhart, Phys. Rev. 51, 735 (1937).

55. L. G. Lang, "Angular Correlation of Annihilation Radiation from Solids", Carnegie Institute of Technology Report (1956).

56. R. D. Evans, op. cit. p. 683.

57. P. B. Moon, Proc. Phys. Soc. 63 A, 1189 (1950).

58. C. R. Hatcher, W. E. Millet and L. Brown, Phys. Rev. 111, 12 (1958).

59. D. P. Kerr and B. G. Hogg, J. Chem. Phys. 36, 2109 (1962).

60. M. Deutsch, Mass. Inst. Technol. Lab. Nuclear Sci. and Engr. Progress Report (1952).

61. C. R. Hatcher, J. Chem. Phys. 35, 2266 (1961).

62. T. L. Cottrell, "The Strengths of Chemical Bonds" Butterworths (1958).

63. K. Watanabe, J. Chem. Phys. 26, 542 (1957).

64. F. H. Field and J. L. Franklin, "Electron Impact Phenomena", Academic Press (1957).

65. A. Streitweiser, "Molecular Orbital Theory", p. 218, Wiley and Sons (1961).

66. S. Kahana, Phys. Rev. 129, 1622 (1963).

67. A. T. Stewart, Phys. Rev. 133, 1651 (1964).

68. Hughes and Starr, Phys. Rev. 55, 343 (1939).

69. C. A. Coulson and W. E. Duncanson, Proc. Camb. Phil. Soc. 37, 406 (1941).

70. C. A. Coulson and W. E. Duncanson, Proc. Camb. Phil. Soc. 38, 100 (1942).

71. R. S. Mulliken, Phys. Rev. 74, 736 (1948).